Co(III) Complexes as Pro-drugs for Cancer Therapy

by

Chen Zhang

B.Sc., Sichuan University, 2013

Thesis Submitted in Partial Fulfillment of the
Requirements for the Degree of
Master of Science

in the
Department of Chemistry
Faculty of Science

Chen Zhang 2016

SIMON FRASER UNIVERSITY

Summer 2016

Approval

Name: **Chen Zhang**

Degree: **Master of Science (Chemistry)**

Title: ***Co(III) Complexes as Pro-drugs for Cancer Therapy***

Chair: Dr. David J. Vocadlo
Professor

Examining Committee:

Dr. Tim Storr
Senior Supervisor
Associate Professor

Dr. Charles J. Walsby
Co-Supervisor
Associate Professor

Dr. Jeffrey J. Warren
Supervisor
Assistant Professor

Dr. Hua-Zhong Yu
Supervisor
Professor

by written consultation (Chongqinq, China) [ ]

Dr. Loren Kaake
Internal Examiner
Assistant Professor

Date Defended/Approved: May 13, 2016

Abstract

Cancer is the leading cause of death in Canada and is characterized by irregular and uncontrolled cell growth. In many cases this uncontrolled cell growth results in a solid mass of cells called a tumor. When the inner part of a tumor is sequestered from blood vessels, the nutrient and oxygen levels decrease. The term “hypoxia” is used to describe low oxygen level in tissue. Hypoxia induces more reducing conditions in a tumor in comparison to normal tissue. The objective of this project was to generate a series of octahedral Co(III) complexes for the treatment of cancer. We designed pro-drugs that are initially administered to the body in an inactive form, and can be selectively activated under the hypoxic (reducing) conditions in tumors.

In this work, a series of octahedral Co(III) salen complexes were synthesized incorporating 1-methylimidazole in axial positions. We investigated the stability of the complexes in solution, and the effect of different *para*-ring substituents on the Co(III) / Co(II) reduction potential. We concluded that the reduction potentials of the complexes were correlated with the electron donating ability of the *para*-ring substituents, and that a geometry change from octahedral to square-planar upon reduction leads to axial ligand release.

Building on these results, coumarin fluorophores were then attached to the Co(III) complexes via a functionalized imidazole. We found that the fluorescence of the coumarin was largely quenched while bound to the Co(III) center. Ligand release was then studied in the presence of excess competing ligands and in the presence of a reducing agent. Our results suggest that both ligand exchange and reduction play a role in axial ligand release in these systems.

Keywords: Tumor hypoxia; redox-active; anti-cancer agents; cobalt salen complex; fluorescence

Dedication

To my dearest parents (Yan Liu and Dianren Zhang) and beloved Yuxing Zhang, for your unconditional love and support.

Acknowledgements

Years from now, when I open this thesis again, what will come to my mind will not only be the work I had done in Storr lab, but also a lot of amazing people and unforgettable stories. Three years overseas living in a beautiful country, speaking in a complicated language, working in a new fascinating field, I have been learning and enjoying so much. All of these would not exist without your company and help.

To Prof. Tim Storr, thank you for taking a chance on an international student. If it was not you, I would not have an opportunity to work in such a fun lab and enjoy my life here in Vancouver. I am so lucky to have such a knowledgeable, patient, and considerable supervisor! Thank you for your wise guidance and kindness.

To Prof. Charles Walsby, thank you for your help in NMR, EPR and good suggestions on my thesis. I am lucky to have you as my supervisor. Thank you for always being patient with me.

To the past and present people in Storr lab: Linus Chiang (thank you for teaching me so many things in the lab, driving me home after lab dinners, and also charging our car when it was dead!!), Ryan Clarke (you are my trouble shooter! Helpful in X-ray and tears, always make me feel better with Jolly rancher and Kitkat!), Rafael Vieira (I still remember that one egg is too much for a day, from “grandpa”), Christine Dyrager (Energetic mom, always helped me with synthesis, I like your roar!), Michael Jones (food is always very tasty when I was eating with you), Dustin Duncan, Jessica Miller, Makrum Guterres, Tiffany Jeen, Misaki Nakai, Chaofeng Zhang, Mathew Sutherland (I was so lucky to have the best undergrad’s help), and Tiffany Tree.

To my dearest girls: Luiza Gomes (xuxu, who always support me like a sister), Emilie Mathieu (ma shihi, the singer who’s famous for “Chenchen song”), Serena Rigo (schatzli, my twin sister, even though we were born several days apart), Khrystyna Herasymchuk (cat lady, smart, sweet, considerable, pretty and nice, you are always the first one to think about when I get in trouble!), Camila Vargas Garcia (pretty cat lady II, slim but fit), Lalangi Asha Chandrasena (only we know what we went through!), Danqing Liu (so happy to have you here in Vancouver). I will always remember the happy time we spent together.

To the past and present instructors and supervisors: Prof. Jeff Warren (a nice supervisor and a good friend), Prof. Hogan Yu and Dr. Julie Lunniss (I would love to be a TA for your course again!). Prof. Bingyun Sun, Prof. Peng Liang, Prof. Fangdong Zou, Prof. Xiangzhen Li (Without your help, I would not be sitting here and writing my thesis)

To Mitacs: Thanks to Globalink Program for sending me here in 2012, and supporting me for two years in pursuing my degree!

I would like to thank Dr. Andrew Lewis (NMR), Colin Zhang (NMR), John Thompson (X-ray), Kate Prosser (EPR), Paul Mulyk (EA) and Chemistry Department Secretaries, especially Lynn Wood, Nathalie Fournier, and Evon Khor.

To my family: Thank you for always supporting and encouraging me since I was a little kid. I love you all!

To Yuxing (Martin) Zhang: I cannot even imagine the life without you. Thank you so much for deciding to come here; I know what that means to you. Thank you so much for your love, care, understanding and support.

To my beloved parents: I knew it would be very difficult since the beginning, but the more time I have spent here, the more I understood how much I love you. I miss you. Dad, I know how worried you are about me, but you never say it. Thank you for encouraging me, and always bringing me good news from China to make me happy. Mom, you are the best lady in the whole world. Without your comfort, I could not have stayed as strong. Thank you so much for always believing in me!

Table of Contents

List of Tables

List of Figures

List of Schemes

List of Acronyms

1-MeIm	1-Methylimidazole
A	Absorbance
acacen	N,N'-ethylenebis(acetylacetone iminate)
AQ2CH	Anthraquinone-2-carboxylic acid
ATP	Adenosine triphosphate
ATSM	Diacetyl-bis(N4-methylthiosemicarbazone)
C	Concentration
C343H	Coumarin-343
ca.	Approximately
cm	Centimeters
Cu-ATSM	Copper(II)-diacetyl-bis(N4-methylthiosemicarbazone)
Cu-PTSM	Copper(II)-pyruvaldehyde-bis(N4-methylthiosemicarbazone)
Cu-GTSM	Copper(II)-glyoxal-bis(N4-methylthiosemicarbazone)
CV	Cyclic Voltammetry
cyclam	1,4,8,11-tetraazacyclotetradecane
d	Doublet (NMR)
DCM	Dichloromethane
DMF	Dimethylformamide
$E_{1/2}$	Reduction potential
E_a	Anodic peak potential
EA	Elemental analysis
E_c	Cathodic peak potential
eq.	Equivalent
ESI (+)	positive ion-mode electrospray ion
EtOH	Ethanol
F	Faraday's constant
Fc	Ferrocene
Fc^+	Ferrocenium
FITC	Fluorescein isothiocyanate
FL	Fluorescein
GFP	Green fluorescent protein

GSH	Glutathione
GTSM	Glyoxal-bis(N4-methylthiosemicarbazone)
HIFs	Hypoxia-inducible factors
IC	Internal conversion
ISC	Intersystem crossing
IV	Intravenous therapy
J	*J* coupling constant
K	Kelvin
K_a	Acid Dissociation Constant
λ_{em}	Emission wavelength
λ_{ex}	Excitation wavelength
m	Multiplet (NMR)
M	Molar concentration (mol/L)
m/z	mass-to-charge ratio
MeOH	Methanol
mg	Milligrams
mL	Milliliters
mm	Millimeters
mmol	Millimoles
mV	Millivolts (Electrochemistry)
m/z	Mass-to-charge ratio
NADH	β-nicotinamide adenine dinucleotide
NADPH	β-nicotinamide adenine dinucleotide phosphate
NHE	Normal Hydrogen Electrode
nm	Nanometers
NMR	Nuclear Magnetic Resonance
NSCLC	Non-small-cell lung cancer
OAc	Acetate
PBS	Phosphate buffered saline
$Pt(IV)(FL)_2$	*c,c,t*-$[Pt(NH_3)_2Cl_2(OCO(CH_2)_2NH(FL))_2]$
$Pt(IV)(FITC)_2$	*c,c,t*-$[Pt(NH_3)_2Cl_2(OCO(CH_2)_2NH(FITC))_2]$
PTSM	Pyruvaldehyde-bis(N4-methylthiosemicarbazone)
pO_2	Partial pressure of oxygen

ppm	Parts per million
R	Gas constant
ROS	Reactive oxygen species
s	Singlet (NMR)
Salen	*bis*-(Schiff base) *bis*-(phenol)
SFU	Simon Fraser University
t	Triplet (NMR)
T	Temperature
THF	Tetrahydrofuran
TMEDA	Tetramethylethylenediamine
Trx	Thioredoxin
UV-Vis	Ultraviolet-Visible spectroscopy
V	Volts (Electrochemistry)
VEGF	Vascular endothelial growth factor
vs.	Versus
ΔE_p	Peak-to-peak difference
ε	Molar extinction coefficient (UV-Vis)
λ_{em}	Wavelength of maximum emission
λ_{ex}	Wavelength of excitation
μL	Microliters
σ	Hammett parameter (para substitution)

Chapter 1.

Introduction

1.1. Cancer Overview

Cancer is a heterogeneous disease in which cell growth is uncontrolled. Cancer leads either to a solid mass of cells known as a malignant tumor or to leukemia and lymphoma.[1] This disease involves dynamic changes in the genome, which can be caused by environmental factors (e.g., smoking, diet, and obesity) and/or genetic factors.[2,3] The process in which genetic alterations drive the progressive transformation of normal human cells into a tumor (benign or malignant) is known as tumorigenesis.[4] Cancer cells sustain proliferative signaling, evade growth suppressors, activate invasion and metastasis, enable replicative immortality, induce angiogenesis and resist programmed cell death (apoptosis).[5] Abnormal cells grow out of control, gather, and gradually disrupt the normal organized structure of a tissue by growing into a tumor.[4] Benign tumors may have similar abilities to avoid natural death, but they are non-cancerous, growing slowly at one place, and not spreading to other parts of the body. While malignant tumors, on the other hand, are cancerous, and always invade other tissue. In the absence of a blood supply, a tumor can grow into a mass of up to 10^6 cells, equivalent to a sphere of about 2 mm in diameter.[6,7] Vascular endothelial growth factor (VEGF) and other growth factors diffuse out to trigger angiogenesis (the formation of new blood vessels).[8] Cancer cells can move and penetrate blood and lymphatic vessels nearby and transit in blood (intravasation).[8] Motile cancer cells then attach to the vessel wall, and start proliferation within or outside vessels at adjacent or distant organs (metastasis).[9,10]

Cancer is a disease that affects people of all ages, but is most common in people over 50 years of age.[11-15] Cancers are among the leading causes of mortality and morbidity worldwide, accounting for 8.2 million deaths in 2012.[3] Cancer is also the number one

cause of death in Canada, with the overall incidence and mortality rates increasing mainly due to our growing and aging population.[11-15] In 2015, 196,900 Canadians will be diagnosed with cancer and 78,000 Canadians will die of cancer.[16]

Chemotherapy, surgery and radiation therapy are the main treatments for cancer.[3] Surgery and radiation therapy damage and/or kill cancer cells, but may not be able to treat metastasized or cancer cells that have spread a significant distance from the primary tumor. In certain cases, chemotherapy can target cancer cells specifically. For these reasons, chemotherapy is often used in combination with surgery and/or radiation therapy in the treatment for patients.[17] Although the various types of treatments for cancer, there is a need to develop more effective therapies for this disease.

1.2. Cancer Chemotherapy

Chemotherapy involves the use of chemical compounds to destroy cancer cells and/or limit their proliferation. Chemotherapy drugs can be classified into many different categories based on their chemical structure, their mechanism of action, or their relationship to other drugs. Owing to the limitless replicative potential of cancer cells, traditional anticancer drugs were developed to target important cellular processes, such as DNA synthesis, DNA function, and the synthesis or breakdown of mitotic spindles.[1] Thus, these drugs were designed to selectively inhibit faster cell growth in comparison to normal tissue.[18]

Listed below are four general categories of approved cancer therapeutics:

1. Compounds that damage DNA directly, inhibiting cancer cell growth and metastasis. Alkylating agents, such as Bendamustine (a type of nitrogen mustard) shown in **Figure 1.1**, are able to damage DNA by crosslinking guanine bases in DNA double strands, leading to cell death.[19] Another example is the Pt complex cisplatin **(Figure 1.1)**, which also binds to DNA. Following administration of cisplatin, one of the chloride ligands slowly exchanges with water. The water ligand in the resulting $[PtCl(H_2O)(NH_3)_2]^+$ is easily displaced, resulting in Pt binding to bases on one DNA strand, usually with guanine. Subsequent to formation of $[PtCl(guanine\text{-}DNA)(NH_3)_2]^+$, crosslinking can occur via

displacement of the other chloride ligand, typically by another guanine.[20] Cisplatin can lead to irreversible inter-strand and/or intra-strand crosslinks,[21] interfering with cell division, triggering apoptosis, and leading to cell death.[22]

2. Drugs termed antimetabolites are similar in chemical structure to specific metabolites, but have additional chemical features that allow them to interfere with normal metabolic processes. Examples of such compounds in chemotherapy include those that participate in the synthesis of DNA and RNA by substituting for normal nucleobases, resulting in DNA and RNA damage and eventually triggering apoptosis. Clinically used examples of these types of compounds include 5-fluorouracil (5-FU), and 6-mercaptopurine (6-MP) shown in **Figure 1.1**.

3. Cytotoxic antibiotics are a group of drugs that have a different mechanism of action, such as inhibiting the function of enzymes involved in DNA replication, intercalating DNA strands (e.g., daunorubicin shown **Figure 1.1**), preventing RNA synthesis.

4. Mitotic inhibitors are drugs that inhibit mitosis and cell division. They hinder the formation of microtubules, interfering with mitotic spindle assembly and/or disassembly in the cell mitosis process. For example, Paclitaxel (**Figure 1.1**) interferes with mitotic spindle assembly, chromosome segregation and cell division.[23]

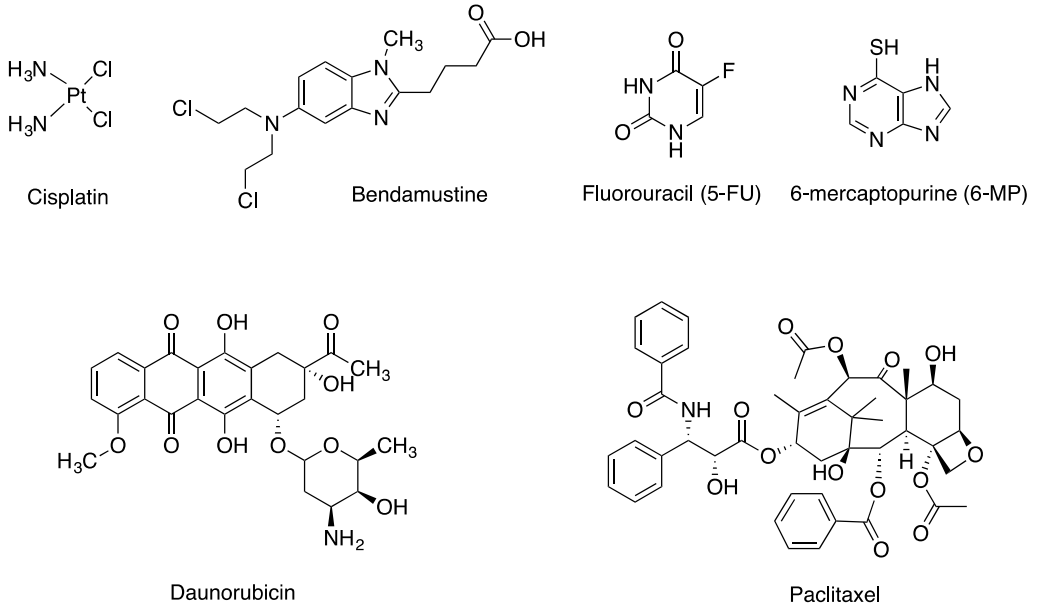

Figure 1.1 Chemical structures of some approved anticancer drugs.

However, all of the drugs detailed above also have drawbacks. They can target cellular processes non-specifically, leading to damage to both cancerous cells and healthy tissues. To overcome off-target toxicity, researchers have developed drugs that target differences between cancerous tissue and normal tissue to enhance selectivity. In comparison to normal tissue, cancerous tissue exhibits uncontrolled growth and thus exhibits an increased need for nutrients and has increased and/or altered receptor expression.[18,24-27] Examples include substances produced only in cancer cells that can be used as tumor markers, and tumor-specific enzymes that selectively activate pro-drugs in cancer cells.[28] In addition, certain tumors can exhibit a lower pH microenvironment in comparison to normal cells.[29] Tumor hypoxia (low oxygen concentration) is also a common feature found in most tumors and is further discussed in Section 1.3.

1.3. Tumor Hypoxia

O_2 concentration in tumor tissue is dependent on the oxygen supply, consumption rate, and the diffusion properties of the tissue. Hypoxia is a condition in which tissues in the body have an inadequate supply of oxygen, with tumor hypoxia being strongly related to tumor proliferation. As cancer cells grow into a tumor, blood vessels are located at the outer part of the tumor, which leads to the inadequate perfusion at longer distances (> 70 μm) from blood vessels.[30] Therefore, regions of low oxygen concentration develop in tumors as shown in **Figure 1.2**. Physiologists define hypoxia as a state of decreased O_2 availability or partial pressures (pO_2) below a critical threshold. Arterial blood oxygen levels in healthy individuals are considered to be 80-100 mmHg, and pO_2 in normal tissues are 24–66 mmHg. However, direct measurements of oxygen levels in human tumors display a drastically lower range of 10–30 mmHg, and even as low as 0.08 mmHg.[31]

Hypoxia can cause treatment resistance in various ways. In radiotherapy, radiation causes damage to DNA, and oxygen readily reacts with damaged ends of DNA, resulting in oxygenated species that are not as easily repaired by the cell. However, the lack of oxygen in tumor hypoxia protects DNA from further damage by oxygen, thus affecting cellular radiation sensitivity, leading to resistance to radiotherapy. The long distance from blood vessels also decreases the effect of intravenous (IV) therapy, leading to lower drug concentrations in the hypoxic cells (**Figure 1.3**). Hypoxia-inducible factors (HIFs) alter

transcriptional activity and cellular metabolism, which inactivate drug cytotoxicity and also enhance genetic instability of the cells, leading to more rapid development of drug resistant cancerous cells.[32]

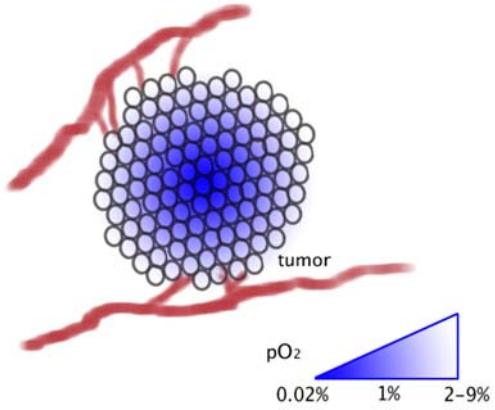

Figure 1.2 Examples of differential oxygen levels in a tumor.

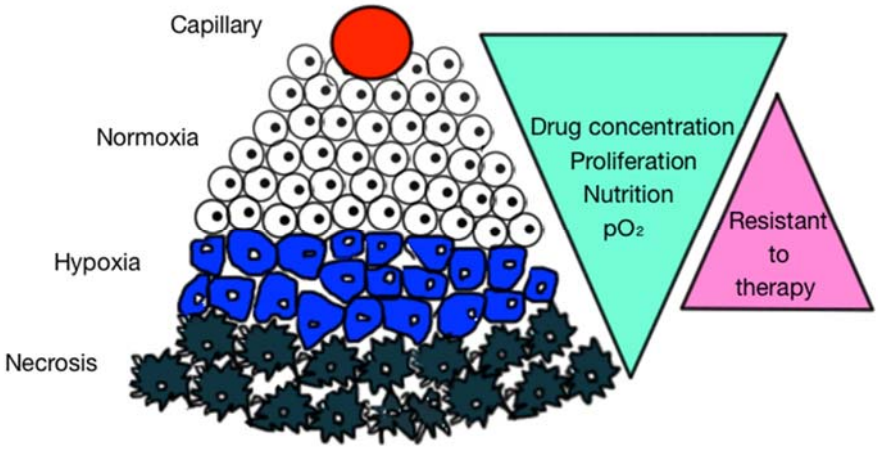

Figure 1.3 Hypoxia in solid tumors.
With increasing distance between cancer cells and blood vessels, drug concentration, cell proliferation, nutrition and oxygen concentration all decrease, while the resistance to chemotherapy and radiotherapy increases.[31]

Normal cells chiefly metabolize glucose to pyruvate for growth and survival, and O_2 is required as the final acceptor of electrons to fully oxidize pyruvate to CO_2 and generate 36 ATP per glucose.[33] As a consequence of tumor hypoxia (limiting oxygen), cancer cells switch their glucose metabolism pathway from tricarboxylic acid to glycolysis in order to accelerate cell proliferation at the expense of generating only two ATPs per

glucose.[33] The metabolism difference is shown in **Figure 1.4**.[34] In order to accelerate cell proliferation, cancer cells convert glucose to excess lactic acid, which is then transported out of cells. As a result, the pH of the intracellular fluid can be higher than 7.4,[35] and the extracellular environment lower than 6.0.[29]

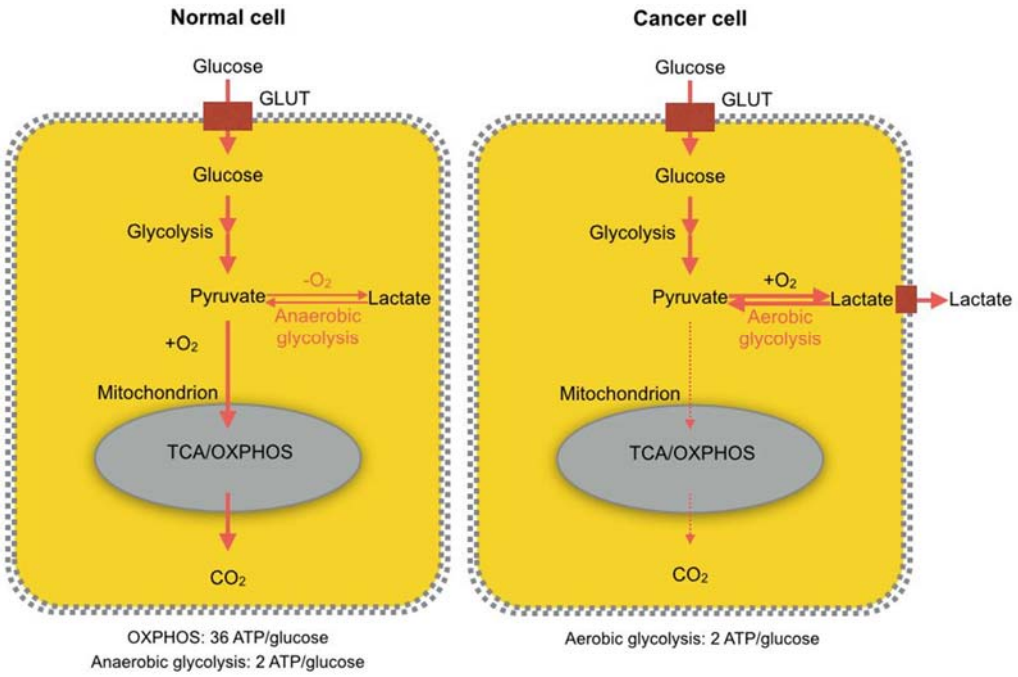

Figure 1.4 The metabolism difference between a normal cell and a cancer cell.

In eukaryotic cells, the redox level is highly controlled, compartmentalized, and crucial for physiological reactions and processes. The intracellular redox potential is regulated by a variety of reductants and oxidants, such as glutathione (GSH), thioredoxin (Trx), nicotinamide adenine dinucleotide (NADH), nicotinamide adenine dinucleotide phosphate (NADPH), and reactive oxygen species (ROS).[36] Traditionally, the intracellular redox potential is calculated by quantifying the oxidized and reduced forms of glutathione. However, this requires cell fractionation and it cannot take into account differences among organisms.[37] Small molecule redox probes have been developed for specific oxidants or reductants, but these probes have limitations with regards to calibration, selectivity, and sensitivity.[38] Fluorescent proteins (such as green fluorescent protein, GFP) based redox sensors (termed roGFP) have been a big success for monitoring redox homeostasis noninvasively. The oxidized and reduced states have different excitation wavelengths,[39] but their use is limited due to the narrow potential window and slow reaction kinetics.

Methods to measure redox potential in cells are progressively improving so that the redox potential in different cellular compartments in living cells or organisms are gradually being reported with increased accuracy.[40-45] Mitochondria are the most reducing compartment in eukaryotic cells, and are very sensitive to oxidation.[36,46] Nuclei also exhibit a reducing environment, but are resistant to oxidation due to two major antioxidant systems dependent on GSH and Trx1.[47] The cytoplasm contains few endogenous oxidants and is less reducing in comparison to the nucleus.[36] Extracellular fluids are maintained at stable potentials.[36] Peroxisomes, the endoplasmic reticulum, and lysosomes exhibit reduction potentials dominated by their own redox system.[36] Thus, each compartment of cells can exhibit a different reduction potential, which leads to an approximate cell potential window: -420mV to -150mV versus the normal hydrogen electrode (NHE).[46] Because of the more negative tumor microenvironment (a result of hypoxia), the reduction potential of a tumor is usually at the lower end of this range.[48] Since hypoxia is a key environmental feature that exists within all solid tumors, but not normal tissues, it has been extensively studied and developed as a selective cancer therapeutic targeting strategy.

1.4. Metal-Based Anticancer Agents

Transition metals, such as iron, copper, zinc, manganese, and cobalt are essential to the human body, due to the fact that they are an integral part of many metalloproteins involved in important biological processes. They can also function as components of cofactors, which are non-protein molecules that are essential for enzyme activity. Advantages of using transition metal complexes as anticancer agents include the ability to vary coordination number, geometry, and redox states. There is considerable design flexibility possible for such complexes in terms of overall charge, geometry, and reactivity in the body. Metals can also change the pharmacological properties of organic-based drugs by forming coordination complexes with them in different three-dimensional configurations.[49] Some metal complexes coordinate to biomolecules by ligand exchange without a change in oxidation state, such as cisplatin. Of central importance of this work, the metal centers in these types of compounds can often exist in different oxidation states under physiological conditions, and this feature allows for ligand exchange and structural rearrangement upon oxidation or reduction of the metal center. Additionally, metal cations

(or positively charged complexes) can bind negatively charged biological molecules, such as DNA, RNA, and proteins.[50,51]

The discovery of the anticancer activity of cisplatin (**Figure 1.1**) in the 1960s steered research in the direction of developing metal-based anticancer drugs. Cisplatin has been widely approved to treat ovarian, head, neck, non-small-cell lung (NSCLC), and cervical cancers. Nevertheless, its clinical application is restricted because of severe side effects and acquired resistance.[52] Due to these limitations, the 2nd generation platinum drug carboplatin and and the 3rd generation oxaliplatin were designed and approved for use (shown in **Figure 1.5**).[53] Other metal-containing anticancer drugs have been developed, with the most promising complexes including copper,[54] iron,[55] ruthenium,[56] gold,[57] and gallium.[58]

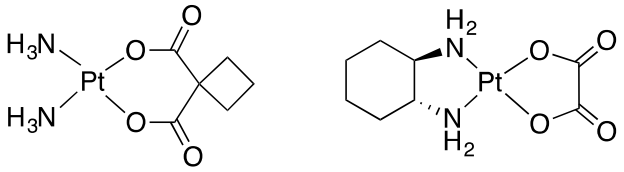

Carboplatin Oxaliplatin

Figure 1.5 Chemical structure of carboplatin and oxaliplatin.

Ruthenium-containing anticancer drugs, such as NAMI-A[59] and KP1019[60] (**Figure 1.6**), are the most well-studied non-Pt metal complexes. Ru(III) complexes generally exhibit fewer side effects in comparison to platinum-containing medicines and show good stability.[61] NAMI-A has low activity in primary tumors but exhibits high efficacy against metastases.[62] KP1019 shows activity against colon cancer, and improved stability and uptake by cells in comparison to NAMI-A.[60] Although NAMI-A and KP1019 can both form DNA adducts, and KP1019 also binds to transferrin, their mechanism of action is still unclear.[63]

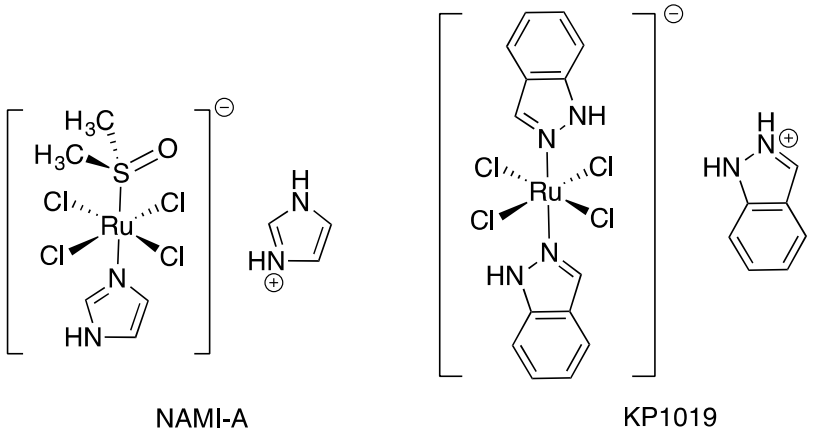

Figure 1.6 Chemical structures of NAMI-A and KP1019.

1.5. Hypoxia-activated Metal-containing Anticancer Agents

The reducing tumor microenvironment provides an opportunity for selective activation so that inert oxidized metal pro-drugs can be delivered and reduced to their activated form.[64] One example of this is copper-62-ATSM, which was designed as a hypoxia-imaging agent with high membrane permeability and a low reduction potential **Figure 1.7**.[54] Cu(II)-ATSM can easily pass through the cell membrane, however under normal cell conditions it has a short cellular retention time. Interestingly, in a reducing environment, Cu(II) can be reduced to Cu(I), and the charged complex can remain trapped in the cell.[65] In addition, using an appropriate Cu radioisotope allows for hypoxia imaging. Other Cu-ATSM analogues were developed with different numbers of methyl groups in the backbone (**Figure 1.7**), which increased reduction potentials.[65]

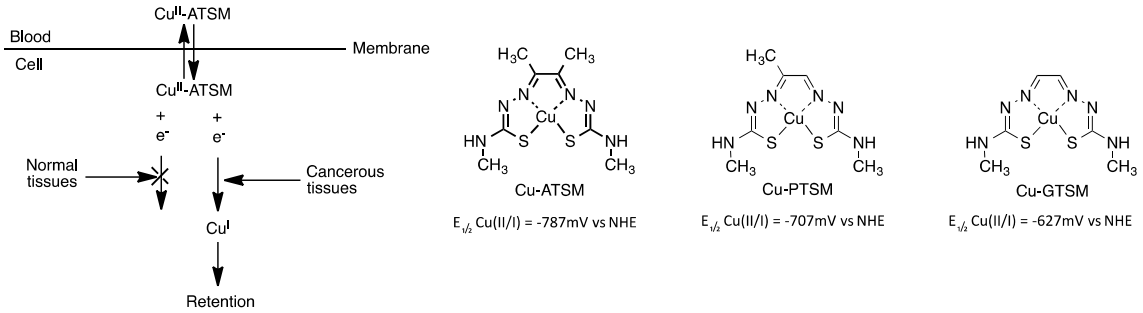

Figure 1.7 Copper(II) bis(thiosemicarbazone) complexes and their reduction potentials.

Another example of hypoxia-activated pro-drugs are Co(III) nitrogen mustard conjugates, which were designed to release cytotoxic nitrogen mustard agents upon reduction under hypoxic conditions.[66,67] Coordination of the mustard agent nitrogen lone pair to Co(III) suppresses its toxicity (**Figure 1.8**). Nitrogen mustards are known to form DNA cross-links, which leads to cell death.[54]

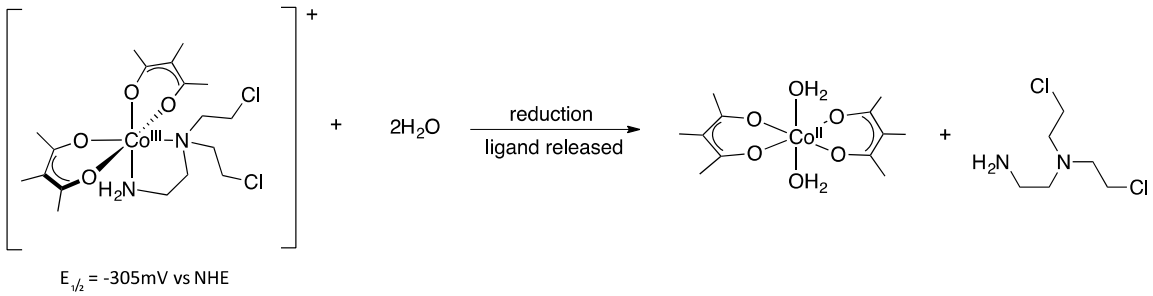

Figure 1.8 Example of a Co(III) nitrogen mustard complex.
One-electron reduction of the inert Co(III) complex results in a labile Co(II) species, leading to facile ligand substitution by water, releasing the cytotoxic nitrogen mustard.[66]

1.6. Cobalt and Vitamin B_{12}

This thesis details the design of Co-containing anti-cancer agents. This section introduces the biological uses and speciation of this metal. Cobalt is an essential element in humans for formation of vitamin B_{12} (cobalamin), shown in **Figure 1.9**. Vitamin B_{12} is the only vitamin found to contain a metal and the only known cobalt-containing compound in the human body.[68] Only about 1 μg of Co daily is essential in human nutrition. Cobalamin and related enzymes catalyze important reactions in body, such as the synthesis of methionine, the metabolism of purines and folates, and the formation of methylmalonic acid, which is important to the tricarboxylic acid cycle.[68,69] Vitamin B_{12} strongly affects DNA synthesis and regulation, fatty acid metabolism, and amino acid metabolism.[69]

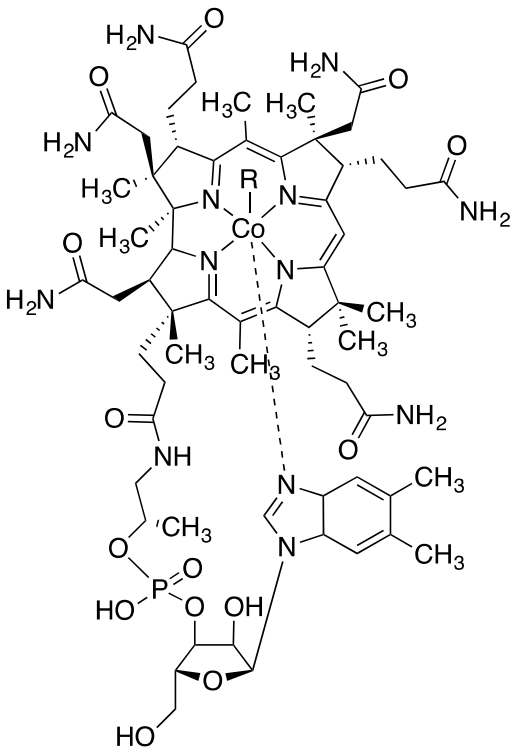

Figure 1.9 The chemical structure of Vitamin B_{12}.

The highest concentration of cobalt in normal subjects is in the liver (median 30 μg Co/kg, with range 6-151 μg Co/kg), followed by the kidney.[70] There is no accumulation of cobalt in the body with age.[71] Most of the absorbed dose of cobalt (80-90%) has a biological half-life of several days, and is eliminated rapidly, appearing in the urine.[69]

Cobalt has two common oxidation states under biological conditions, Co(III) and Co(II). Co(III) complexes are defined as kinetically inert due to the high ligand field stabilization energy of the low spin d^6 electronic configuration, which results in very slow ligand exchange processes. Compared to Co(III) complexes, octahedral d^7 Co(II) complexes are much more labile, and readily undergo ligand exchange reactions. As an example, at 25 °C, the exchange rate constant for water molecules ligated to Co(III) is slow ($< 10^{-6}$ s^{-1}), while for Co(II) the water exchange rate is much faster (3×10^6 s^{-1}).[72] Many bioactive Co complexes have been designed to take advantage of the difference in ligand lability between the Co(III) and Co(II) oxidation states. Reduction of stable d^6 Co(III) complexes to more labile d^7 Co(II) complexes can lead to structure rearrangement and/or

ligand release, providing a means to change the biological activity of the complex. This property is especially useful in the case of hypoxia, in which selective drug activation can occur in the hypoxic (reducing) tumor environment.

1.7. Thesis Outline

The reducing environment in a tumor due to hypoxia is a common characteristic and can be used as a unique feature for drug targeting. This research aims to take advantage of the reducing environment by designing Co(III) complexes with fluorescent ligands that are quenched by the cobalt center, and can be selectively reduced under the reducing conditions. Reduction of stable d^6 Co(III) complexes to more labile d^7 Co(II) complexes lead to structure rearrangement and ligand release. Thus, ligand release leads to increased fluorescence as a proof-of-principle for the attachment of cytotoxic compounds to the Co(III) center. **Scheme 1.1**

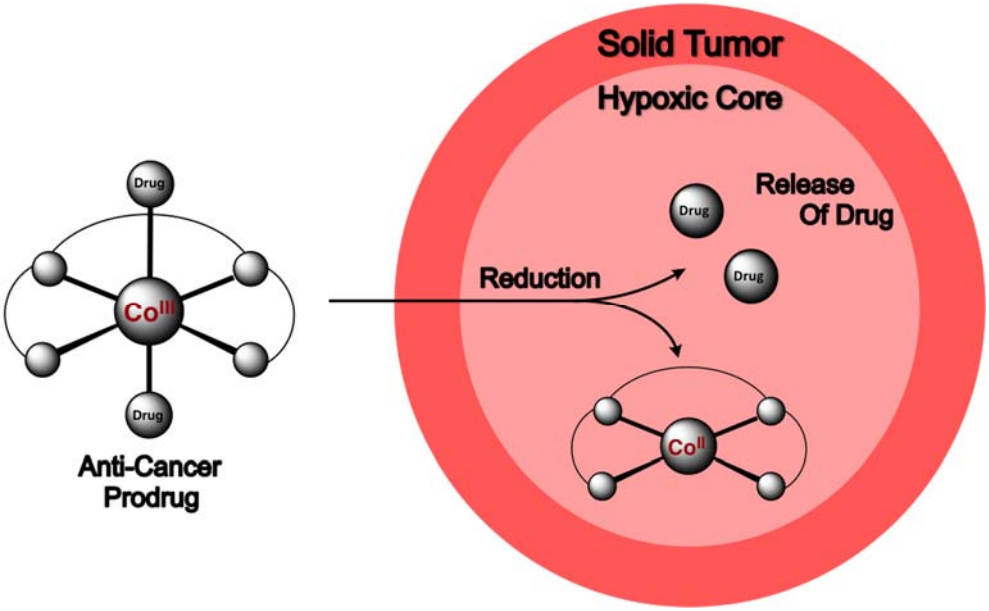

Scheme 1.1 Activation mechanism of Co^{III} pro-drugs.

The design, synthesis, characterization, and electrochemical properties of tetradentate Co(II) salen complexes, as well as the model compounds $[Co^{III}(salen^{R})(1\text{-MeIm})_2]ClO_4$ (**Figure 1.10**) will be illustrated in **Chapter 2**. The binding of fluorescent molecules (e.g., coumarin) to the cobalt ion is used as a proof-of-principle for axial ligand release upon reduction. The synthetic routes, characterization, and electrochemical

properties of $[Co^{III}(salen^{R})(coumarin)_2]Cl$ complexes (**Figure 1.10**) will be discussed in detail in **Chapter 3**. Fluorescence intensity of $[Co^{III}(salen^{R})(coumarin)_2]Cl$ complexes in the presence of a reducing agent and in the presence of a competing ligand will be discussed in **Chapter 4**. Finally, ongoing and future work will be discussed in **Chapter 5.**

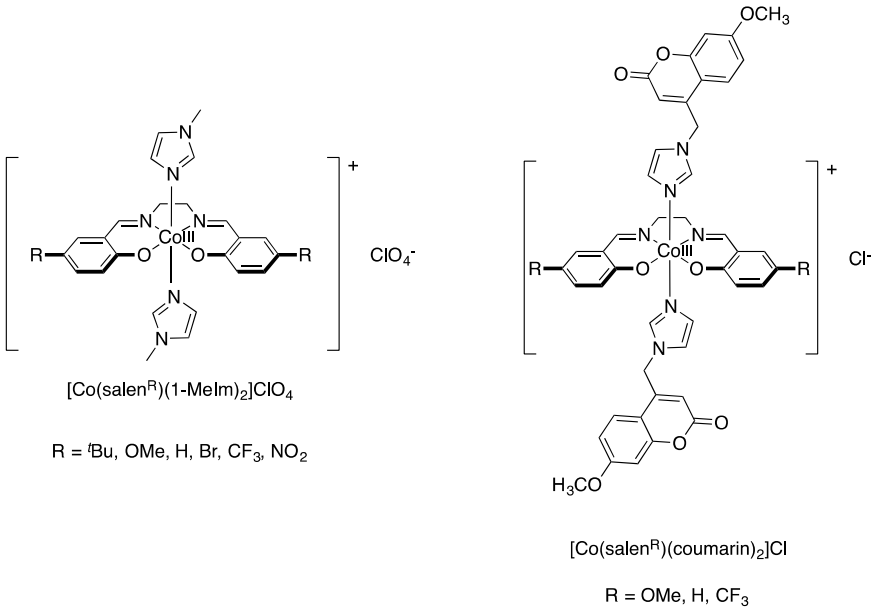

Figure 1.10 Chemical structures of $[Co^{III}(salen^{R})(1\text{-MeIm})_2]ClO_4$ and $[Co^{III}(salen^{R})(coumarin)_2]Cl$.

Chapter 2.

Synthesis and Characterization of Cobalt(III) Salen Imidazole Complexes

John Thompson and Ryan Clarke collected X-ray data and solved the crystal structures in this chapter.

2.1. Introduction

Salen ligands (a common abbreviation for N_2O_2 bis-Schiff-base bis-phenolates) and their complexes are of interest for a wide range of applications in the chemical sciences,[73] and have found application in catalysis and materials chemistry.[11] In addition, certain metal salens have shown antibacterial,[74] antiviral,[75] and anticancer activity.[76]

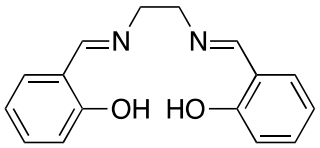

Figure 2.1 An example of salen ligands.

Salen ligands are widely used due to their modular synthesis, the possibility to vary both steric and electronic properties at the metal center *via* substituents on the phenolate, and the ability to form stable complexes with many different metals and oxidation states.[77-85] Salen complexes are often referred to as "privileged chiral catalysts", and examples include Mn salen catalysts developed by Jacobsen and co-workers for epoxidation of unfunctionalized olefins (**Scheme 2.1**).[78-80] In addition, salen complexes have been reported as catalysts for myriad asymmetric transformations, such as aziridinations,[81] epoxide ring opening,[82-84] and the hydrolytic kinetic resolution of epoxides.[85] The ligand radical chemistry of metal salen complexes has also been investigated. Storr and co-workers, as well as other groups, have shown that varying the electron donating ability of phenolate substituents influences the redox potentials of the metal complexes and/or ligand radical localization.[12,86-88]

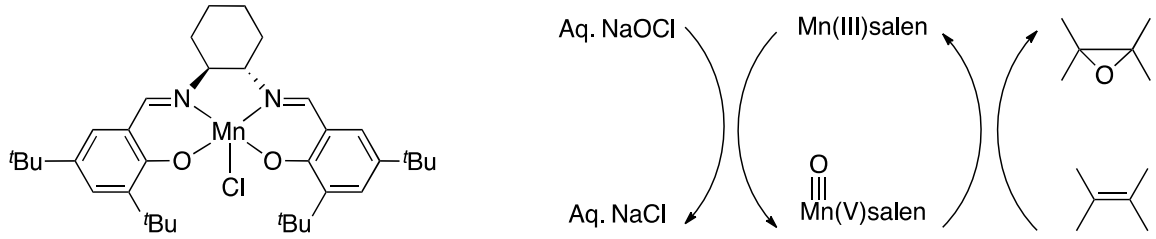

Scheme 2.1 Scheme for the epoxidation of olefins by Jacobsen's Mn^{III}-salen catalyst.

In this chapter, a series of Co(II) salen complexes were synthesized and reacted with 1-methylimidazole under aerobic conditions to form octahedral Co(III) complexes (**Figure 2.2).**

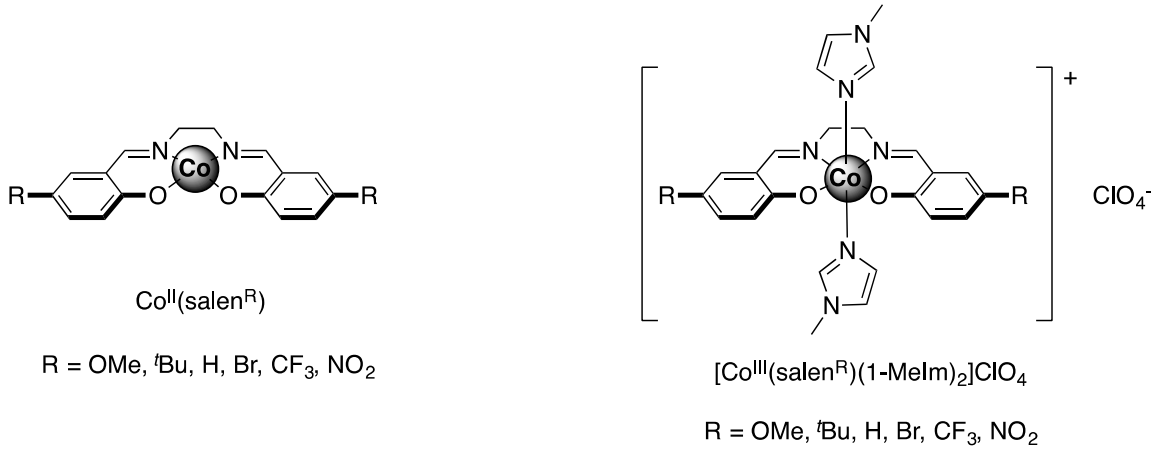

Figure 2.2 Chemical structure of the complexes studied.

Co(III) d^6 low spin octahedral complexes are kinetically inert, due to the strong ligand field stabilizing energy (LFSE). The activation energy required for substitution reactions is relatively high.[89] Upon reduction to a Co(II) d^7 low spin complex (**Figure 2.3**), a degenerate electronic state is formed and a geometrical distortion (Jahn-Teller distortion)[90] may occur depending on the geometry to lower the energy of the species. In the case of the Co(II) salen complexes shown in **Figure 2.2**, elongation of the Co-imidazole bonds is the most likely geometrical distortion. A change from low spin to high spin Co(II) d^7 is also possible (**Figure 2.3**) depending on the coordinating ligands. Both low spin and high spin octahedral Co(II) complexes are kinetically labile, and in the case

of the octahedral Co(II) salen complexes shown in **Figure 2.2**, axial ligands can be released to give a low spin Co(II) d^7 square planar complex.

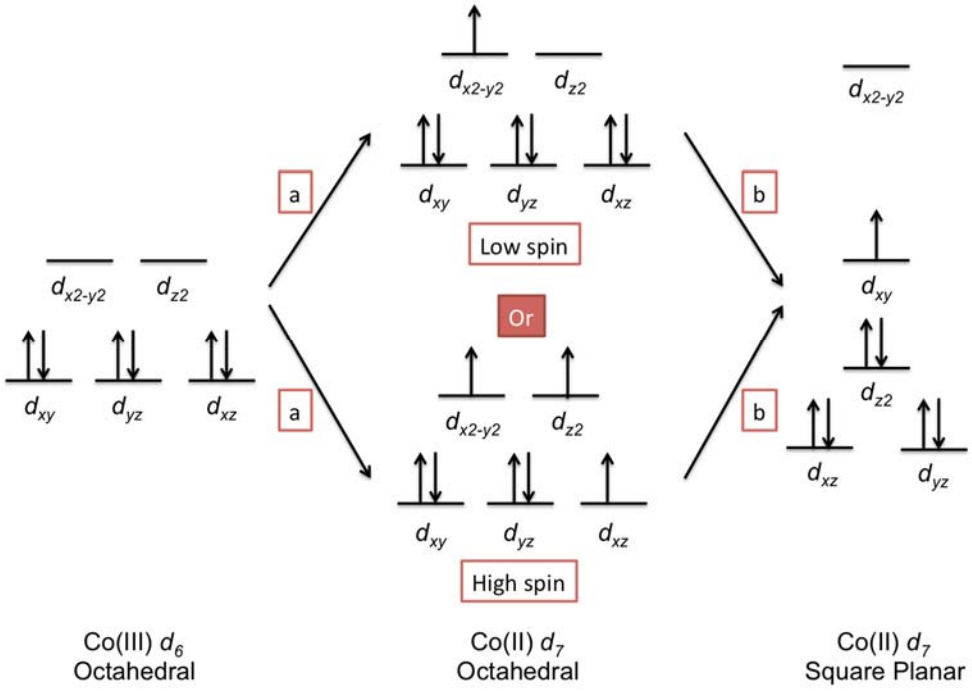

Figure 2.3 d-orbital splitting diagram of Co(III) and Co(II) salen complexes (a: reduction; b: rearrangement).

The structural change upon reduction detailed above provides a means to control ligand release from a complex and facilitate selective drug activation.[64] Indeed, this mechanism of selective drug activation has been investigated for Pt(IV),[91] Fe(III),[92] and Co(III) complexes.[28,93-95] In the work described in this chapter, a series of octahedral Co(III) salen complexes have been synthesized, employing 1-methylimidazole in the axial positions (**Figure 2.2**). The planar tetradentate salen ligand provides the opportunity to bind mono-dentate ligands axially in an octahedral Co(III) complex, that could subsequently be released upon reduction to Co(II). In addition, *para*-phenolate substituents with different electron-donating abilities (*i.e.,* OMe, ^{t}Bu, H, Br, CF_3, NO_2) were used in this work to study the effect of salen ligand electronics on the Co(III) / Co(II) reduction potential.

2.2. Experimental

2.2.1. Materials

All reagents and solvents used for synthesis were from commercial sources and used as received. Literature methods were used or adapted to prepare the salen ligands (R= OMe, ^{t}Bu, H, Br, CF_3, NO_2),[96] $Co^{II}(salen^R)$ complexes (R= OMe, ^{t}Bu, H, Br, CF_3, NO_2),[97] and $[Co^{III}(salen^R)(1\text{-MeIm})_2]ClO_4$ complexes (R= OMe, ^{t}Bu, H, Br, CF_3, NO_2).[98]

2.2.2. Instrumentation

^{1}H NMR spectra were recorded on Bruker AV-400 or AV-500 instruments. Mass spectra (positive ion) were obtained on an Agilent 6210 TOF ESI-MS instrument. Elemental analyses (C, H, N) were performed by Mr. Paul Mulyk at Simon Fraser University on a Carlo Erba EA1110 CHN elemental analyzer. Cyclic voltammetry (CV) was performed on a PAR-263A potentiometer, equipped with a glassy carbon working electrode and a platinum counter electrode, and a BASi MF-2062 non-aqueous electrode kit was used to make a silver/silver nitrate reference electrode with $^n Bu_4NClO_4$ (0.1 M) solutions in DMF. Ferrocene was used as an internal standard.

2.2.2.1 X-ray Structure Determination

Single crystal X-ray crystallographic analyses of selected $[Co^{III}(salen^R)(1\text{-MeIm})_2]ClO_4$ complexes were performed on a Bruker X8 APEX II diffractometer and each crystal was mounted on a glass fiber. For $[Co^{III}(salen^{OMe})(1\text{-MeIm})_2]ClO_4$, data collection was completed with graphite monochromated Mo Kα radiation. Data were collected at 296 ± 2 K to a maximum 2θ value of 61.0°, in a series of φ and ω in 0.50° widths with 30.0 s exposures. The crystal-to-detector distance was 50 mm. For $[Co^{III}(salen^H)(1\text{-MeIm})_2]ClO_4$, data were collected at 296 ± 2 K to a maximum 2θ value of 57.2°, in a series of φ and ω in 0.50° widths with 10.0 s exposures. The crystal-to-detector distance was 50 mm. For $[Co^{III}(salen^{CF3})(1\text{-MeIm})_2]ClO_4$, data collection was performed with graphite monochromated Cu Kα radiation. Data were collected at 149 ± 2 K to a maximum 2θ value of 133.3°, in a series of φ and ω in 0.80° widths with 10.0 s exposures. The crystal-to-detector distance was 40 mm.

The structures were solved by direct methods (SIR92)26[99] and refined by least-

squares procedures using SHELXL-2013.[100] All non-hydrogen atoms were refined anisotropically. All C−H hydrogen atoms were placed in calculated positions, but were not refined. All crystal structure plots were produced using ORTEP-3 and rendered with POV-Ray (v.3.6.2). A summary of the crystal data and experimental parameters for structure determinations are shown in **Table 2.1**.

Table 2.1 Selected crystallographic data for $[Co^{III}(salen^{R})(1\text{-MeIm})_2]ClO_4$

$[Co^{III}(salen^{R})(1\text{-MeIm})_2]ClO_4$	R = OMe	R = H	R = CF_3
Formula	$C_{26}H_{30}ClN_6O_8Co$	$C_{24}H_{26}ClN_6O_6Co$	$C_{26}H_{24}ClN_6O_6F_6Co$
Formula weight	648.94	588.89	724.89
space group	P-1	P 21 21 21	P-1
a (Å)	8.4249(4)	12.4129(7)	10.9036(5)
b (Å)	11.8610(6)	13.1381(8)	11.0510(5)
c (Å)	15.0154(8)	15.6039(9)	14.3468(7)
α (°)	74.3740(10)	90	106.780(4)
β (°)	81.6870(10)	90	96.598(3)
γ (°)	76.8910(10)	90	105.318(3)
V [$Å^3$]	1401.76(12)	2544.7(3)	1561.74
Z, D_{calc} [g/cm^3]	2	4	2
T (K)	150(2)	296(2)	149(2)
ρ_{calcd} ($g\ cm^{-3}$)	1.537	1.537	1.542
λ (Å)	0.71073	0.71073	1.54178
μ (cm^{-1})	0.768	0.832	5.871
R indices[a] with I>2σ(I) (data)	0.0285	0.0512	0.0746
wR_2	0.0731	0.1413	0.2032
R_1	0.0373	0.0623	0.0893
Goodness-of-fits on F^2	1.029	0.903	1.438

2.2.2.2 Stability studies (NMR) of $[Co^{III}(salen^{R})(1\text{-MeIm})_2]ClO_4$

Phosphate buffered saline (PBS) (1 mL, 0.01 M, pH 7.4) was dried *in vacuo* and redissolved in the same amount of D_2O to obtain a deuterated PBS solution. The complexes were first solubilized in DMSO-d_6 and then diluted in deuterated PBS solution. Hence, 2% DMSO-d_6 in deuterated PBS solution was used as the NMR solvent for stability tests.

2.2.3. Synthesis

2,2'-((1*E*,1'*E*)-(ethane-1,2-diylbis(azanylylidene))bis(methanylyl-idene))diphenol (**Salen^{H}**) (**1**).

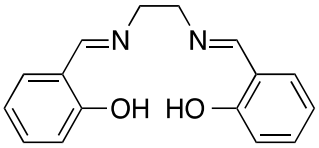

This compound was synthesized following a literature procedure.[97] 2-hydroxybenzaldehyde (0.90 g, 7.38 mmol) and ethane-1,2-diamine (0.22 g, 3.67 mmol) were dissolved in EtOH (15 mL) at 298 K. After the mixture was stirred for 15 min at room temperature a yellow precipitate was formed. The solid was collected by vacuum filtration and washed with EtOH, then dried *in vacuo* overnight. Yield: 0.83 g, 83%. ^{1}H NMR (400 MHz, $CDCl_3$) δ 8.36 (s, 2H), 7.29 (ddd, *J* = 8.3, 7.3, 1.7 Hz, 2H), 7.23 (dd, *J* = 7.6, 1.7 Hz, 2H), 6.97-6.91 (m, 2H), 6.86 (td, *J* = 7.5, 1.1 Hz, 2H), 3.95 (s, *J* = 0.6 Hz, 4H). ESI(+)-MS m/z (relative intensity) = 269.1283 ([**1**+H]$^{+}$). The synthetic procedure for this compound has been reported and characterization matches literature data.[101]

2,2'-((1*E*,1'*E*)-(ethane-1,2-diylbis(azanylylidene))bis(methanyl-ylidene))bis(4-nitrophenol) (**Salen^{NO2}**)(**2**).

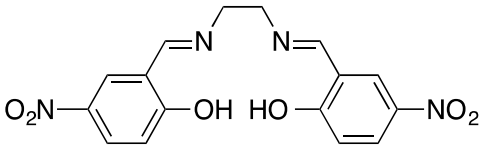

This compound was synthesized following a literature procedure.[97] 5-nitrosalicylaldehyde (0.99 g, 2.78 mmol) and ethane-1,2-diamine (0.083 g, 1.39 mmol) were used. Yield: 0.33 g, 66%. ^{1}H NMR (400 MHz, DMSO-d_6) δ 8.78 (s, 2H), 8.44 (d, *J* = 3.0 Hz, 2H), 8.09 (dd, *J* = 9.6, 3.0 Hz, 2H), 6.77 (d, *J* = 9.5 Hz, 2H), 4.02 (s, 4H). ESI(+)-MS m/z (relative intensity) = 359.0987 ([**2**+H]$^{+}$). The Synthetic procedure for this compound has been reported and characterization matches literature data.[102]

2,2'-((1*E*,1'*E*)-(ethane-1,2-diylbis(azanylylidene))bis(methanyl-ylidene))bis(4-bromophenol) (**Salen^{Br}**) (**3**).

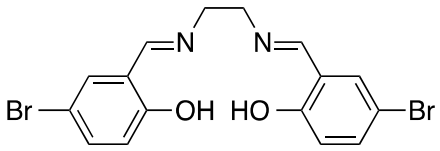

This compound was synthesized following a literature procedure.[97] 5-bromosalicylaldehyde (1.98 g, 4.68 mmol) and ethane-1,2-diamine (0.14 g, 2.34 mmol) were used. Yield: 0.74 g, 73%. ^{1}H NMR (400 MHz, $CDCl_3$) δ 8.29 (s, 2H), 7.38 (dd, *J* = 8.7, 2.5 Hz, 2H), 7.34 (d, *J* = 2.4 Hz, 2H), 6.85 (d, *J* = 8.7 Hz, 2H), 3.96 (s, 4H). ESI(+)-MS m/z (relative intensity) = 424.9487 ([**3**+H]$^+$). The synthetic procedure for this compound has been reported and characterization matches literature data.[102]

2,2'-((1*E*,1'*E*)-(ethane-1,2-diylbis(azanylylidene))bis(methanyl-ylidene))bis(4-(*tert*-butyl)phenol) (**Salen$^{t\mathrm{Bu}}$**) (**4**).

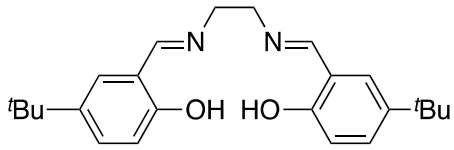

This compound was synthesized following a literature procedure.[97] 5-*tert*-butyl-2-hydroxybenzaldehyde (1.98 g, 5.22 mmol) and ethane-1,2-diamine (0.16 g, 2.61 mmol) were used. Yield: 0.28 g, 87%. ^{1}H NMR (400 MHz, CD_3CN) δ 8.44 (s, 2H), 7.37 (dd, *J* = 8.6, 2.5 Hz, 2H), 7.34 (d, *J* = 2.5 Hz, 2H), 6.80 (d, *J* = 8.6 Hz, 2H), 3.92 (s, 4H), 1.27 (s, 18H). ESI(+)-MS m/z (relative intensity) = 381.2539 ([**4**+H]$^+$). The synthetic procedure for this compound has been reported and characterization matches literature data.[101]

2,2'-((1*E*,1'*E*)-(ethane-1,2-diylbis(azanylylidene))bis(methanyl-ylidene))bis(4-methoxyphenol) (**Salen$^{\mathrm{OMe}}$**) (**5**).

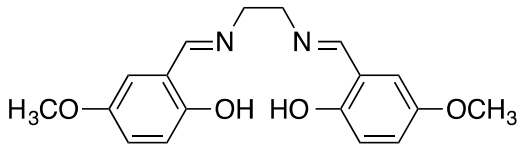

This compound was synthesized following a literature procedure.[97] 2-hydroxy-5-methoxybenzaldehyde (1.08 g, 3.29 mmol) and ethane-1,2-diamine (0.1 g, 1.65 mmol)

were used. Yield: 0.40 g, 72%. ^{1}H NMR (400 MHz, $CDCl_3$) δ 8.31 (s, 2H), 6.93-6.86 (m, 4H), 6.73 (dd, *J* = 2.8, 0.7 Hz, 2H), 3.94 (s, 4H), 3.75 (s, 6H). ESI(+)-MS m/z (relative intensity) = 329.1493 ([**5**+H]$^+$). The synthetic procedure for this compound has been reported and characterization matches literature data.[101,102]

2-(4-(Trifluoromethyl)phenoxy)tetrahydro-2*H*-pyran (**6**).[103]

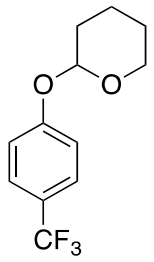

This compound was synthesized using a modified literature procedure.[103] One drop of concentrated HCl (38% in H_2O) was diluted in dioxane (2 mL) and then added into a solution of 3,4-dihydro-2H-pyran (0.72 mL, 7.93 mmol) in CH_2Cl_2. 4-(trifluoromethyl)phenol (0.429 g, 2.64 mmol) was then added dropwise at 298 K. After stirring overnight, the residue was purified by column chromatography (silica gel, eluent = hexanes), and dried *in vacuo* to afford a white solid. Yield: 0.18 g, 28%. ^{1}H NMR (400 MHz, $CDCl_3$) δ 7.58-7.49 (m, 2H), 7.15-7.07 (m, 2H), 5.48 (t, *J* = 3.2 Hz, 1H), 3.89-3.81 (m, 1H), 3.62 (dtd, *J* = 11.4, 4.1, 1.5 Hz, 1H), 2.08-1.95 (m, 1H), 1.91-1.84 (m, 2H), 1.78-1.57 (m, 3H).

2-Hydroxy-5-(trifluoromethyl)benzaldehyde (**7**).[104]

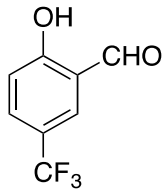

This compound was synthesized with minor changes to a literature procedure.[104] A 5 mL round-bottomed flask was cooled and then charged with TMEDA (0.88 g, 1.13 mmol). N-Butyllithium in hexane (2.88 mL, 1.6 M, 1.15 mmol) was added to the stirred TMEDA over a period of 30 min at 263 K. After a further 45 min compound **6** (0.80 g, 0.812 mmol) was added into the reaction, and precipitation of a white solid was observed. After 2 h, DMF (0.37 g, 1.13 mmol) was added to give a cloudy solution. After a further 15 min, this solution was added dropwise to a solution of HCl (38%, 1.6 mL) diluted in H_2O (1.00 mL). The reaction temperature was maintained below 45 °C. The reaction mixture was then extracted with DCM (3 × 2 mL). The combined organic fractions were dried with anhydrous Na_2SO_4 and evaporated *in vacuo* to afford a yellow oil which was purified by column chromatography (silica gel, eluent = DCM : Hexane (1:6)), to afford the title product as a white crystalline solid. Yield: 0.30 g, 48%. ^{1}H NMR (500 MHz, $CDCl_3$) δ 9.95 (s, 1H), 7.89-7.84 (m, 1H), 7.76 (dd, *J* = 8.8, 2.3 Hz, 1H), 7.11 (d, *J* = 8.8 Hz, 1H).

2,2'-((1*E*,1'*E*)-(ethane-1,2-diylbis(azanylylidene))bis(methanylylidene))bis(4-(trifluoromethyl)phenol) (**Salen^{CF3}**) (**8**)

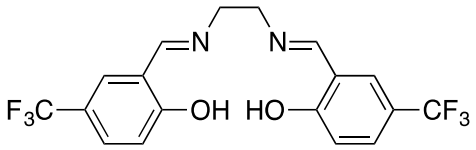

This compound was synthesized following a literature procedure.[97] 2-hydroxy-5-(trifluoromethyl)benzaldehyde (**7)** (0.59 g, 1.47 mmol) and ethane-1,2-diamine (0.049 g, 0.810 mmol) were used. Yield: 0.206 g, 69%. ^{1}H NMR (500 MHz, $CDCl_3$) δ 8.41 (s, 2H), 7.56 – 7.50 (m, 4H), 7.03 (d, *J* = 8.6 Hz, 2H), 4.00 (s, 4H). ^{19}F NMR (500 MHz, $CDCl_3$) δ -61.63 (s). ESI(+)-MS m/z (relative intensity) = 405.1025 ([**8**+H]$^+$).

$Co^{II}(salen^{H})$ (**9**)[97]

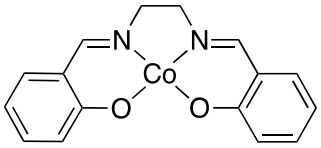

To a solution of **Salen^{H}** (0.20 g, 0.75 mmol) in degassed Et_2O (5 mL) was added a solution of $Co(OAc)_2 \bullet 4H_2O$ (0.186 g, 0.75 mmol) in degassed MeOH (5 mL) at 298 K. After stirring the mixture under N_2 for 15 min, a dark red precipitate formed. The solid was collected by vacuum filtration, washed with MeOH, and then dried *in vacuo* overnight. Yield: 0.15 g, 62%. ESI(+)-MS m/z (relative intensity) = 325.0396 ([**9**]$^+$). Elemental analysis calculated for $Co^{II}(salen^{H}) \bullet 0.5H_2O$ ($C_{16}H_{15}N_2O_{2.5}Co$) C: 57.50%, H: 4.59%, N: 8.38%, Found C: 57.17%, H: 5.09%, N: 8.63%.

$Co^{II}(salen^{NO2})$ (**10**)

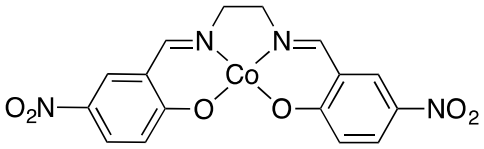

This complex was synthesized following the same procedure as for compound **9**, combining **Salen^{NO2}** (0.15 g, 0.419 mmol) and $Co(OAc)_2 \bullet 4H_2O$ (0.10 g, 0.419 mmol). Yield: 0.16 g, 92%. ESI(+)-MS m/z (relative intensity) = 415.0091 ([**10**]$^+$). Elemental analysis calculated for $Co^{II}(salen^{NO2}) \bullet CH_3OH$ ($C_{17}H_{16}N_4O_7Co$) C: 45.65%, H: 3.61%, N: 12.53%, Found C: 45.58%, H: 4.12%, N: 13.05%.

$Co^{II}(salen^{Br})$ (**11**)

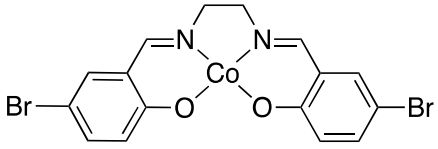

This complex was synthesized following the same procedure as for compound **9**, combining **Salen^{Br}** (0.22 g, 0.516 mmol) and $Co(OAc)_2 \bullet 4H_2O$ (0.129 g, 0.516 mmol). Yield: 0.23 g, 92%. ESI(+)-MS m/z (relative intensity) = 482.8595 ([**11**]$^+$). Elemental analysis calculated for $Co^{II}(salen^{Br}) \bullet H_2O$ ($C_{16}H_{14}N_2O_3Co$) C: 38.36%, H: 2.82%, N: 5.59%, Found C: 38.00%, H: 3.03%, N: 5.38%.

$Co^{II}(salen^{tBu})$ (**12**)

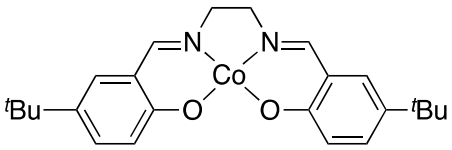

This complex was synthesized following the same procedure as for compound **9**, combining **Salen^{tBu}** (0.20 g, 0.526 mmol) and $Co(OAc)_2 \bullet 4H_2O$ (0.13 g, 0.526 mmol). Yield: 0.20 g, 88%. ESI(+)-MS m/z (relative intensity) = 437.1647 ([**12**]$^+$). Elemental analysis calculated for $Co^{II}(salen^{tBu})$ ($C_{24}H_{30}N_2O_2Co$) C: 65.90%, H: 6.91%, N: 6.40%, Found C: 65.49%, H: 6.96%, N: 6.60%.

$Co^{II}(salen^{OMe})$ (**13**)

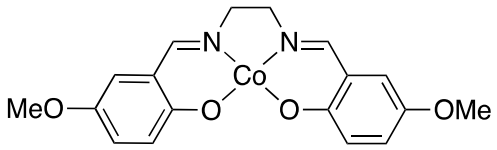

This complex was synthesized following the same procedure as for compound **9**, combining **Salen^{OMe}** (0.4 g, 1.22 mmol) and $Co(OAc)_2 \bullet 4H_2O$ (0.33 g, 1.34 mmol). Yield: 0.38 g, 81%. ESI(+)-MS m/z (relative intensity) = 385.0596 ([**13**]$^+$). Elemental analysis calculated for $Co^{II}(salen^{OMe}) \bullet 0.6H_2O$ ($C_{18}H_{19.2}N_2O_{4.6}Co$) C: 54.58%, H: 4.89%, N: 7.07%, Found C: 54.12%, H: 5.02%, N: 7.60%.

$Co^{II}(salen^{CF3})$ (**14**)

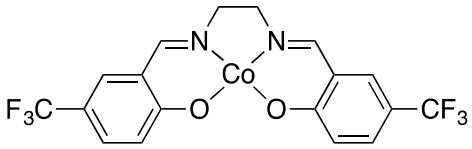

This complex was synthesized following the same procedure as for compound **9**, combining **Salen^{CF3}** (0.03 g, 0.07 mmol) and $Co(OAc)_2 \bullet 4H_2O$ (0.018 g, 0.07 mmol). Yield: 0.01 g, 29%. ESI(+)-MS m/z (relative intensity) = 462.0256 ([**14+H**]$^+$).

$[Co^{III(}salen^H)$-OTs] (**15**)[105]

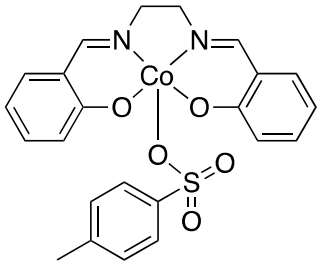

This compound was synthesized according to a literature procedure.[105] Complex **9** (0.02 g, 0.063 mmol) in DCM and *p*-toluenesulfonic acid (0.012 g, 0.063 mmol) in 2 mL DCM and 2 mL acetone were combined and stirred in the air at 298 K for 2 h, in which time a brown precipitate formed. The product was filtered, washed with DCM and dried *in vacuo*. Yield: 0.13 g, 84%. ^{1}H NMR (400 MHz, DMSO-d_6) δ 8.45 (s, 2H), 8.32-8.25 (m, 2H), 7.51-7.45 (m, 5H), 7.43-7.36 (m, 2H), 7.14-7.09 (m, 2H), 6.70-6.63 (m, 2H), 4.20-4.12 (m, 4H), 2.31-2.26 (s, 3H). ESI(+)-MS m/z (relative intensity) = 519.0386 ([**15**+Na]$^+$). This data is consistent with the literature.[105] Elemental analysis calculated for $[Co^{III}(salen^H)$-OTs]$\bullet C_3H_6O \bullet 2H_2O$ ($C_{26}H_{31}N_2SO_8Co$) C: 52.88%, H: 5.29%, N: 4.74%, Found C: 52.54%, H: 4.59%, N: 4.18%.

$[Co^{III}(salen^{H})(1\text{-MeIm})_2]ClO_4$ (**16**)

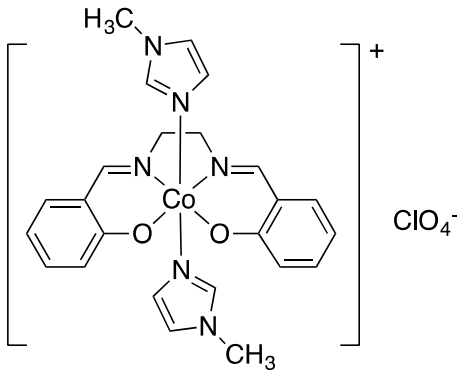

To complex **9** (0.1 g, 0.3 mmol) in a MeOH/ DCM solution (25/25 mL) was added 3 equivalents of 1-methylimidazole (0.076g, 0.920 mmol). The solution was stirred at 298 K for 2 h and turned a dark red colour. $NaClO_4$ (0.23 g, 1.80 mmol) in MeOH (2 mL) was then added, and stirring in the air at 298 K was continued for 1 day. Slow evaporation of the solvent afforded dark red crystals after 1 day that were collected by filtration, washed with cold MeOH, and dried in *vacuo*. Yield: 0.14 g, 79%. ^{1}H NMR (400 MHz, MeOD) δ 8.20 (s, 2H), 7.46 (s, 2H), 7.32 – 7.25 (m, 4H), 7.18 (d, *J* = 8.3 Hz, 2H), 6.94 (t, *J* = 1.6 Hz, 2H), 6.69 (t, *J* = 1.5 Hz, 2H), 6.63 – 6.57 (m, 2H), 4.06 (s, 4H), 3.60 (s, 6H). ^{13}C NMR (101 MHz, MeOD) δ 168.71, 164.95, 138.94, 135.24, 134.51, 127.65, 122.77, 118.35, 115.21, 56.97, 33.61. ESI(+)-MS m/z (relative intensity) = 489.1466 ($[Co^{III}(salen^{H})(1\text{-MeIm})_2]^{+}$). Elemental analysis calculated for $[Co^{III}(salen^{H})(1\text{-MeIm})_2]ClO_4$ ($C_{24}H_{26}N_6ClO_6Co$) C: 48.95%, H: 4.45%, N: 14.27%, Found C: 48.71%, H: 4.65%, N: 14.11%.

$[Co^{III}(salen^{NO2})(1\text{-MeIm})_2]ClO_4$ (**17**)

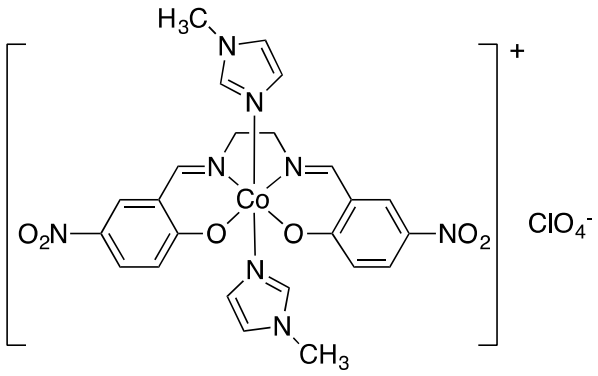

This complex was synthesized following the same procedure as for compound **16**, combining complex **10** (0.1 g, 0.240 mmol), 1-methylimidazole (0.06 g, 0.722 mmol) and $NaClO_4$ (0.176 g, 1.44 mmol). Yield: 0.11 g, 79%. ^{1}H NMR (400 MHz, DMSO-d_6) δ 8.48 (s, 2H), 8.46 (d, J = 2.7 Hz, 2H), 8.07 (dd, J = 9.3, 2.8 Hz, 2H), 7.68 (s, 2H), 7.23 – 7.14 (m, 4H), 6.67 (s, 2H), 4.12 (s, 4H), 3.59 (s, 6H). ^{13}C NMR (101 MHz, DMSO-d_6) δ 170.58, 169.56, 139.14, 135.62, 132.54, 128.91, 127.12, 122.89, 122.77, 117.59, 57.41, 34.67. ESI(+)-MS m/z (relative intensity) = 579.1008 ($[Co^{III}(salen^{NO2})(1\text{-MeIm})_2]^+$). Elemental analysis calculated for $[Co^{III}(salen^{NO2})(1\text{-MeIm})_2]ClO_4$ ($C_{24}H_{24}N_8ClO_{10}Co$) C: 42.46%, H: 3.56%, N: 16.51%, Found C: 42.87%, H: 3.68%, N: 16.04%.

$[Co^{III}(salen^{Br})(1\text{-MeIm})_2]ClO_4$ (**18**)

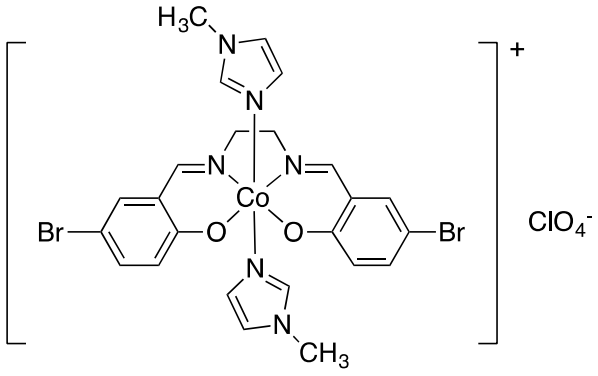

This complex was synthesized following the same procedure as for compound **16**, combining complex **11** (0.1 g, 0.207 mmol), 1-methylimidazole (0.05 g, 0.621 mmol) and $NaClO_4$ (0.15 g, 1.24 mmol). Yield: 0.12 g, 78%. ^{1}H NMR (500 MHz, DMSO-d_6) δ 8.19 (s, 2H), 7.56 (s, 2H), 7.46 (d, *J* = 2.7 Hz, 2H), 7.27 (dd, *J* = 9.1, 2.7 Hz, 2H), 7.09 (d, *J* = 1.6 Hz, 2H), 6.98 (d, *J* = 9.1 Hz, 2H), 6.61 (d, *J* = 1.5 Hz, 2H), 3.99 (s, 4H), 3.56 (s, 6H). ^{13}C NMR (101 MHz, DMSO-d_6) δ 168.05, 164.37, 138.86, 137.02, 135.83, 127.31, 124.57, 122.30, 119.64, 104.17, 57.06, 34.56. ESI(+)-MS m/z (relative intensity) = 646.9651 ($[Co^{III}(salen^{Br})(1\text{-MeIm})_2]^+$). $[Co^{III}(salen^{Br})(1\text{-MeIm})_2]ClO_4 \bullet 0.5CH_2Cl_2$ ($C_{24.5}H_{25}N_6Cl_2O_6CoBr_2$) C: 37.29%, H: 3.19%, N: 10.65%, Found C: 37.16%, H: 3.59%, N: 10.65%.

$[Co^{III}(salen^{tBu})(1\text{-MeIm})_2]ClO_4$ (**19**)

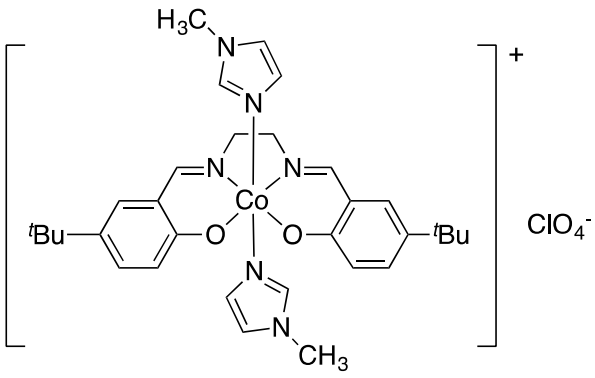

This complex was synthesized following the same procedure as for compound **16**, combining complex **12** (0.063 g, 0.145 mmol), 1-methylimidazole (0.036 g, 0.435 mmol) and $NaClO_4$ (0.1 g, 0.869 mmol). Yield: 0.06 g, 90%. ^{1}H NMR (500 MHz, DMSO-d_6) δ 8.21 (s, 2H), 7.57 (d, *J* = 1.5 Hz, 2H), 7.30 (dd, *J* = 8.9, 2.7 Hz, 2H), 7.19 (d, *J* = 2.7 Hz, 2H), 7.07 (t, *J* = 1.6 Hz, 2H), 7.01 (d, *J* = 8.9 Hz, 2H), 6.66 (t, *J* = 1.5 Hz, 2H), 4.04 (s, 4H), 3.57 (s, 6H), 1.21 (s, 18H). ^{13}C NMR (100 MHz, DMSO-d_6) δ 168.60, 163.44, 138.63, 135.75, 132.94, 129.93, 127.42, 122.04, 121.98, 116.66, 56.73, 34.51, 33.29, 31.14. ESI(+)-MS m/z (relative intensity) = 601.2696 ($[Co^{III}(salen^{tBu})(1\text{-MeIm})_2]^+$). Elemental analysis calculated for $[Co^{III}(salen^{tBu})(1\text{-MeIm})_2]ClO_4 \bullet 2H_2O \bullet 2CH_2Cl_2$ ($C_{34}H_{50}N_6Cl_5O_8Co$) C: 45.02%, H: 5.56%, N: 9.27%, Found C: 44.43%, H: 5.32%, N: 9.74%.

$[Co^{III}(salen^{OMe})(1\text{-}MeIm)_2]ClO_4$ (**20**)

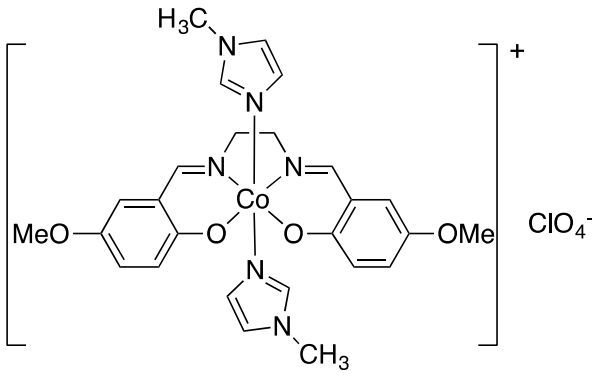

This complex was synthesized following the same procedure as for compound **16**, combining complex **13** (0.1 g, 0.260 mmol), 1-methylimidazole (0.064 g, 0.780 mmol) and $NaClO_4$ (0.19 g, 1.56 mmol). X-ray quality crystals were isolated by slow evaporation from MeOH. Yield: 0.163 g, 97%. ^{1}H NMR (400 MHz, DMSO-d_6) δ 8.18 (s, 2H), 7.54 (t, J = 1.5 Hz, 2H), 7.08 (t, J = 1.6 Hz, 2H), 6.99 (d, J = 9.1 Hz, 2H), 6.93 (dd, J = 9.2, 3.1 Hz, 2H), 6.79 (d, J = 3.1 Hz, 2H), 6.64 (t, J = 1.5 Hz, 2H), 4.00 (s, 4H), 3.65 (s, 6H), 3.57 (s, 6H). ^{13}C NMR (101 MHz, DMSO-d_6) δ 167.90, 160.42, 148.20, 138.67, 127.42, 124.81, 123.02, 121.97, 116.30, 114.66, 56.85, 55.45, 34.47. Elemental analysis calculated for $[Co^{III}(salen^{OMe})(1\text{-}MeIm)_2]ClO_4$ ($C_{26}H_{30}N_6ClO_8Co$) C: 48.12%, H: 4.66%, N: 12.95%, Found C: 48.30%, H: 4.96%, N: 12.76%.

$[Co^{III}(salen^{CF3})(1\text{-}MeIm)_2]ClO_4$ (**21**)

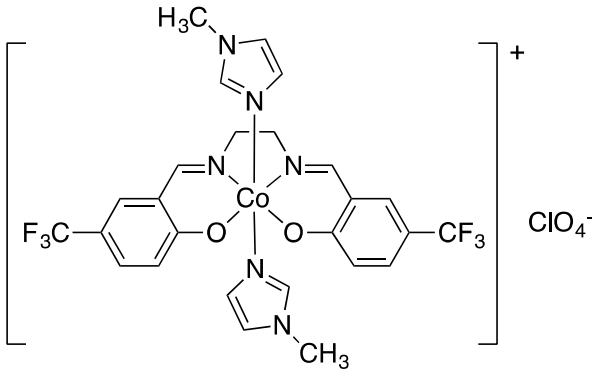

To a stirring solution of **Salen^{CF3}** (0.03 g, 0.0742 mmol) (in Et_2O) under N_2, $Co(OAc)_2 \bullet 4H_2O$ (0.018 g, 0.0742 mmol) in MeOH was added. The mixture was stirred for 20 min and then 3 eq. of 1-methylimidazole (0.018 g, 0.223 mmol) were added to the reaction. The solution was then stirred under an aerobic atmosphere overnight and then concentrated under low pressure and a precipitate formed. A dark red powder was collected by filtration, washed with cold methanol, and dried *in vacuo*. Yield: 0.04 g, 71%. X-ray quality crystals were isolated by slow evaporation from MeOH. ^{1}H NMR (400 MHz, DMSO-d_6) δ 8.38 (s, 2H), 7.75 (d, *J* = 2.4 Hz, 2H), 7.64 (s, 2H), 7.48 (dd, *J* = 9.1, 2.6 Hz, 2H), 7.19 (d, *J* = 8.9 Hz, 2H), 7.14 (t, *J* = 1.6 Hz, 2H), 6.66 (t, *J* = 1.6 Hz, 2H), 4.07 (s, 4H), 3.59 (s, 6H). ^{13}C NMR (101 MHz, DMSO-d_6) δ 169.47, 168.19, 139.45, 130.93, 127.73, 126.50, 123.69, 122.98, 118.05, 115.24, 114.91, 57.62, 35.08. ^{19}F NMR (500 MHz, $CDCl_3$) δ -59.50 (s). ESI(+)-MS m/z (relative intensity) = 625.1393 ($[Co^{III}(salen^{CF3})(1\text{-MeIm})_2]^+$). Elemental analysis calculated for $[Co^{III}(salen^{CF3})(1\text{-MeIm})_2]ClO_4 \bullet 2H_2O$ ($C_{26}H_{28}N_6ClO_8Co$) C: 41.04%, H: 3.71%, N: 11.04%, Found C: 40.60%, H: 3.37%, N: 11.47%.

(1*H*-imidazol-5-yl) methyl 3-methoxybenzoate hydrochloride (**22**).

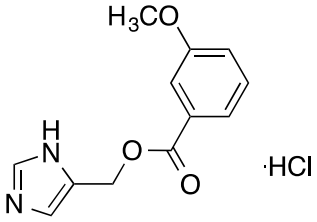

A mixture of finely dispersed (1*H*-imidazol-5-yl)methanol (0.40 g, 2.97 mmol) and benzoic acid chloroanhydride (0.452 g, 5.9 mmol) was heated without solvent for 5 h. The reaction temperature was maintained between 363 and 373 K. Reaction completion was assumed when the evolution of gas (hydrogen chloride) ceased. After cooling, a pink solid was obtained, washed with diethyl ether, acetone, and dried *in vacuo.* Yield: 0.73 g, 92%. ^{1}H NMR (400 MHz, DMSO-d_6) δ 9.16 (d, *J*= 1.4 Hz, 1H), 7.86- 7.79 (m, 1H), 7.58 (ddd, *J*= 7.7, 1.6, 1.0 Hz, 1H), 7.49 (dd, *J*= 2.7, 1.5 Hz, 1H), 7.45 (dd, *J*= 8.3, 7.7 Hz, 1H), 7.25 (ddd, *J*= 8.3, 2.7, 1.0 Hz, 1H), 5.40 (d, *J*= 0.7 Hz, 2H), 3.81 (s, 3H). The synthetic procedure for this compound has been reported and characterization matches literature data.[106]

[Co^{III}(salen)((1*H*-imidazol-5-yl) methyl 3-methoxybenzoate)$_2$]ClO_4 (**23**)

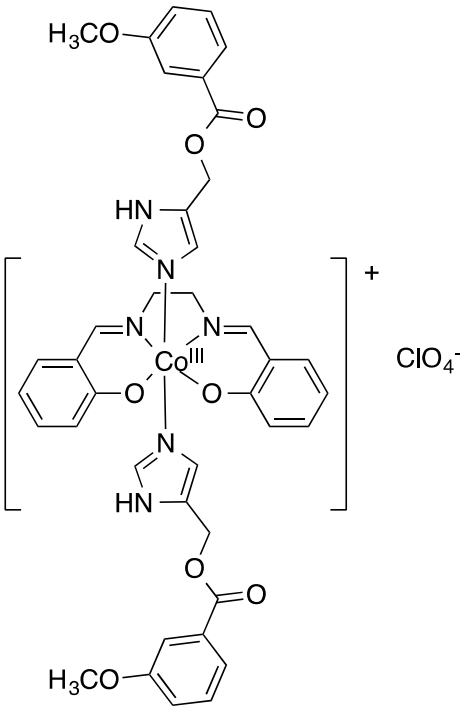

To complex **9** (0.053 g, 0.16 mmol) in a MeOH/ DCM solution (5/5 mL) was added 3 equivalents of compound **14** (0.11g, 0.49 mmol). The solution was stirred at 298 K for 2 h in which time the reaction turned dark red in color. $NaClO_4$ (0.12 g, 0.98 mmol) in methanol (2 mL) was then added, and stirring at 298 K was continued for 1 day. Slow evaporation of the solvent afforded a dark red powder that was collected by filtration, washed with cold methanol, and dried *in vacuo*. The crude product was purified by silica-gel chromatography (1:15, MeOH: DCM eluent) to afford compound **23** as a brown solid. Yield: 0.029 g, 20%. ^{1}H NMR (400 MHz, MeOD) δ 8.22 (s, 2H), 7.54 (d, *J*=1.3 Hz, 2H), 7.44 (dt, *J*= 7.7, 1.3 Hz, 2H), 7.38 (dd, *J*= 2.7, 1.5 Hz, 2H), 7.35-7.27 (m, 4H), 7.21 (ddd, *J*= 8.6, 6.8, 1.8 Hz, 2H), 7.17-7.11 (m, 4H), 6.86 (d, *J*= 1.3 Hz, 2H), 6.54 (ddd, *J*= 8.0, 6.8, 1.3 Hz, 2H), 5.12 (s, 4H), 4.06 (s, 4H), 3.78 (s, 6H). ^{13}C NMR (101 MHz, MeOD) δ 170.30, 167.24, 166.22, 161.12, 139.51, 136.69, 135.98, 132.02, 130.65, 128.84, 128.54, 123.73, 122.83, 120.36, 119.79, 116.71, 115.41, 58.53, 57.27, 55.89. ESI(+)-MS m/z (relative intensity) = 789.2075 [Co(salen)((1*H*-imidazol-5-yl) methyl 3-methoxybenzoate)$_2$]$^+$.

2.3. Results and Discussion

2.3.1. Synthesis

2.3.1.1 Synthesis of salen ligands and $Co^{II}(salen^{R})$ complexes

The salicylaldehyde starting materials were purchased except for 2-hydroxy-5-(trifluoromethyl)benzaldehyde which was prepared in two steps from commercially available 4-(trifluoromethyl)phenol.[11,103] The yield of 2-hydroxy-5-(trifluoromethyl)benzaldehyde (**6**) was lower in comparison to the literature report,[103] likely due to the sensitivity of the reaction to the amount of acid added. The salen ligands were synthesized by condensation of ethane-1,2-diamine in the presence of two equivalents of salicylaldehyde (**Scheme 2.2**). Salen ligands were obtained in a moderate yield (66-87%), and characterized by ^{1}H NMR, ^{13}C NMR and MS. **$Co^{II}(salen^{R})$** (**9-14**) (R= OMe, ^{t}Bu, H, Br, CF_3, NO_2) complexes were synthesized in moderate yields (62-92%) by reacting the salen ligands with $Co(OAc)_2$•$4H_2O$ under anaerobic conditions (**Scheme 2.2).** The synthesis of **$Co^{II}(salen^{CF3})$** using this procedure resulted in a very low yield (29%), likely due to the increased solubility of the complex and limited precipitation. ^{1}H NMR was used to characterize the d^7 Co(II) complexes further (**Figure 2.4**). The wide chemical shift range and broadened peaks in the spectra indicate the formation of a paramagnetic Co(II) species. The spectra are similar to those reported in the literature for similar compounds.[87] Minor sharp peaks observed in the diamagnetic region could be due to a small amount of oxidized Co(III) complexes.

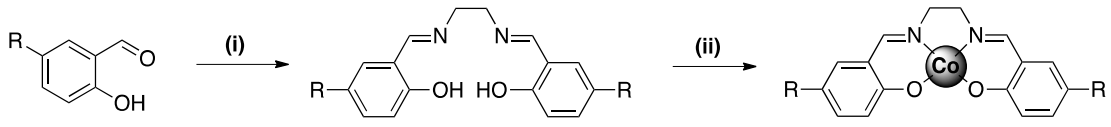

Scheme 2.2 Synthesis route for $[Co(salen^{R})(1\text{-}MeIm)_2]ClO_4$ complexes
(R = OMe, ^{t}Bu, H, Br, NO_2). Reaction Conditions: (i) 0.5 eq. ethane-1,2-diamine, EtOH, 298 K; (ii) N_2, $Co(OAc)_2$•$4H_2O$, MeOH/DCM, 298 K.

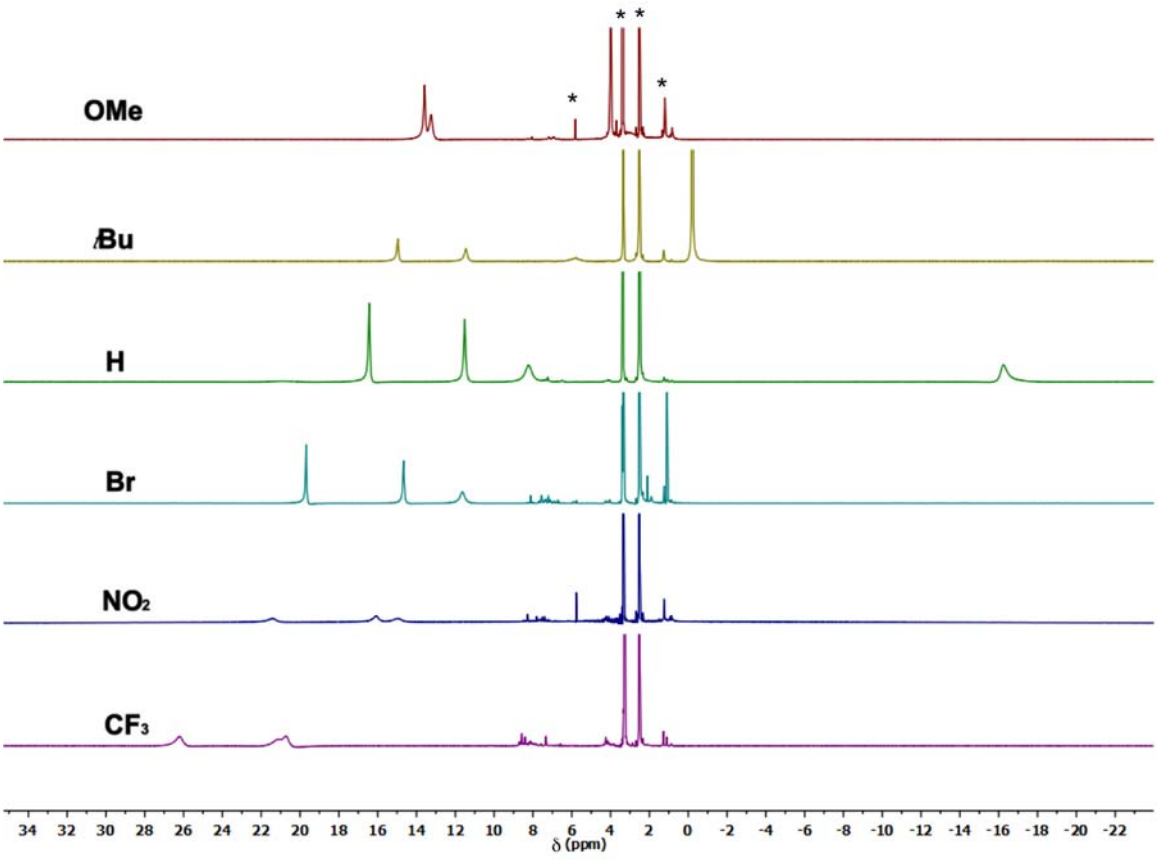

Figure 2.4 **^{1}H NMR spectra of Co^{II}(salen^{R}) in DMSO-*d*$_6$.**
(*solvent peaks. Dichloromethane (5.8 ppm), H_2O (3.3 ppm), DMSO (2.5 ppm) Diethyl ether (1.1 ppm))

2.3.1.2 Synthesis of Co(III) complexes

Once the Co(II) salen complexes were obtained, we investigated the synthesis of the associated octahedral Co(III) salen complexes with different axial ligands. Initially, we investigated the reactions of the Co(II) salens with a number of different organic acids.[105,107,108] However, it was difficult to isolate the desired Co(III) complexes. Analysis of 1H NMR spectra suggests that a mixture of complexes with one or two acids bound axially was formed, even though a large excess of acid was employed. Only **[Co(salen^{H})-OTs]** (**15**) was isolated during these studies.[105] We then turned to neutral donors, in order to ensure the formation of Co(III) complexes in an octahedral geometry.

1-Methylimidazole was chosen as a neutral donor, due to the numerous reports of this ligand binding in an axial fashion to Co complexes of salen and salen analogues.[109, 111] **[Co^{III}(salen^{R})(1-MeIm)$_2$]ClO$_4$** (R= OMe, ^{t}Bu, H, Br, NO_2) complexes were synthesized

using the $Co^{II}(salen^{R})$ complexes as starting materials with three equivalents of 1-methylimidazole and excess $NaClO_4$ in air (**Scheme 2.3**). Compounds precipitated from solution, and were isolated by filtration in moderate yield. Characterization included ^{1}H and ^{13}C NMR, mass spectrometry, elemental analysis and, in certain cases, X-ray crystallography.

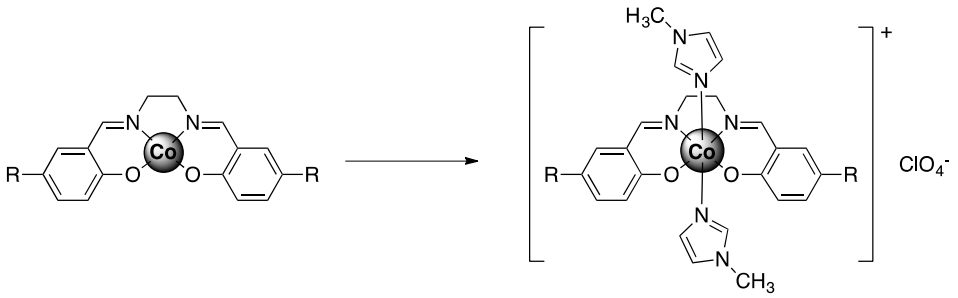

Scheme 2.3 Synthesis route for $[Co^{III}(salen^{R})(1\text{-MeIm})_2]ClO_4$ complexes.
(R= OMe, ^{t}Bu, H, Br, NO_2). Reaction Conditions: (i) Air, 3 eq. 1-methylimidazole, $NaClO_4$, MeOH/DCM, 12 h, 298 K.

Due to the difficulty in isolating **$Co^{II}(salen^{CF3})$, $[Co^{III}(salen^{CF3})(1\text{-MeIm})_2]ClO_4$** was synthesized in a one-pot reaction by first reacting $salen^{CF3}$ (**8**) and $CoCl_2$ under N_2, and then adding 1-methylimidazole and $NaClO_4$ to the reaction mixture and exposing to air (**Scheme 2.4**).

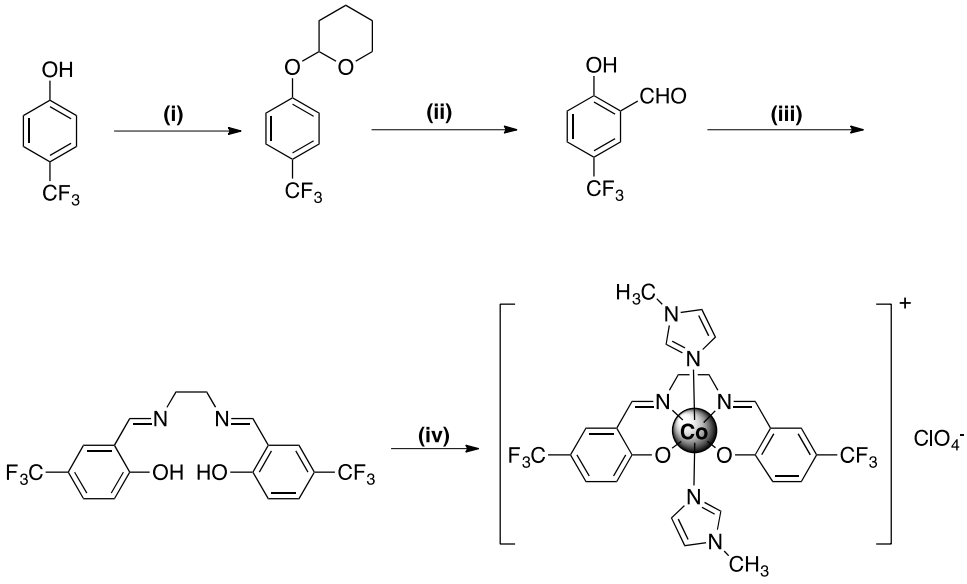

Scheme 2.4 Synthesis route for $[Co^{III}(salen^{CF3})(1\text{-MeIm})_2]ClO_4$ complex.
Reaction Conditions: (i) 3eq. 3,4-dihydro-2H-pyran, H^+, DCM; (ii) *n*BuLi, TMEDA, DMF, 263 K; (iii) 0.5 eq. ethane-1,2-diamine, MeOH; (iv) $CoCl_2$ and then 3 eq. 1-MeIm, MeOH/DCM, 12 h, 298 K.

2.3.2. X-ray Structure Determination

X-ray quality crystals of $[Co^{III}(salen^{OMe})(1\text{-MeIm})_2]ClO_4$, $[Co^{III}(salen^{H})(1\text{-MeIm})_2]ClO_4$ and $[Co^{III}(salen^{CF3})(1\text{-MeIm})_2]ClO_4$ were grown by slow evaporation of concentrated MeOH solutions. The three X-ray structures were solved by J. R. Thompson and R. M. Clarke and are shown in Figures **2.5** to **2.7**. A number of other Co(III) salen imidazole complexes have been reported in the literature,[109-111] and the bond length data and geometries found in this work are in agreement with those reports.

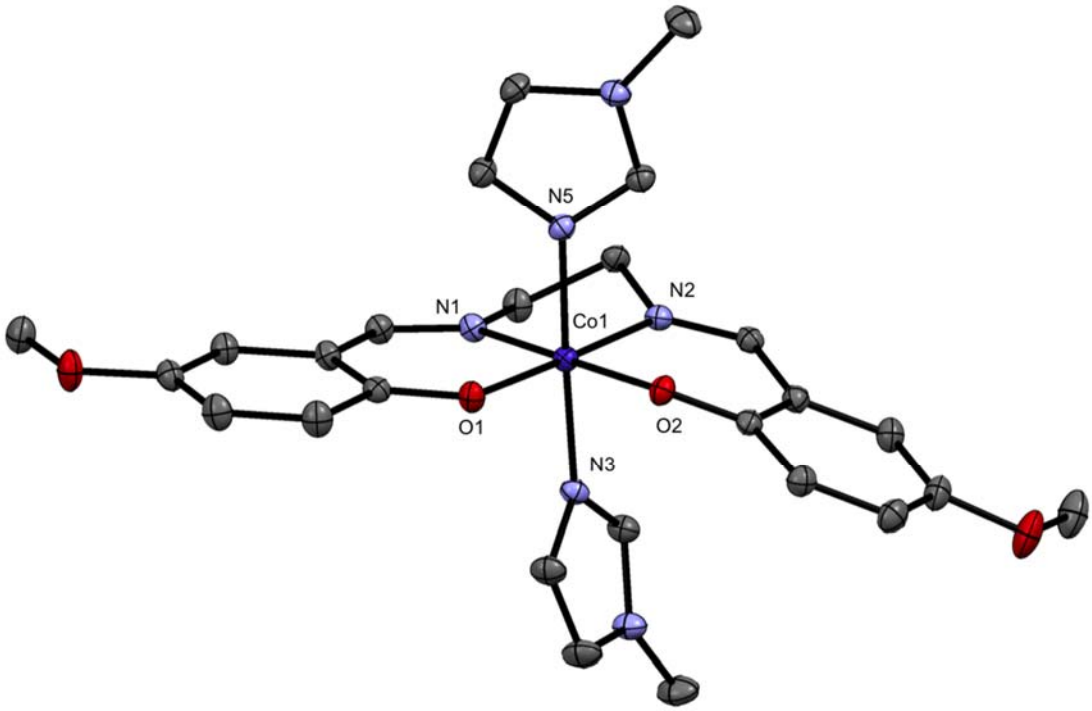

Figure 2.5 Crystal structure of $[Co^{III}(salen^{OMe})(1\text{-MeIm})_2]ClO_4$
(thermal ellipsoids shown at 50% probability). Hydrogen atoms and solvent molecules excluded for clarity.

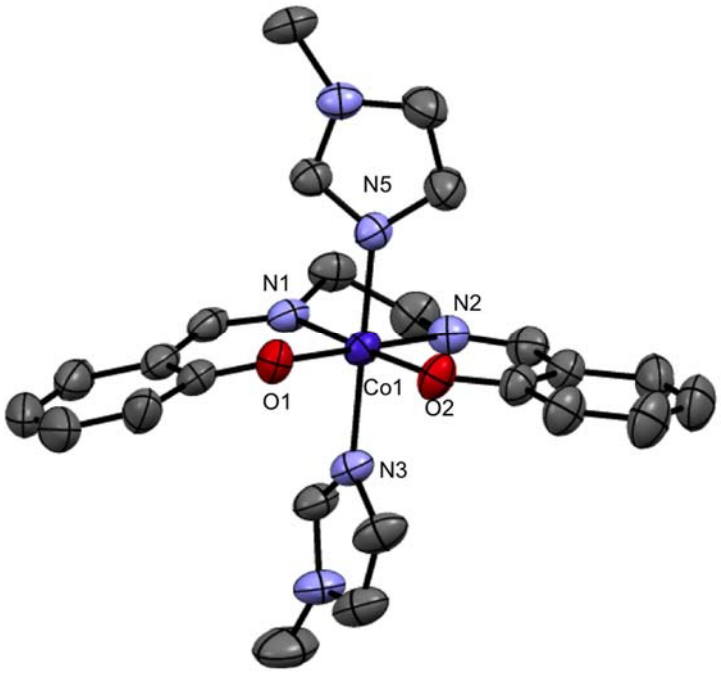

Figure 2.6 Crystal structure of $[Co^{III}(salen^{H})(1\text{-MeIm})_2]ClO_4$
(thermal ellipsoids shown at 50% probability). Hydrogen atoms and solvent molecules excluded for clarity.

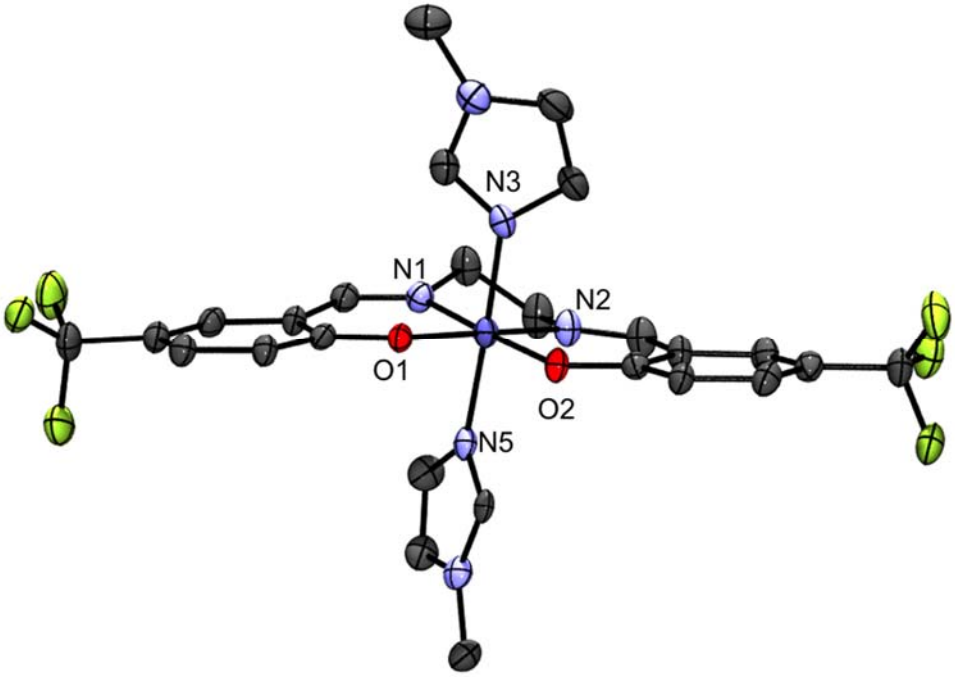

Figure 2.7 Crystal structure of $[Co^{III}(salen^{CF3})(1\text{-MeIm})_2]ClO_4$
(thermal ellipsoids shown at 50% probability). Hydrogen atoms and solvent molecules excluded for clarity.

Table 2.2 Selected bond distances (Å) and angles (°) for $[Co^{III}(salen^{R})(1\text{-}MeIm)_2]ClO_4$ complexes.

$[Co^{III}(salen^{R})(1\text{-}MeIm)_2]ClO_4$	R = OMe	R = H	R = CF_3
Co1 – O1	1.8931(9)	1.895(3)	1.896(3)
Co1 – O2	1.9067(9)	1.893(4)	1.907(3)
Co1 – N1	1.8969(10)	1.889(4)	1.895(4)
Co1 – N2	1.8935(10)	1.902(5)	1.893(4)
Co1 – N3	1.9430(10)	1.964(4)	1.951(4)
Co1 – N5	1.9490(10)	1.940(4)	1.956(4)
O2 – Co1 – N5	88.69(4)	88.5(2)	90.09(15)
N1 – Co1 – N5	92.05(4)	89.2(2)	91.88(17)
N2 – Co1 – N5	89.42(4)	90.8(2)	90.70(17)
O1 – Co1 – N5	89.27(4)	89.7(2)	88.54(15)
O2 – Co1 – N3	87.30(4)	90.1(2)	89.57(16)
N1 – Co1 – N3	91.99(4)	92.2(2)	88.51(17)
N2 – Co1 – N3	91.62(4)	90.1(2)	92.37(18)
O1 – Co1 – N3	89.71(4)	89.5(2)	88.38(15)

In each of the three crystal structures the expected pseudo octahedral geometry is observed, including the tetradentate salen ligand in the equatorial plane and two axial N-methylimidazole molecules. In the **$[Co^{III}(salen^{R})(1\text{-}MeIm)_2]ClO_4$** complexes, the Co(III) ion is coordinated by two oxygen atoms (O1, O2) and two nitrogen atoms (N1 ,N2) from the tetradentate salen ligand. The O2–Co1–N5, N1–Co1–N5, N2–Co1–N5, O1–Co1–N5, O2–Co1–N3, N1–Co1–N3, N2–Co1–N3, and O1–Co1–N3 angles differ only slightly from 90° as indicated in **Table 2.2**. The bond distances between the Co(III) centre and the axial imidazole ligands (Co1 – N3 and Co1 – N5) are longer in comparison to the equatorial bond lengths (both Co-O and Co-N), suggesting that the binding of axial ligands is weaker in comparison to the equatorial salen ligand (**Table 2.2**). This is likely due to the geometrical constraints (chelation effect) imposed by the tetradentate salen ligand and Jahn-Teller distortion.[90] We also investigated if a change in the electron-donating ability of the *para*-ring substituents would alter the coordination sphere bond lengths systematically. Analysis of X-ray distances for square-planar Cu(II) salen derivatives have shown a small but significant decrease in Cu-O bond lengths (CF_3 > ^{t}Bu > OMe) as the electron donating ability of the *para*-ring substituent is increased.[112-114] The same trend in Ni-O bond lengths is also observed for square-planar Ni(II) salen complexes.[86,112,113]

However, comparison of the Co-O distances for each of the complexes (**Table 2.2**) does not show a statistically significant change across the three complexes. In addition, no obvious trend is apparent in the Co-N distances, either equatorial or axial, in the three structures. The electronic effect of the *para*-ring substituents may not be strong enough to alter the coordination sphere bond lengths in these octahedral derivatives. Alternatively, crystal packing forces may dominate in these solid state structures.

2.3.3. Stability Studies of $[Co^{III}(salen^{R})(1\text{-MeIm})_2]ClO_4$

The stability of the $[Co^{III}(salen^{H})(1\text{-MeIm})_2]ClO_4$ complex in 2% DMSO-d_6 in deuterated PBS solution was examined using ^{1}H NMR spectroscopy. The first spectrum was collected within 10 min of dissolving the complex. The sealed sample was kept in a 37 °C water bath, and another spectrum was collected after 24 h. The NMR spectrum at t = 10 min shows only signals assigned to the Co(III) complex. At the t = 24 h time point, several new minor signals appear, which are consistent with free 1-methylimidazole. This indicates that ligand exchange is likely slowly occurring in solution, with ca. 10% exchange over 24h based on NMR. (**Figure 2.8**) This experiment indicates that the $[Co^{III}(salen^{R})(1\text{-MeIm})_2]ClO_4$ complexes are relatively stable at 37 °C.

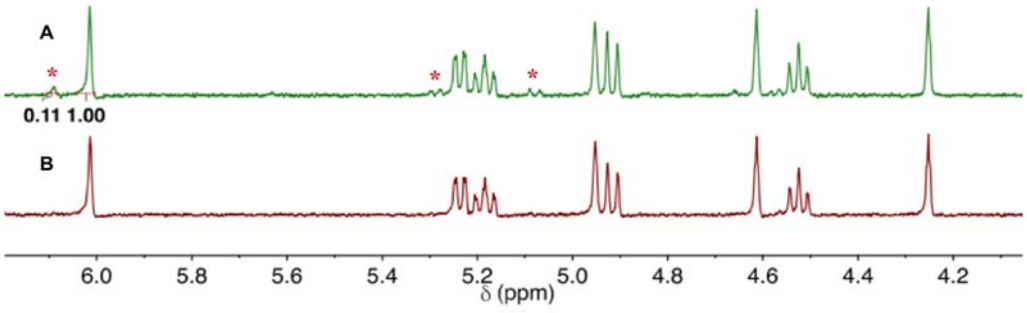

Figure 2.8 ^{1}H NMR spectra of $[Co(salen^{H})(1\text{-MeIm})_2]ClO_4$.
*Peaks of free 1-methylimidazole. Expanded spectra (4.2-6.0 ppm). Red, spectrum at t = 10 min (B); Green, spectrum at t = 24 h (A). Conditions: 2% DMSO-d_6 in deuterated PBS, 37 °C.

The stability of other $[Co^{III}(salen^{R})(1\text{-MeIm})_2]ClO_4$ complexes (R= OMe, ^{t}Bu, Br, CF_3, NO_2) was tested using the same method as $[Co^{III}(salen^{H})(1\text{-MeIm})_2]ClO_4$ (**Appendix 2.1 - 2.5**). The complexes $[Co^{III}(salen^{R})(1\text{-MeIm})_2]ClO_4$ (R= OMe, ^{t}Bu, Br) exhibit a similar change in comparison to $[Co^{III}(salen^{H})(1\text{-MeIm})_2]ClO_4$ (above), indicating

that this series of complexes exhibit only minor decomposition (ca. 10 %) in solution over 24 h. Interestingly, $[Co^{III}(salen^{CF3})(1\text{-MeIm})_2]ClO_4$ and $[Co^{III}(salen^{NO2})(1\text{-MeIm})_2]ClO_4$ exhibited no obvious ligand exchange over 24 h, indicating that the complexes with electron-withdrawing *para*-ring substituents are more stable to axial ligand exchange. The increased stability can be attributed to the increased Lewis acidity of the Co(III) centre, a result of the electron-withdrawing effect of these *para*-substituents.[97]

2.3.4. Electrochemistry

2.3.4.1 Cyclic voltammetry (CV) of $Co^{II}(salen^{R})$

The electrochemical behavior of the $Co^{II}(salen^{R})$ complexes (R = OMe, ^{t}Bu, H, Br, NO_2) has been studied after isolating by CV in DMF (**Figure 2.9**). Due to difficulty in isolating, the CV of $Co^{II}(salen^{CF3})$ could not be measured. A more negative redox potential was expected for complexes with electron-donating phenolate *para*-substituents (OMe > ^{t}Bu > H > Br > NO_2), due to the expected increase in electron density at the Co centre.

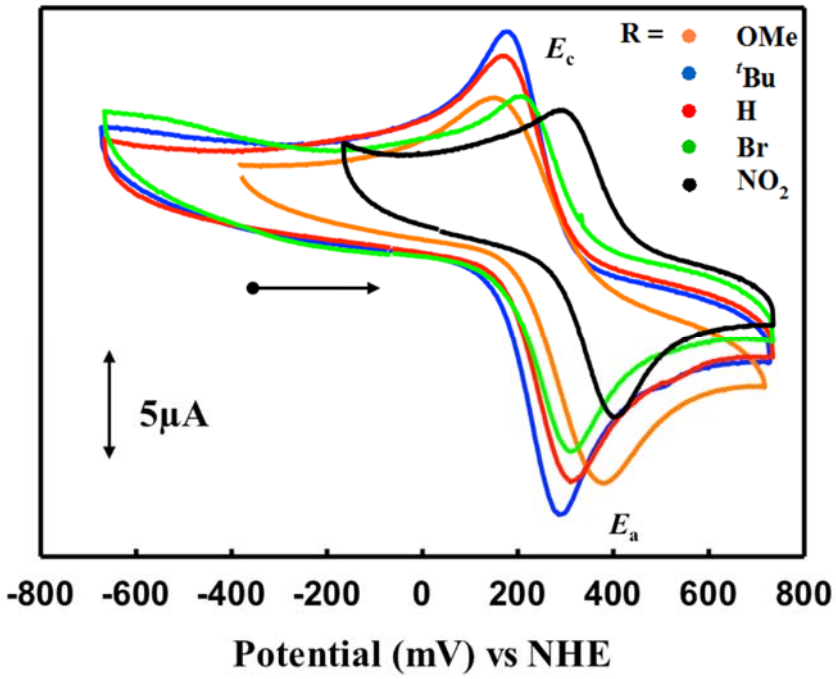

Figure 2.9 Cyclic voltammetry of $Co^{II}(salen^{R})$, where R accounts for the *para*-ring substitution.

The direction of the arrow signifies the initial direction of the scans. Conditions: 1 mM complex, 0.1 M $^{n}Bu_4NClO_4$, scan rate 100 mV s^{-1}, DMF, 298 K.

The reduction potential ($E_{1/2}$) can be obtained from a cyclic voltammogram by the mean of anodic (E_a) and cathodic peaks (E_c)[115], as shown in **Equation 2.1**:

$$E_{1/2} = \frac{E_c + E_a}{2} \quad \textbf{(2.1)}$$

The reduction potentials ($E_{1/2}$) for the five derivatives (Shown in **Table 2.3**) correlate with the relative electronic properties of the phenolate *para*-substituents (OMe > ^{t}Bu > H > Br > NO_2) as expected. The $E_{1/2}$ values for the $Co^{II}(salen^R)$ complexes could be shifted from 215 mV to 335 mV (120 mV difference) by the different *para*-substituents. This result is consistent with similar complexes that were previously reported in the Storr group.[97] The separation between the anodic and the cathodic peak potentials, ΔE_p, can be used to determine the electrochemical reversibility for a redox couple, with **Equation 2.2** describing the reversible case at 25 °C under ideal conditions[115] (n is the number of electron from the balanced redox reaction, in this case, n= 1).

$$\Delta E_p = \frac{59 \text{ mV}}{n} \quad \textbf{(2.2)}$$

However, in practice, the theoretical value for ΔE_p is rarely observed. Ferrocene (Fc) is a known reversible standard used in electrochemistry, and is used in this experiment to characterize the reversibility of the synthesized Co complexes. The measured ΔE_p value for Fc is 100 mV under our experimental conditions (**Table 2.3**). The ΔE_p values for the $Co^{II}(salen^R)$ complexes (R = ^{t}Bu, H, NO_2) are slightly higher in comparison to the value for Fc, indicating that the Co(III) / Co(II) redox process is quasi-reversible for these complexes. The ΔE_p value for the $Co^{II}(salen^{OMe})$ complex (230 mV) is much larger, which may due to the slow electron transfer kinetics.

Table 2.3 Electrochemical data (mV) for $Co^{II}(salen^R)$ versus the normal hydrogen electrode (NHE).

$Co^{II}(salen^R)$	E_c	E_a	$E_{1/2}$	ΔE_p[a]
OMe	150	380	215	230
^{t}Bu	180	290	235	110
H	170	310	240	140
Br	210	310	260	100
NO_2	300	410	355	110

[a]Peak-to-peak differences ($\Delta E_p = |E_a - E_c|$). Peak-to-peak difference for the Fc^+/Fc couple at 298 K is 100 mV.

2.3.4.2 CV of $[Co^{III}(salen^R)(1\text{-}MeIm)_2]ClO_4$.

The electrochemical properties of the $[Co^{III}(salen^R)(1\text{-}MeIm)_2]ClO_4$ complexes were assessed to better understand how the different *para*-substituents and/or axial ligands shift the Co(III) / Co(II) redox couple. The complexes investigated here are models for axial ligand release from the Co(III) salen ligand scaffold in a reducing environment. In order to tune the reduction potential, $[Co^{III}(salen^R)(1\text{-}MeIm)_2]ClO_4$ complexes with phenolate *para*-substituents (OMe, ^{t}Bu, H, Br, CF_3, NO_2) of different electron-donating ability were synthesized. A more negative Co^{III} / Co^{II} redox potential was expected for complexes with electron-donating *para*-phenolate ring substituents (OMe > ^{t}Bu > H > Br > CF_3 > NO_2). In addition, the complexes are expected to exhibit an irreversible redox couple if structural rearrangement (*i.e.*, ligand loss) occurs upon reduction.

As shown in **Figure 2.10 and Table 2.4**, there is a large value of ΔE_p and a different current response for the reduction (E_c) and oxidation (E_a) processes. These results suggest an irreversible electrochemical process for $[Co^{III}(salen^R)(1\text{-}MeIm)_2]ClO_4$. Scanning towards negative potential, the $[Co^{III}(salen^R)(1\text{-}MeIm)_2]ClO_4$ complexes are likely reduced (E_c) to $[Co^{II}(salen^R)(1\text{-}MeIm)_2]$ (**Scheme 2.5, step 1**). The axial ligands in the reduced Co(II) complex can then undergo ligand release in solution (**Scheme 2.5, step 2**) as structural re-arrangement likely occurs to a square planar Co^{II}salen complex. Subsequent oxidation to Co^{III}salen (E_a) then occurs, likely via the process shown in **Scheme 2.5, step 3.**

The trend in reduction potential ($E_{1/2}$) for the octahedral Co(III) derivatives match the relative electronic properties of the phenolate *para*-substituents (OMe > ^{t}Bu > H > Br > CF_3 > NO_2) as expected. Overall, using the different *para*-ring substituents allowed for tuning of the $E_{1/2}$ value from -140 mV to 80 mV (220 mV difference), and E_c value from -570 mV to -230 mV (340 mV difference). It should also be noted that the E_a values of the $Co^{II}(salen^R)$ complexes (**Table 2.3**) and associated $[Co^{III}(salen^R)(1\text{-}MeIm)_2]ClO_4$ complexes (**Table 2.4**) with same *para*-substituent are comparable, likely due to the fact that a similar reduced species is re-oxidized in the associated electrochemistry experiments.

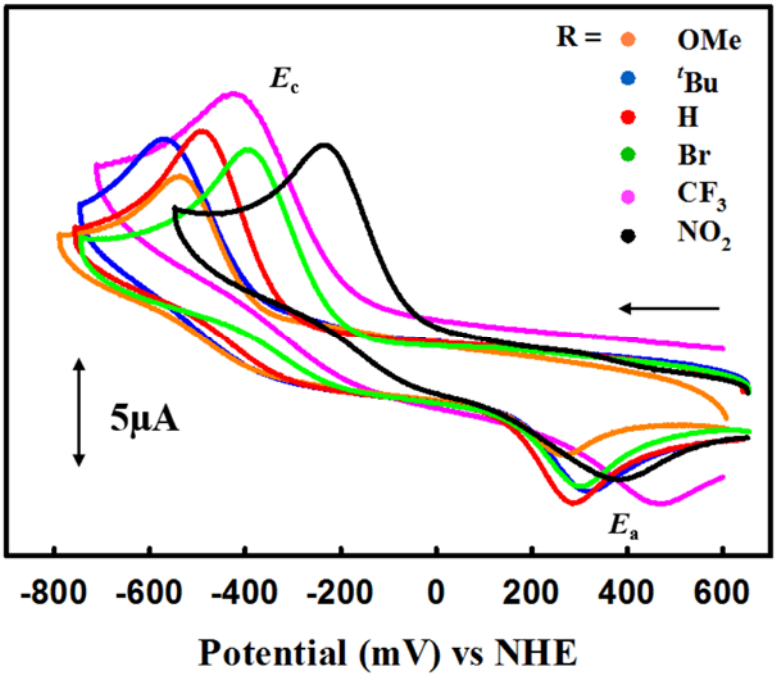

Figure 2.10 **Cyclic voltammetry of $[Co^{III}(salen^{R})(1\text{-MeIm})_2]ClO_4$. The direction of the arrow signifies the direction of the scans.**

Conditions: 1 mM complex, 0.1 M $^{n}Bu_4NClO_4$, scan rate 100 mV s^{-1}, DMF, 298 K.

Table 2.4 **Electrochemical data (mV) for $[Co^{III}(salen^{R})(1\text{-MeIm})_2]ClO_4$ versus NHE.**

$[Co(salen^{R})(1\text{-MeIm})_2]ClO_4$	E_c	E_a	$E_{1/2}$	$\Delta E_p{}^a$
OMe	-540	260	-140	800
^{t}Bu	-570	320	-125	890
H	-490	290	-100	780
Br	-400	300	-50	700
CF_3	-420	470	25	790
NO_2	-230	390	80	620

[a]Peak-to-peak differences ($\Delta E_p = |E_a - E_c|$). Peak-to-peak difference for the Fc^{+}/Fc couple at 298 K is 130 mV.

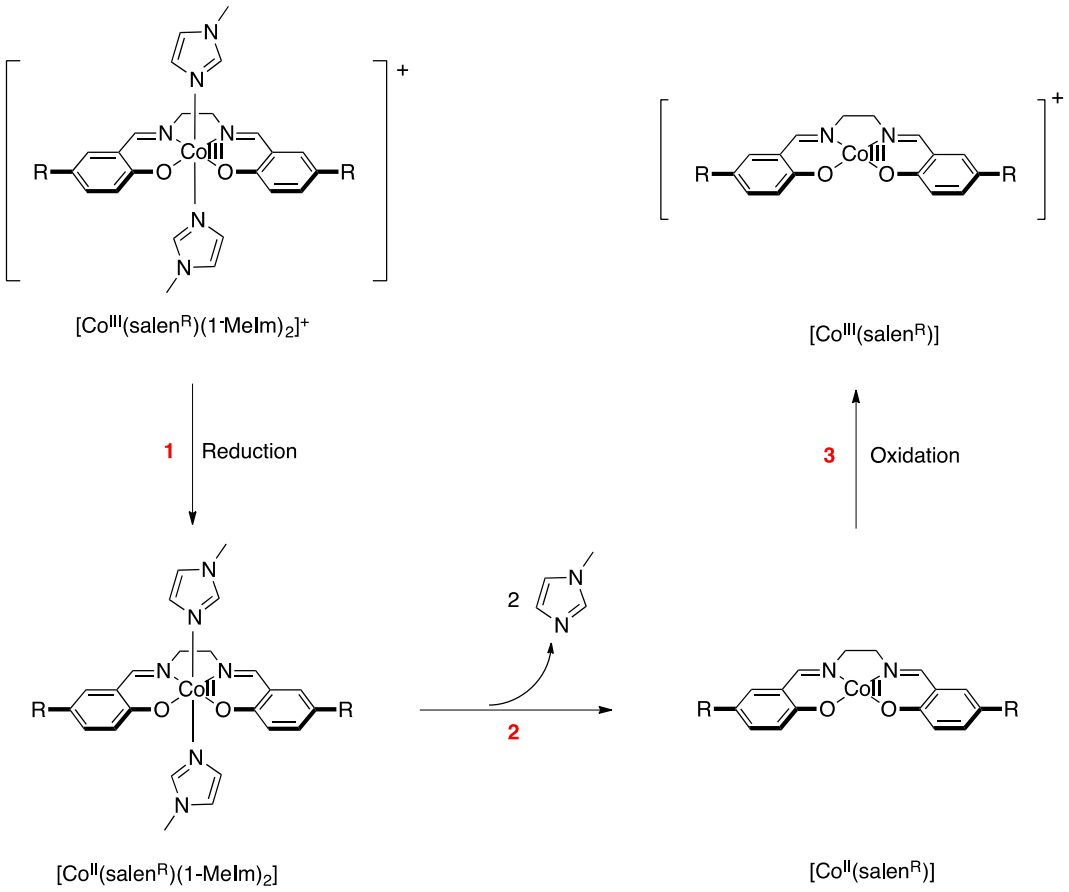

Scheme 2.5 Illustration of redox processes associated with Figure 2.10
Step 1: Reduction of $[Co^{III}(salen^{R})(1\text{-MeIm})_2]ClO_4$ to $[Co^{II}(salen^{R})(1\text{-MeIm})_2]$; Step 2: Axial ligand release due to structural rearrangement; Step 3: Oxidation of square planar $Co^{II}(salen^{R})$ complexes to $[Co^{III}salen]^+$ complexes.

As discussed above, the reduction potentials of the $[Co^{III}(salen^{R})(1\text{-MeIm})_2]ClO_4$ complexes versus NHE follow a trend consistent with the electron-donating abilities of the *para*-ring substituents. We further investigated this trend by plotting the $E_{1/2}$ values against Hammett substituent constants (σ_{para}) as shown in **Figure 2.11**.[116,117] A linear correlation (R^2 value is 0.992) is observed, demonstrating that the reduction potential is predominantly affected by the donating ability of the *para*-ring substituents. The E_c values of these series of complexes were also plotted against Hammett substituent constants, however the fitting was not as good as $E_{1/2}$ (**Appendix 2.6**)

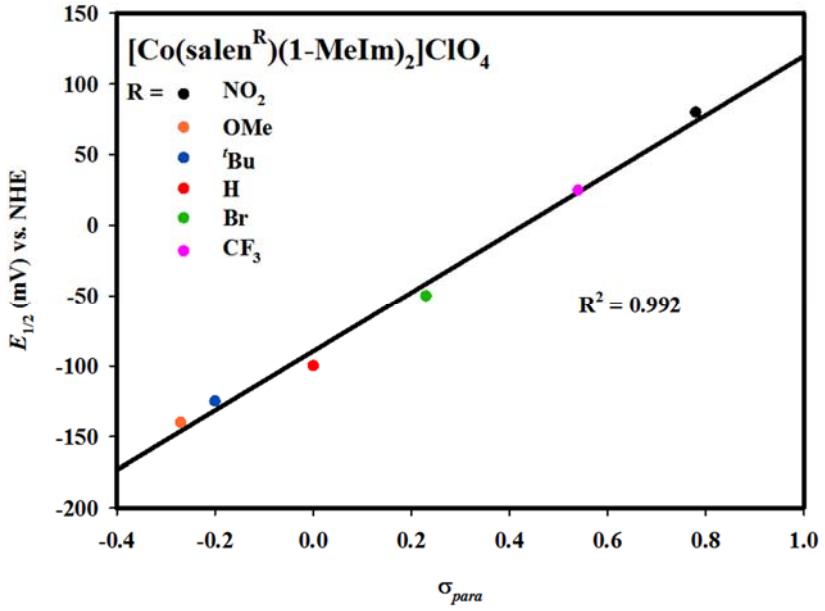

Figure 2.11 Hammett plot of the $E_{1/2}$ value of the $[Co^{III}(salen^R)(1\text{-MeIm})_2]ClO_4$ complexes versus σ_{para} of the *para*-ring substituents.

2.4. Conclusion

In this chapter, $Co^{II}(salen^R)$ and $[Co^{III}(salen^R)(1\text{-MeIm})_2]ClO_4$ (R = OMe, ^{t}Bu, H, Br, CF_3, NO_2) were synthesized and characterized by ^{1}H and ^{13}C NMR, mass spectrometry, elemental analysis, and, in certain cases, (R = OMe, H, CF_3) X-ray crystallography. An NMR stability study indicates that the $[Co^{III}(salen^R)(1\text{-MeIm})_2]ClO_4$ series of complexes exhibit only a small amount of axial ligand exchange in solution over 24 h, signifying that these Co(III) complexes are relatively stable. The reduction potentials of the complexes were correlated with the electronic properties of the phenolate *para*-substituents. As expected, electron-rich *para*-ring substituents on the salen ligand results in a low reduction potential of the complex. The large difference in reduction potential and current response of the $[Co^{III}(salen^R)(1\text{-MeIm})_2]ClO_4$ complexes indicates an irreversible electrochemical process, and likely axial ligand loss upon reduction. A plot of the $E_{1/2}$ of $[Co^{III}(salen^R)(1\text{-MeIm})_2]ClO_4$ complexes against Hammett constants (σ_{para}) indicates that the reduction potential is predominantly affected by the electronic properties of the phenolate *para*-substituents. The $E_{1/2}$ of $[Co^{III}(salen^R)(1\text{-MeIm})_2]ClO_4$ complexes are at the higher end of the physiological range (-420 mV to -150 mV), and the E_c values are at the lower end of physiological range.

Since this series of $[Co^{III}(salen^{R})(1\text{-MeIm})_2]ClO_4$ model complexes show good solution stability and tunable reduction potentials, the sterically more bulky (1*H*-imidazol-5-yl) methyl 3-methoxybenzoate hydrochloride (**21**) and associated $[Co^{III}(salen)((1H\text{-imidazol-5-yl) methyl 3-methoxybenzoate})_2]ClO_4$ (**22**) were also successfully synthesized (**Figure 2.12)**. This indicates that axial imidazole ligation is possible, even if a bulkier imidazole is used. On the basis of these results, we examined the chemistry of coumarin functionalized imidazoles bound to the Co(III) salens due to the potential for a fluorescent response upon ligand release. Details are presented in Chapters 3 and 4.

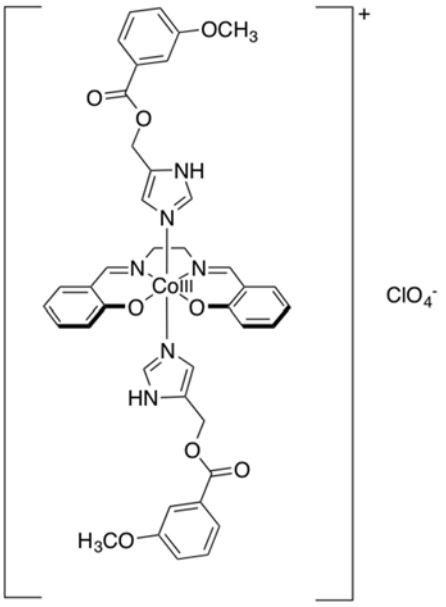

Figure 2.12 Chemical structure of $[Co^{III}(salen)((1H\text{-imidazol-5-yl)methyl-3-methoxybenzoate})_2]ClO_4$.

Chapter 3.

Synthesis and Characterization of Cobalt(III) Salen Coumarin-Imidazole Complexes

John Thompson and Ryan Clarke collected X-ray data and solved the crystal structure. Dr. Andrew Lewis and Colin Zhang assisted with the NMR experiments. Many thanks to Dr. Angela Stefanachi (Dipartimento di Farmacia, Scienze del Farmaco, Universita of Bari Aldo Moro, Italy) for information on the fluorescence of the coumarin-imidazole adduct.

3.1. Introduction

Metal complexes can be activated and undergo structural rearrangement upon reduction, which has been investigated as a means for selective cancer treatment.[28,64,92-95] In recent years, platinum(IV) complexes have been investigated as potential chemotherapeutics, with many acting as pro-drugs that are activated upon reduction to Pt(II)[91]. The octahedral geometry of Pt(IV) complexes allows for the binding of two additional axial ligands in some cases,[91] similar to the Co salen complexes discussed in Chapter 2. Satraplatin (**Figure 3.1**) was designed to act as a pro-drug, in which the axial acetate ligands make the complex more lipophilic in comparison to cisplatin.[118] Once administered orally, satraplatin can be reduced to a Pt(II) complex, which undergoes structural rearrangement to a square planar geometry with release of the acetate ligands. This metabolite is structurally similar to cisplatin, except for the replacement of one ammine group with a cyclohexylamine,[119] and exhibits a similar mechanism of action to cisplatin by inducing apoptosis via DNA cross-linking.[118]

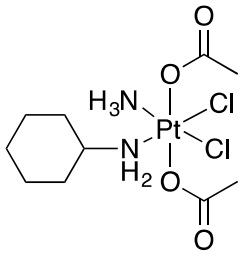

Figure 3.1 Chemical structure of satraplatin.

A recent report detailed Pt(IV) complexes that provide additional information on the reduction process and associated ligand release (**Figure 3.2**).[91] It was shown that *c,c,t*-[$Pt(NH_3)_2Cl_2(OCO(CH_2)_2NH(FL))_2$] ($Pt(IV)(FL)_2$) and *c,c,t*-[$Pt(NH_3)_2Cl_2(OCO(CH_2)_2NH(FITC))_2$] ($Pt(IV)(FITC)_2$) (**Figure 3.2**) can be reduced in a hypoxic environment, releasing the fluorescent axial ligands, to generate an active Pt(II) species. Fluorescence imaging then provides kinetic information on oxidation states and the distribution of the compound in cells.[91]

In the Pt(IV) complexes, the fluorescence of the fluorescein groups was quenched (off-state) through Forster Resonance Energy Transfer (FRET), owing to the close proximity of the fluorescein and Pt. When the fluorophores are excited, energy transfer to Pt effectively quenches the fluorescein fluorescence. The reduction of Pt(IV) to Pt(II) results in the release of the fluorescein groups so that the fluorescence is restored (on-state) (**Figure 3.2**).[91,120]

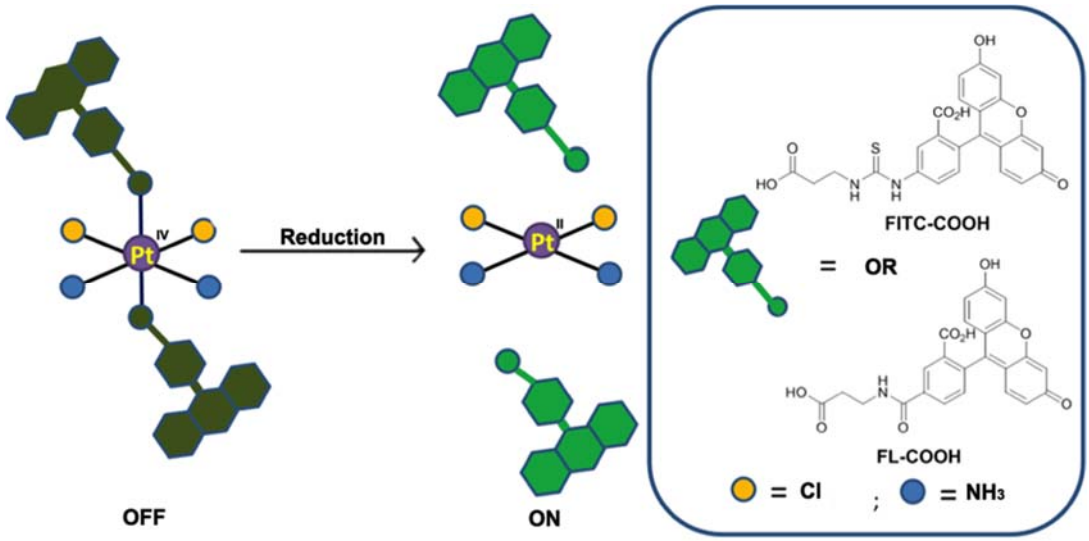

Figure 3.2 Illustration of the fluorescence 'Turn-on' of Pt(IV) Complexes following reduction of Pt(IV) to Pt(II) and release of the axial fluorescein ligands.[91]

Octahedral cobalt(III) complexes can also act as pro-drugs, and a number of interesting compounds have been reported that undergo ligand release upon reduction.[28,93-95] In an example relevant to this research, two Co(III) complexes, $[Co(C343)_2(cyclam)]Cl$ and $[Co(AQ2C)_2(cyclam)]Cl$, were synthesized incorporating the fluorescent anthraquinone-2-carboxylic acid (AQ2CH) or coumarin-343 (C343H) ligands in the axial positions and the tetradentate macrocycle 1,4,8,11-tetraazacyclotetradecane (cyclam) to form octahedral complexes (**Figure 3.3**).[93] $[Co(C343)_2(cyclam)]Cl$ ($E_{1/2}$ = -250 mV vs. NHE) and $[Co(AQ2C)_2(cyclam)]Cl$ ($E_{1/2}$ = -387 mV vs. NHE) were designed to be activated by hypoxic cells and act as a visual reporter of the reduction process and localization upon reduction and ligand release. Co(III) quenches the fluorescence of the ligands and reduction of Co(III) to Co(II) leads to ligand release and the recovery of fluorescence, which enables the detection of the released ligands by confocal microscopy.[93]

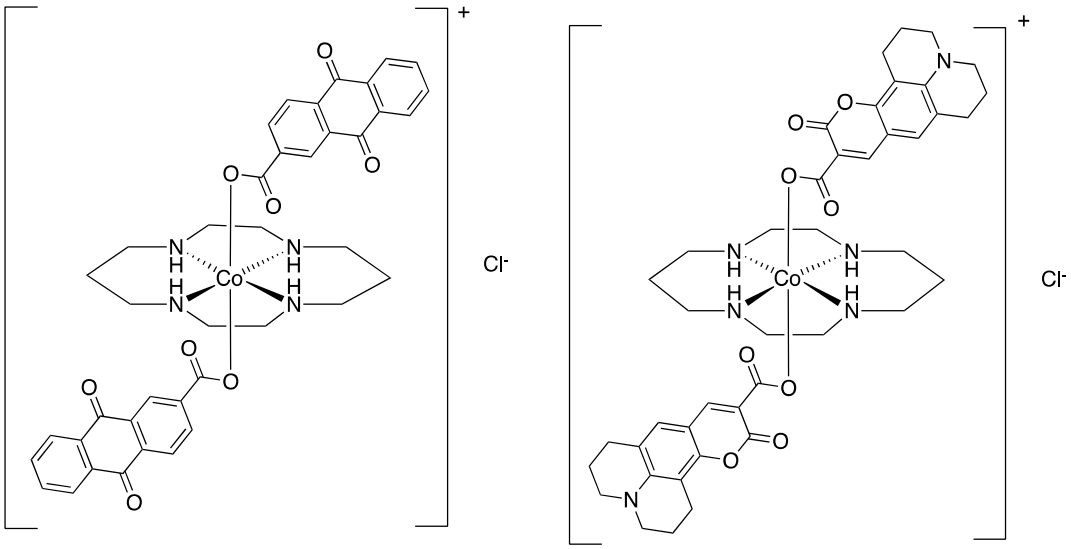

Figure 3.3 Chemical structures of [Co(C343)$_2$(cyclam)]Cl ($E_{1/2}$ = -250 mV vs. NHE) and [Co(AQ2C)$_2$(cyclam)]Cl ($E_{1/2}$ = -387 mV vs. NHE).[93]

3.2. Compound Design

Inspired by the fluorophore-containing metal complexes detailed in the previous section, we designed Co(III) salen complexes incorporating fluorescent molecules into the axial ligands. As discussed in Chapter 2, the lability of the Co(II) salen complex formed upon reduction of the inert Co(III) complex should allow for release of the fluorescent axial ligands, as shown in **Scheme 3.1**.

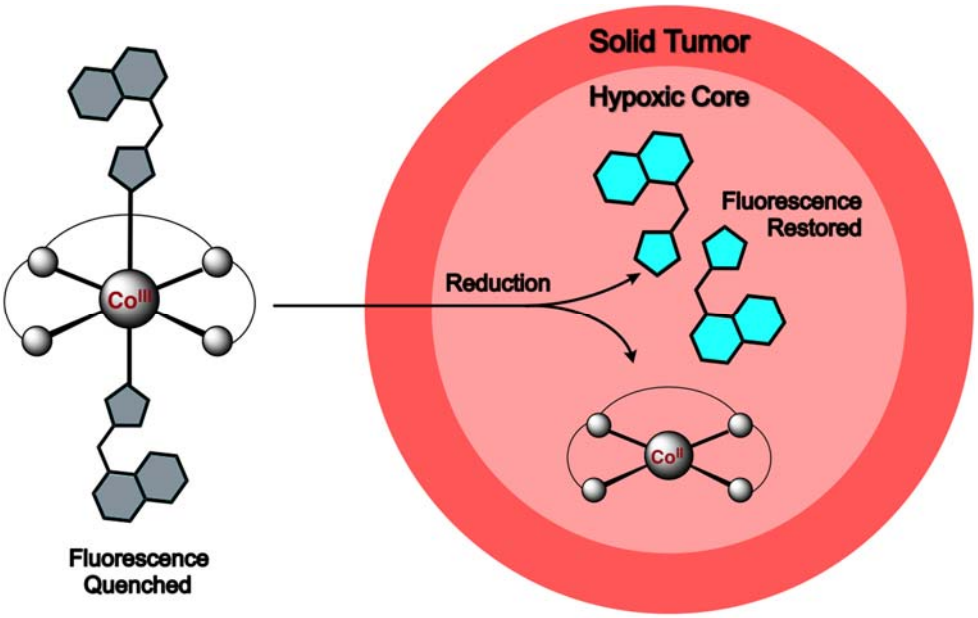

Scheme 3.1 Design of fluorophore-containing Co(III) complexes.
Within a solid tumor, the hypoxic core offers a more reducing environment in comparison to normal tissue, which provides a lower reduction potential to activate the complexes.

In Chapter 2, 1-methylimidazole was employed as an axial ligand, and the resulting octahedral Co(III) complex exhibits limited decomposition over 24 h in solution. In this chapter, a series of octahedral Co(III) salen complexes have been synthesized, using an imidazole-appended coumarin dye[121]as the axial ligand (**Figure 3.4**). Coumarin dyes are widely used in imaging[122,123] and pharmaceutical applications.[124-126]

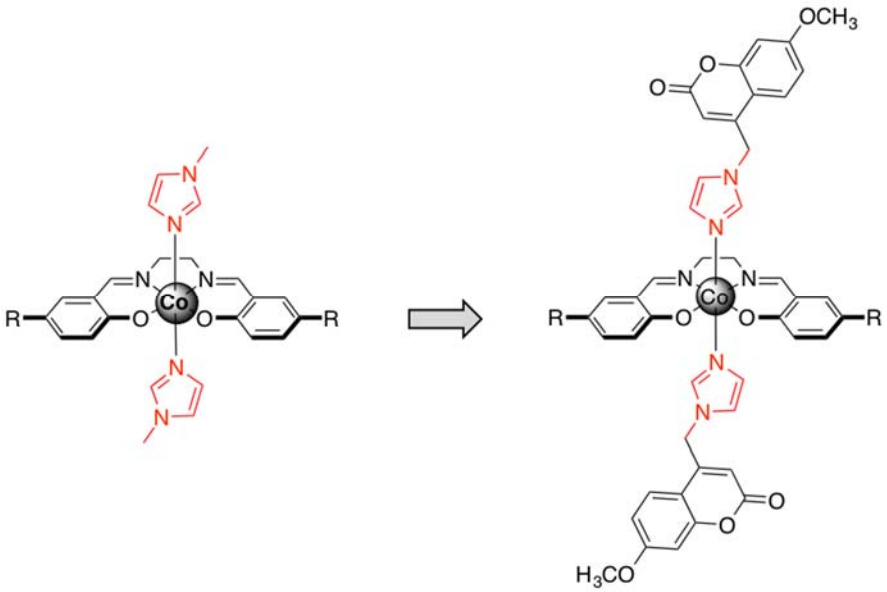

Figure 3.4 Compound design.

Building on the results of Chapter 2, the planar tetradentate salen ligand provides the opportunity to bind two monodentate axial fluorophore-containing ligands to Co(III) to form an octahedral complex, that should undergo release (fluorescence turn-on) upon reduction to Co(II). In addition, alteration of the salen phenolate *para*-substituents allows for tuning the Co(III) / Co(II) reduction potential, which is important for investigating the hypoxic-activation selectivity of the studied compounds. The Co(III) salen coumarin complexes were expected to show similar reduction potentials in comparison to the corresponding $[Co^{III}(salen^{R})(1\text{-MeIm})_2]ClO_4$ complexes detailed in Chapter 2 due to the same binding manner of 1-MeIm to Co.

In this chapter the synthesis of an imidazole-containing coumarin compound was completed, and then $[Co^{III}(salen^{R})(coumarin)_2]ClO_4$ complexes were synthesized following the same procedure as for the $[Co^{III}(salen^{R})(1\text{-MeIm})_2]ClO_4$ complexes detailed in Chapter 2. Due to low aqueous solubility, $[Co^{III}(salen^{R})(coumarin)_2]Cl$ complexes were also synthesized and studied. The chemical structure is shown in **Figure 3.5**.

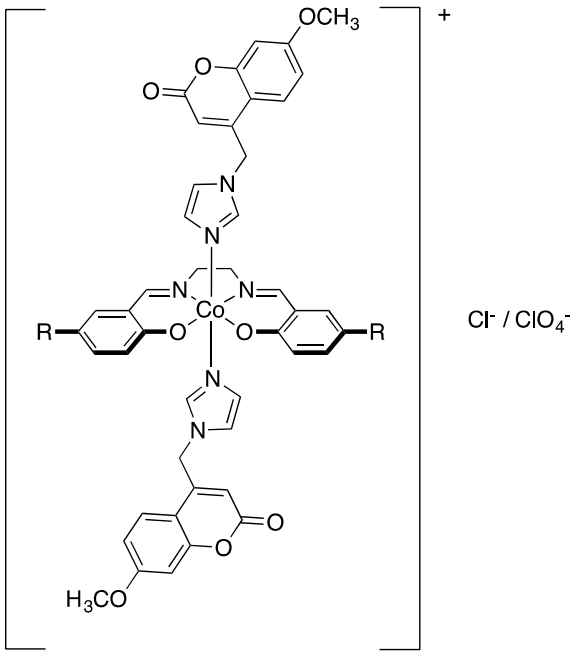

Figure 3.5 Chemical structure of the Co(III) salen coumarin complexes.

3.3. Experimental

3.3.1. Materials

All chemicals used were of the highest grade available and were further purified whenever necessary.

3.3.2. Instrumentation

Single-crystal X-ray crystallographic analysis of a red crystal of $[Co^{III}(salen^{CF3})(coumarin)_2]Cl$ was performed at the Advanced Light Source (Lawrence Berkeley National Laboratory) using synchrotron radiation tuned to λ = 0.7749 Å. Intensity data were collected at 296 K on a D8 goniostat equipped with a Bruker APEXII CCD detector at Beamline 11.3.1. For data collection, frames were measured for a duration of 1 s at 0.3° intervals of ω with a maximum 2θ value of 60°. The data frames were collected using the program APEX2 and processed using the program SAINT routine within APEX2. The data were corrected for absorption and beam corrections based on the multiscan technique as implemented in SADABS. The structure was solved by the intrinsic phasing

method and subsequent refinements were performed using ShelXle. All non-hydrogen atoms were refined anisotropically. All C−H hydrogen atoms were placed in calculated positions but were not refined. The crystal structure plot was produced using ORTEP-3 and rendered with POV-Ray (v.3.6.2). A summary of the crystal data and experimental parameters for the structure determination are given in **Table 3.1**.

Table 3.1 Selected crystallographic data for $[Co^{III}(salen^{CF3})(coumarin)_2]Cl$

$[Co^{III}(salen^{CF3})(coumarin)_2]Cl$	
Formula	$C_{46}H_{36}ClN_6O_8F_6Co$
Formula weight	1027.20
space group	P-1
a (Å)	10.5080(7)
b (Å)	14.4981(10)
c (Å)	16.3735(11)
α (°)	78.449(2)
β (°)	87.379(2)
γ (°)	69.154(2)
V [Å^3]	2283.1(3)
Z, D_{calc} [g/cm^3]	2
T (K)	273(2)
ρ_{calcd} (g cm^{-3})	1.494
λ (Å)	0.7749
μ (cm^{-1})	0.654
R indices[a] with I>2σ(I) (data)	0.0897
wR_2	0.2591
R_1	0.1035
Goodness-of-fits on F^2	1.009

3.3.3. Synthesis

4-((1*H*-imidazol-1-yl) methyl)-7-methoxy-2*H*-chromen-2-one (**24**)[121]

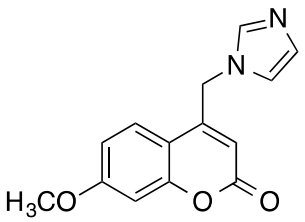

The synthetic procedure followed for this compound was similar to a literature report.[121] K_2CO_3 (4.62 g, 33.4 mmol) and 4-(bromomethyl)-7-methoxy-2*H*-chromen-2-one (2.28 g, 33.4 mmol) were added to a solution of imidazole (3 g, 11.1 mmol) in THF (2 mL). The reaction mixture was refluxed for 5 h, the K_2CO_3 was filtered, washed with warm EtOH, and the solution was concentrated *in vacuo*. The crude residue was recrystallized from EtOH. White crystals of the product were filtered and washed with cold EtOH, and dried *in vacuo*. Yield: 2.5 g, 87%. ^{1}H NMR (400 MHz, DMSO-d_6) δ 7.80 (d, *J* = 1.1 Hz, 1H), 7.78 (d, *J* = 8.8 Hz, 1H), 7.28 (t, *J* = 1.3 Hz, 1H), 7.06 (d, *J* = 2.5 Hz, 1H), 7.03-6.99 (m, 2H), 5.55 (d, *J* = 1.4 Hz, 2H), 5.46-5.42 (m, 1H), 3.87 (s, 3H). ^{13}C NMR (101 MHz, DMSO-d_6) δ 162.67, 159.98, 152.67, 138.20, 128.90, 125.64, 120.31, 112.40, 110.58, 108.84, 101.04, 56.01, 46.02, 18.55. ESI (+)-MS m/z (relative intensity) = 257.0902 ([**24**+H]$^+$). The characterization data matches the literature.[121] **Note that this compound is named 'coumarin' as the ligand in the associated Co(III) complexes below.**

$[Co^{III}(salen^{H})(coumarin)_2]ClO_4$ (**25**)

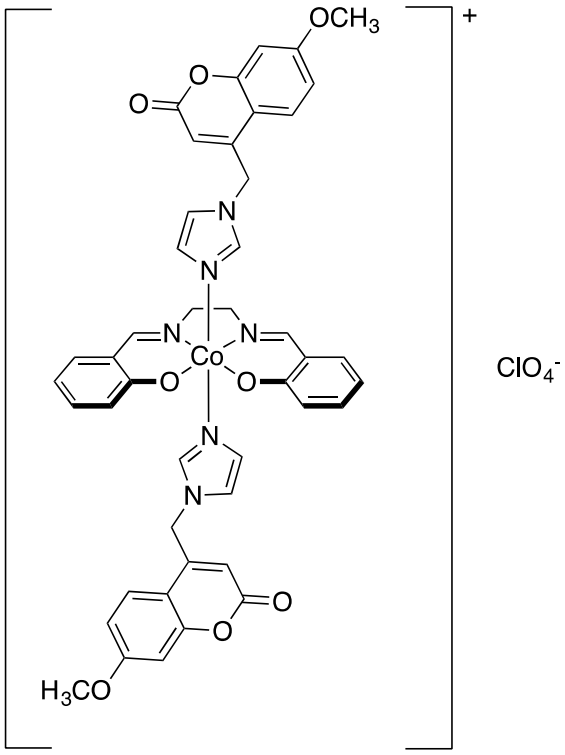

To $Co^{II}(salen^{H})$ (0.05 g, 0.15 mmol) in a 50:50 MeOH/DCM solution was added 3 eq. of 4-((1*H*-imidazol-1-yl) methyl)-7-methoxy-2*H*-chromen-2-one (**24**) (0.117 g, 0.45 mmol). The solution was stirred at room temperature for 2 h and the colour turned to dark red. $NaClO_4$ (0.1120 g, 0.92 mmol) in MeOH (2 mL) was then added, was then stirred at room temperature for 24 h. Slow evaporation of the solvent over 1 day afforded a dark red powder that was collected by filtration, washed with cold MeOH, and dried *in vacuo*. Yield: 0.06 g, 43%. ^{1}H NMR (400 MHz, DMSO-d_6) δ 7.44 (s, 1H), 7.09 (s, 1H), 6.70 (d, *J* = 8.9 Hz, 1H), 6.44-6.39 (m, 2H), 6.36 (t, *J* = 7.6 Hz, 1H), 6.21 (d, *J* = 8.5 Hz, 1H), 6.18 (d, *J* = 2.5 Hz, 1H), 6.04 (dd, *J* = 8.9, 2.5 Hz, 1H), 5.94 (s, 1H), 5.65 (t, *J* = 7.3 Hz, 1H), 4.66 (s, 2H), 4.40 (s, 1H), 3.21 (s, 2H), 3.02 (s, 3H). ^{13}C NMR (101 MHz, DMSO-d_6) δ 168.71, 165.44, 162.66, 159.52, 154.85, 150.89, 139.74, 134.88, 134.51, 128.11, 125.32, 122.30, 121.67, 118.11, 114.38, 112.34, 110.20, 109.17, 101.05, 56.77, 56.03, 47.37. ESI (+)-MS m/z (relative intensity) = 837.1751 ($[Co^{III}(salen^{H})(coumarin)_2]^{+}$).

$[Co^{III}(salen^{tBu})(coumarin)_2]ClO_4$ (**26**)

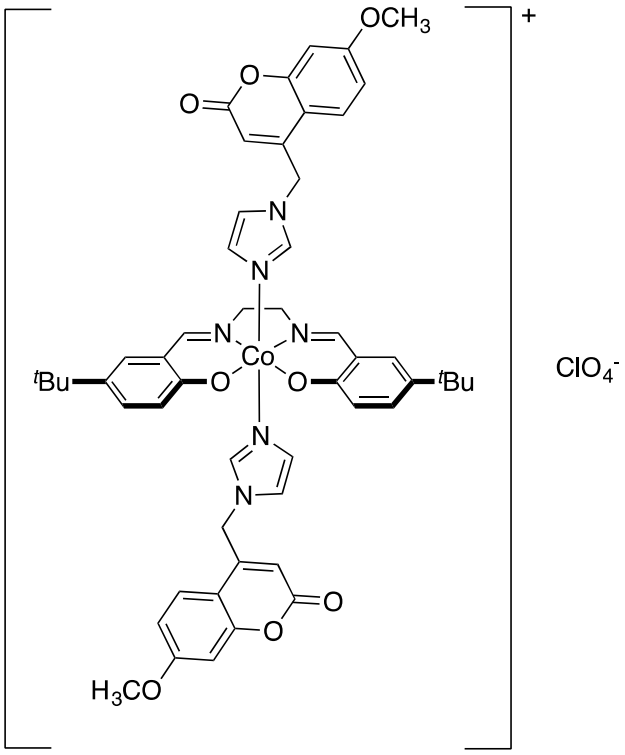

The complex was synthesized following the same procedure as for compound **25**, combining $Co^{II}(salen^{tBu})$ (0.046 g, 0.105 mmol), coumarin (**24**) (0.081 g, 0.315 mmol) and $NaClO_4$ (0.0772 g, 0.630 mmol). Yield: 0.10 g, 91%. ^{1}H NMR (400 MHz, DMSO-d_6) δ 8.29 (s, 1H, CNH), 7.93 (s, 1H), 7.57 (d, J = 9.0 Hz, 1H), 7.36-7.15 (m, 4H), 7.01 (d, J = 11.7 Hz, 1H), 6.90 (d, J = 9.1 Hz, 1H), 6.77 (s, 1H), 5.50 (s, 2H), 5.25 (d, J = 18.9 Hz, 1H), 4.03 (s, 2H), 3.86 (s, J = 9.4 Hz, 3H), 1.20 (s, 9H). ESI (+)-MS m/z (relative intensity) = 949.3355 ($[Co^{III}(salen^{tBu})(coumarin)_2]^+$). Elemental analysis calculated for $[Co^{III}(salen^{tBu})(coumarin)_2]ClO_4$•0.5 CH_2Cl_2 ($C_{52.5}H_{55}N_6Cl_2O_{12}Co$) C: 57.75%, H: 5.08%, N: 7.70%, Found C: 57.41%, H: 4.83%, N: 8.14%.

$[Co^{III}(salen^{Br})(coumarin)_2]ClO_4$ (**27**)

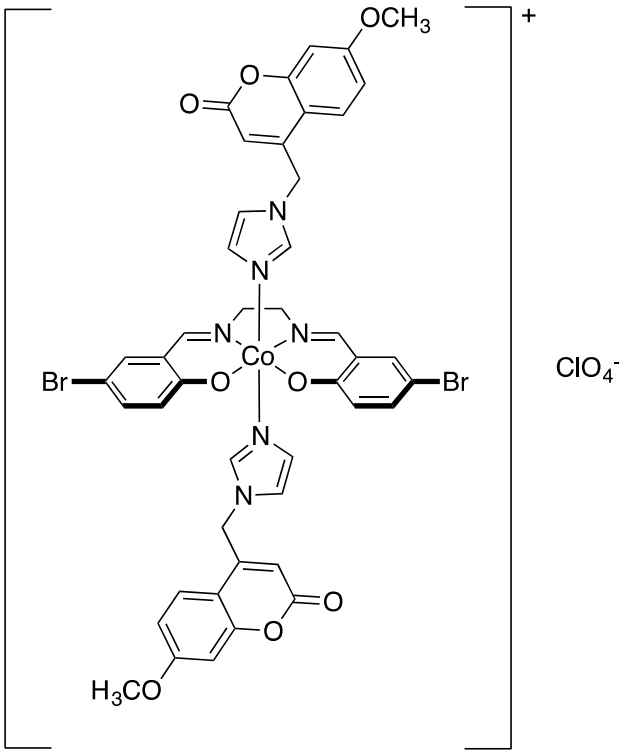

The complex was synthesized following the same procedure as for compound **25**, combining $Co^{II}(salen^{Br})$ (0.05 g, 0.104 mmol), coumarin (**24**) (0.080 g, 0.311 mmol) and $NaClO_4$ (0.076 g, 0.621 mmol). Yield: 0.05 g, 45%. ^{1}H NMR (400 MHz, DMSO-d_6) δ 8.28 (s, 1H), 7.92 (s, 1H), 7.54 (d, J = 8.9 Hz, 1H), 7.47 (d, J = 2.7 Hz, 1H), 7.31-7.27 (m, 2H), 7.03 (d, J = 2.5 Hz, 1H), 6.99 (d, J = 9.0 Hz, 1H), 6.89 (dd, J = 8.9, 2.5 Hz, 1H), 6.76 (t, J = 1.6 Hz, 1H), 5.49 (s, 2H), 5.31 (d, J = 1.4 Hz, 1H), 4.04 (d, J = 1.4 Hz, 2H), 3.86 (s, 3H). ESI (+)-MS m/z (relative intensity) = 995.0277 ($[Co^{III}(salen^{Br})(coumarin)_2]^+$).

$[Co^{III}(salen^{OMe})(coumarin)_2]ClO_4$ (**28**)

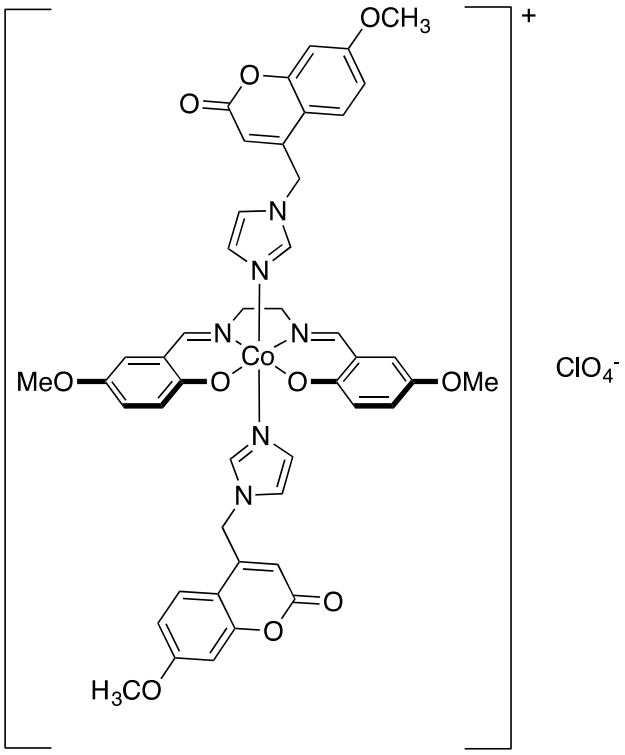

The complex was synthesized following the same procedure as for compound **25**, combining $Co^{II}(salen^{OMe})$ (0.10 g, 0.260 mmol), coumarin (**24**) (0.146 g, 0.570 mmol) and $NaClO_4$ (0.191 g, 1.56 mmol). Yield: 0.24 g, 92%. ^1H NMR (400 MHz, $CDCl_3$) δ 8.10 (s, 1H), 7.72 (t, *J* = 1.5 Hz, 1H), 7.20 (t, *J* = 8.7 Hz, 2H), 7.01-6.96 (m, 1H), 6.87 (t, *J* = 1.5 Hz, 1H), 6.80-6.71 (m, 3H), 6.68 (d, *J* = 3.2 Hz, 1H), 5.46 (d, *J* = 3.2 Hz, 1H), 5.23 (s, 2H), 4.16 (s, 2H), 3.86 (s, 3H), 3.74 (s, 3H).

$[Co^{III}(salen^{H})(coumarin)_2]Cl$ (**29**)

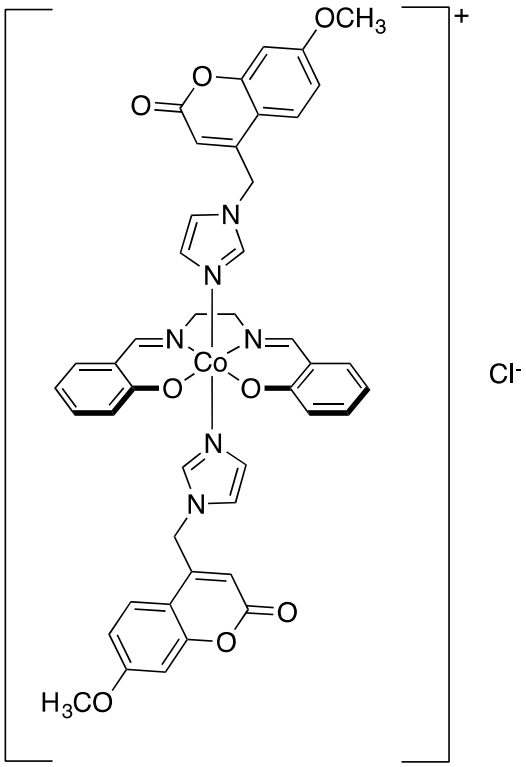

Three drops of NEt_3 was added to a solution of $Salen^{H}$ (0.123 g, 0.378 mmol in DCM) in a round-bottom flask under N_2. $CoCl_2$ (0.050 g, 0.385 mmol in MeOH) was added into the flask, which was then purged with N_2 for 20 min. Then coumarin (**24)** (0.213 g, 0.831 mmol) was added to the reaction. The solution was stirred in air overnight. The solvent was then removed *in vacuo*, and a brown solid was obtained. The solid was washed with EtOAc and filtered, and then the crude product was further purified by size exclusion chromatography using a Sephadex® (LH-20; MeOH eluent). Yield: 0.28 g, 83%. ^{1}H NMR (400 MHz, MeOD) δ 8.21 (s, 1H), 7.74 (t, *J* = 1.5 Hz, 1H), 7.42 (d, *J* = 8.8 Hz, 1H), 7.27-7.18 (m, 2H), 7.14-7.08 (m, 2H), 6.85 (d, *J* = 2.5 Hz, 1H), 6.83-6.78 (m, 2H), 6.58-6.53 (m, 1H), 5.40 (d, *J* = 1.4 Hz, 2H), 5.27 (d, *J* = 1.3 Hz, 1H), 4.08 (s, 2H), 3.85 (s, 3H). ^{13}C NMR (101 MHz, MeOD) δ 170.42, 166.26, 164.89, 162.26, 156.74, 151.99, 141.09, 136.96, 135.86, 129.65, 125.99, 123.83, 122.94, 119.86, 117.03, 113.94, 110.73, 111.69, 111.40, 102.11, 58.37, 56.51. ESI (+)-MS m/z (relative intensity) = 837.2088 ($[Co^{III}(salen^{H})(coumarin)_2]^{+}$). Elemental analysis calculated for

$[Co^{III}(salen^{H})(coumarin)_2]Cl•CH_2Cl_2$ ($C_{45}H_{40}N_6Cl_3O_8Co$) C: 56.41%, H: 4.21%, N: 8.77%, Found C: 56.19%, H: 4.03%, N: 9.26%.

$[Co^{III}(salen^{OMe})(coumarin)_2]Cl$ (**30**)

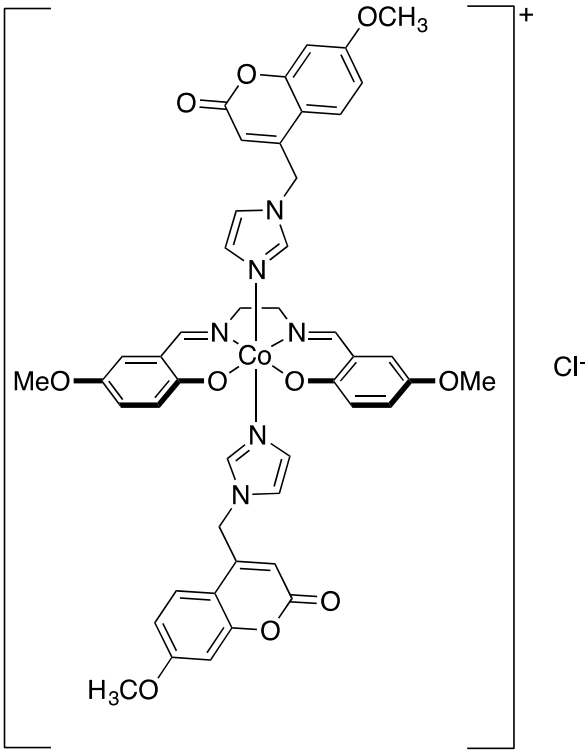

The complex was synthesized following the same procedure as for **29**, combining $Salen^{OMe}$(0.13 g, 0.385 mmol), $CoCl_2$ (0.05 g, 0.385 mmol) and coumarin **24** (0.22 g, 0.847 mmol). Yield: 0.35 g, 97%. ^{1}H NMR (400 MHz, MeOD) δ 8.19 (s, 1H), 7.73 (t, *J* = 1.4 Hz, 1H), 7.45 (d, *J* = 9.0 Hz, 1H), 7.14 (t, *J* = 1.7 Hz, 1H), 7.07 (d, *J* = 9.2 Hz, 1H), 6.96 (dd, *J* = 9.2, 3.1 Hz, 1H), 6.91 (d, *J* = 2.5 Hz, 1H), 6.85 (dd, *J* = 8.9, 2.5 Hz, 1H), 6.82 (t, *J* = 1.5 Hz, 1H), 6.77 (d, *J* = 3.2 Hz, 1H), 5.43 (d, *J* = 1.3 Hz, 2H), 5.38-5.34 (m, 1H), 4.09 (s, 2H), 3.89 (s, 3H), 3.73 (s, 3H). ^{13}C NMR (101 MHz, MeOD) δ 169.90, 164.89, 162.27, 161.02, 157.26, 156.76, 152.07, 151.31, 141.05, 129.61, 126.98, 125.98, 124.48, 122.93, 118.50, 115.77, 113.92, 111.69, 110.86, 102.11, 58.35, 56.50, 56.27. ESI (+)-MS m/z (relative intensity) = 897.2297 ($[Co^{III}(salen^{OMe})(coumarin)_2]^+$). Elemental analysis calculated for $[Co^{III}(salen^{OMe})(coumarin)_2]Cl•1CH_2Cl_2•0.5H_2O$ ($C_{47}H_{45}N_6Cl_3O_{10.5}Co$) C: 54.96%, H: 4.42%, N: 8.18%, Found C: 54.82%, H: 3.87%, N: 8.88%.

$[Co^{III}(salen^{CF3})(coumarin)_2]Cl$ (**31**)

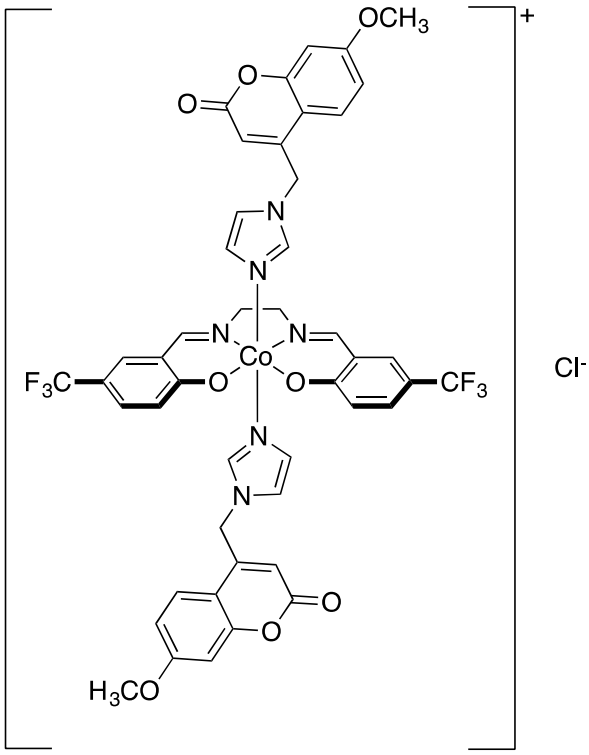

The complex was synthesized following the same procedure as for **29**, combining $Salen^{CF3}$ (0.071 g, 0.176 mmol), $CoCl_2$ (0.023 g, 0.176 mmol) and coumarin **24** (0.09 g, 0.351 mmol). Yield: 94%. ^{1}H NMR (400 MHz, MeOD) δ 8.37 (s, 1H), 7.86 (t, *J* = 1.4 Hz, 1H), 7.71-7.67 (m, 1H), 7.50 (d, *J* = 8.8 Hz, 2H), 7.27 (d, *J* = 9.0 Hz, 1H), 7.19 (t, *J* = 1.7 Hz, 1H), 6.91 (d, *J* = 2.5 Hz, 1H), 6.89 – 6.83 (m, 2H), 5.47 (d, *J* = 1.4 Hz, 2H), 5.31 (s, 1H), 4.20 (s, 2H), 3.89 (s, 3H). ^{19}F NMR (400 MHz, MeOD) δ -62.95 (s). ^{13}C NMR (101 MHz, MeOD) δ 170.82, 168.64, 164.95, 162.26, 156.77, 152.17, 141.22, 134.98, 132.69, 129.51, 125.95, 124.57, 123.48, 119.34, 113.99, 111.64, 110.49, 102.05, 68.86, 58.68, 56.49, 47.95, 9.22. ESI (+)-MS m/z (relative intensity) = 973.1085 ($[Co^{III}(salen^{CF3})(coumarin)_2]^+$). Elemental analysis calculated for $[Co^{III}(salen^{CF3})(coumarin)_2]Cl \bullet 0.5CH_2Cl_2 \bullet 3H_2O$ ($C_{46.5}H_{43}N_6Cl_2O_{11}CoF_6$) C: 50.51%, H: 3.92%, N: 7.60%, Found C: 50.48%, H: 4.53%, N: 7.54%.

3.4. Results and Discussion

3.4.1. Synthesis

The coumarin (4-((1*H*-imidazol-1-yl)methyl)-7-methoxy-2*H*-chromen-2-one) (**24**) was obtained by refluxing K_2CO_3, imidazole with commercially available 4-bromomethyl-7-methoxycoumarin as reported in a literature procedure.[121] Initially, $[Co^{III}(salen^{R})(coumarin)_2]ClO_4$ (R = OMe, *t*Bu, H, Br) complexes were synthesized by reacting the $Co^{II}(salen^{R})$ complexes with excess coumarin (**24**) and $NaClO_4$ (shown in **Scheme 3.2**). The synthesis of $[Co^{III}(salen^{NO2})(coumarin)_2]ClO_4$ was not successful due to the low solubility of $Co^{II}(salen^{NO2})$.

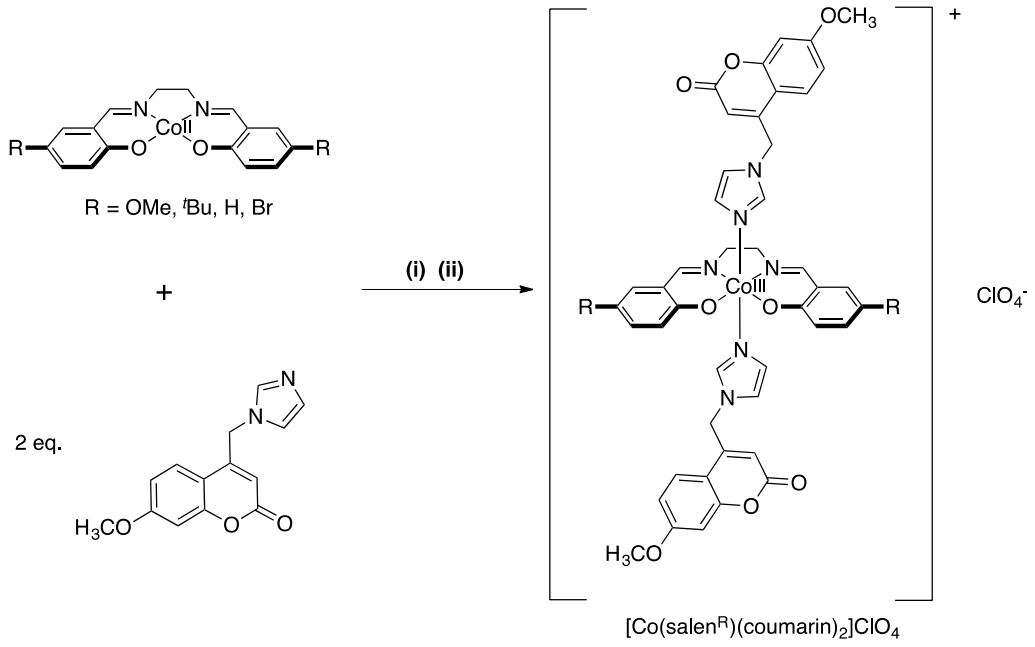

Scheme 3.2 Synthetic route for $[Co^{III}(salen^{R})(coumarin)_2]ClO_4$ complexes.
Reaction conditions: (i) MeOH/DCM, triethylamine, N_2, 298 K, 1 h; (ii) $NaClO_4$, air, MeOH/DCM, 298 K, overnight.

Even though the Co(III) salen complexes precipitated from solution, a free coumarin impurity (less than 5% as detected by ^1H NMR) was present in most of the samples. Changing the reaction conditions, including using exactly 2 eq. of the coumarin ligand (**24**) resulted in the same amount of impurity in the isolated compounds. Further purification of these complexes is a challenge due to low solubility in most solvents including MeOH and water, and decomposition of the complexes on silica gel. For this

reason, elemental analysis and ^{13}C NMR are not presented in the Experimental section for certain $[Co^{III}(salen^{R})(coumarin)_2]ClO_4$ complexes (R = OMe, *t*Bu, Br). Therefore, we investigated the synthesis of the chloride complexes, $[Co^{III}(salen^{R})(coumarin)_2]Cl$, in a one pot procedure by mixing $salen^{R}$ (R = OMe, H, CF_3) ligands with anhydrous $CoCl_2$ and coumarin **24** (shown in **Scheme 3.3**). Further purification was completed using size exclusion chromatography on Sephadex® LH-20. Other salen derivatives (R = Br) could not be obtained with satisfactory purity using this method. Among the $[Co^{III}(salen^{R})(coumarin)_2]Cl$ complexes, complex **30** (R= OMe) exhibits the highest ligand exchange rate (see later), hence the intact molecular ion could not be observed using mass spectrometry. In this study, $[Co^{III}(salen^{R})(coumarin)_2]Cl$ (R = OMe, H, CF_3) complexes were carried forward as high purity samples were obtained.

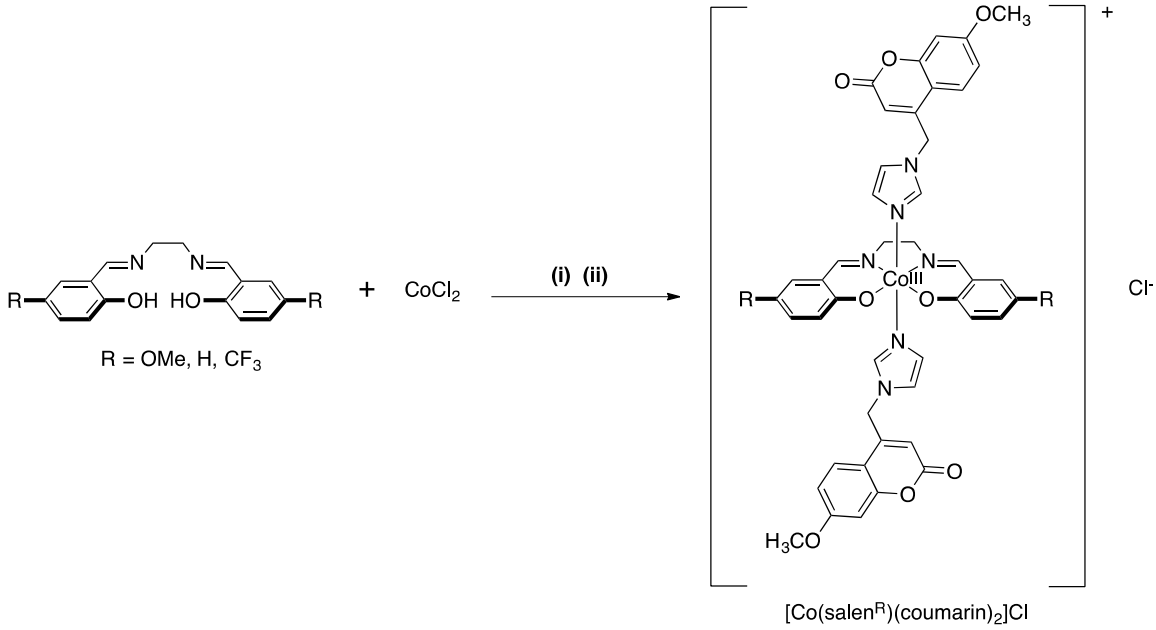

Scheme 3.3 Synthetic route for $[Co^{III}(salen^{R})(coumarin)_2]Cl$ complexes.
Reaction Conditions: (i) MeOH/DCM, triethylamine, N_2, 298 K, 10 min; (ii) 2 eq. coumarin (24), air, MeOH/DCM, 298 K, overnight.

3.4.2. X-ray Structure Determination

X-ray quality crystals of $[Co^{III}(salen^{CF3})(coumarin)_2]Cl$ were grown by slow evaporation of a concentrated MeOH solution. Initial experiments at SFU did not provide a high quality data set and thus the crystal sample was sent to the Stanford Synchrotron Radiation Laboratory to obtain a better data. As shown in **Figure 3.6**, the salen ligand is bound to Co(III), showing in the equatorial plane with the coumarin molecules in the axial positions. However, one of the axial coumarin ligands is very distorted, possibly due to the crystal arrangement; stacking of coumarin molecules between two close complexes. Even though the data set is not ideal, an octahedral geometry and structure of the coumarin ligand can be observed.

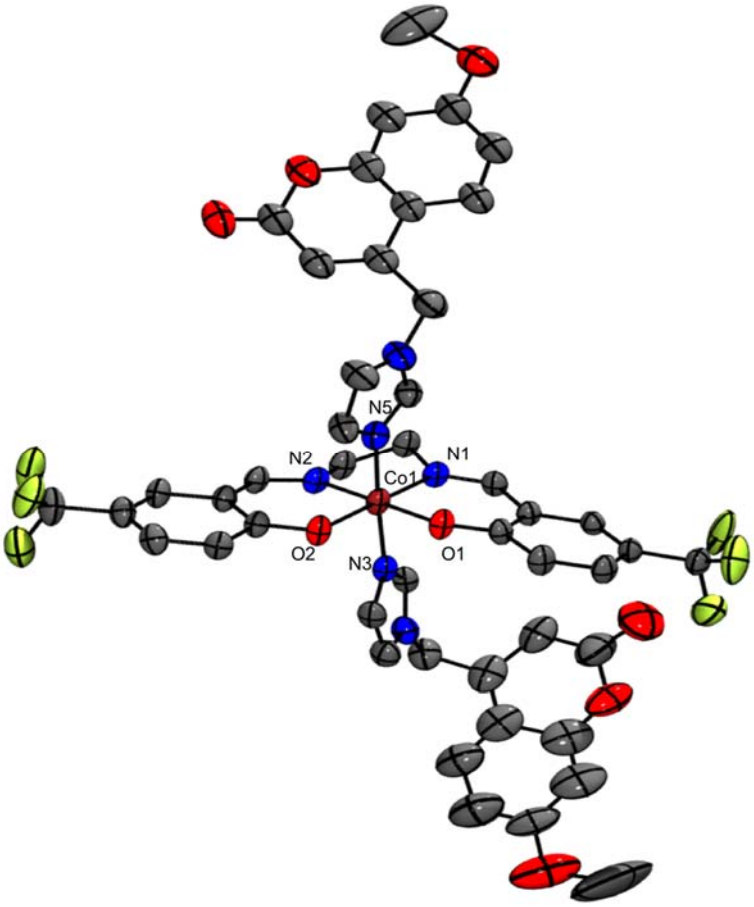

Figure 3.6 Crystal structure of $[Co^{III}(salen^{CF3})(coumarin)_2]Cl$
(thermal ellipsoids shown at 50% probability). Hydrogen atoms and solvent molecules excluded for clarity.

Table 3.2 Selected bond distances (Å) and angles (°) for $[Co^{III}(salen^{CF3})(coumarin)_2]Cl$ complexes.

$[Co(salen^{CF3})(coumarin)_2]Cl$	
Co1 – O1	1.902(3)
Co1 – O2	1.887(3)
Co1 – N1	1.890(4)
Co1 – N2	1.895(4)
Co1 – N3	1.946(4)
Co1 – N5	2.02(3)
O2 – Co1 – N5	88.4(12)
N1 – Co1 – N5	92.6(12)
N2 – Co1 – N5	94.4(12)
O1 – Co1 – N5	86.0(12)
O2 – Co1 – N3	89.24(17)
N1 – Co1 – N3	89.84(18)
N2 – Co1 – N3	91.70(18)
O1 – Co1 – N3	87.82(16)
O1 – Co1 – N2	179.51(18)
O2 – Co1 – N1	179.02(18)

In the **$[Co^{III}(salen^{CF3})(coumarin)_2]Cl$** complexes, the Co(III) ion is coordinated by two oxygen atoms (O1, O2) and two nitrogen atoms (N1 ,N2) from the tetradentate salen ligand. The O2–Co1–N5, N1–Co1–N5, N2–Co1–N5, O1–Co1–N5, O2–Co1–N3, N1–Co1–N3, N2–Co1–N3, and O1–Co1–N3 angles differ only slightly from 90°, and the O2–Co1–N1, O1–Co1–N2 angles differ only slightly from 180° as indicated in **Table 3.2**. The bond distances between the Co(III) centre and the axial imidazole ligands (Co1 – N3 and Co1 – N5) are longer in comparison to the equatorial bond lengths (both Co-O and Co-N), suggesting that the binding of axial ligands is weaker in comparison to the equatorial salen ligand, similar as observed in Chapter 2 for $[Co^{III}(salen^{R})(1\text{-MeIm})_2]ClO_4$ complexes.

3.4.3. Electrochemistry

The electrochemical properties of the $[Co^{III}(salen^{R})(coumarin)_2]Cl$ complexes were assessed to better understand how the different phenolate *para*-substituents shift the Co(III) / Co(II) redox couple in the octahedral Co(III) complexes. The CV experimental set

up is the same as that for $[Co^{III}(salen^{R})(1\text{-MeIm})_2]ClO_4$,as discussed in Chapter 2. A more negative Co(III) / Co(II) reduction potential was expected for complexes with electron-donating *para*-phenolate ring substituents (OMe > H > CF_3). In addition, the complexes are expected to exhibit a similar irreversible redox process in comparison to $[Co^{III}(salen^{R})(1\text{-MeIm})_2]ClO_4$ upon reduction due to the same binding manner of coumarin and 1-MeIm.

As shown in **Figure 3.7** and **Table 3.3**, there is a large value of ΔE_p as well as a different current response for the reduction (E_c) and oxidation (E_a) processes. These results suggest an irreversible electrochemical process for $[Co^{III}(salen^{R})(coumarin)_2]Cl$ that is similar to that detailed for the $[Co^{III}(salen^{R})(1\text{-MeIm})_2]ClO_4$ complexes in Chapter 2. It is proposed that scanning cathodically, the $[Co^{III}(salen^{R})(coumarin)_2]Cl$ complexes are reduced to $[Co^{II}(salen^{R})(coumarin)_2]$ (E_c). Axial ligand release and structural re-arrangement affords square planar $Co^{II}(salen^{R})$ complexes that are then re-oxidized to $[Co^{III}(salen^{R})]$ (E_a). Although the $E_{1/2}$ values of these complexes are similar (**Table 3.3**), ranging from -60 to 45 mV, the $E_{1/2}$ values follow a trend consistent with the relative electron-donating ability of the *para*-phenolate ring substituents (OMe > H > CF_3).

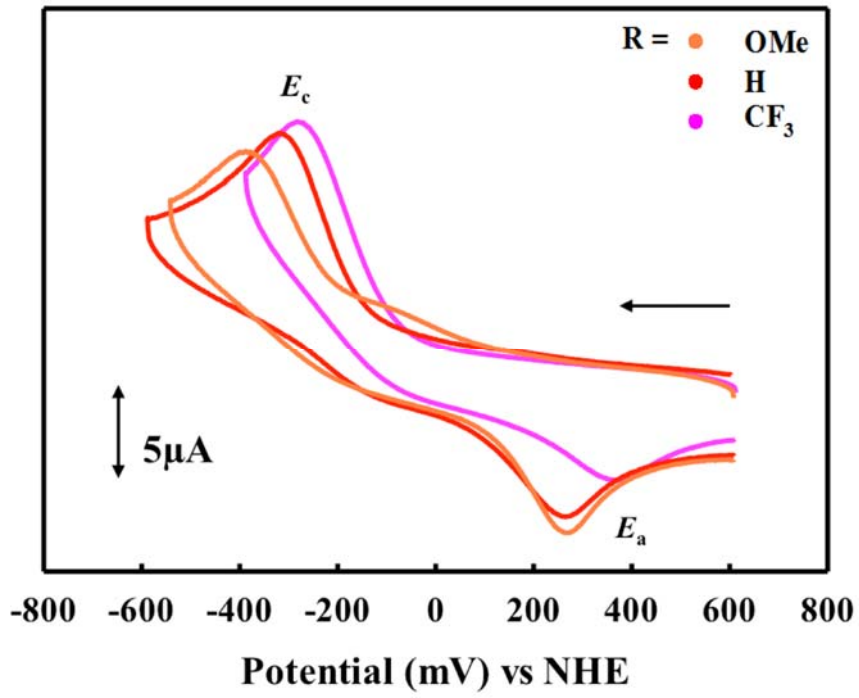

Figure 3.7 Cyclic Voltammogram for $[Co^{III}(salen^{R})(coumarin)_2]Cl$.
The direction of the arrow signifies the direction of the scans. Conditions: 1 mM complex, 0.1 M $^{n}Bu_4NClO_4$, scan rate 100 mV s^{-1}, DMF, 293 K.

Table 3.3 **Reduction potentials (mV) for $[Co^{III}(salen^{R})(coumarin)_2]Cl$ versus NHE.**

$[Co^{III}(salen^{R})(coumarin)_2]Cl$	E_c	E_a	$E_{1/2}$	ΔE_p[a]
R = OMe	-390	270	-60	660
R = H	-310	270	-20	580
R = CF_3	-280	370	45	650

[a] Peak-to-peak differences ($\Delta E_p = |E_a - E_c|$). Peak-to-peak difference for the Fc^+/Fc couple at 298 K is 120 mV.

The $E_{1/2}$ values of these complexes are ca. 80 mV more positive in comparison to the $[Co^{III}(salen^{R})(1\text{-MeIm})_2]ClO_4$ derivatives with the same salen ligands. The reduction potentials of $[Co^{III}(salen^{H})(1\text{-MeIm})_2]ClO_4$, $[Co^{III}(salen^{H})(coumarin)_2]ClO_4$, and $[Co^{III}(salen^{H})(coumarin)_2]Cl$ are compared in Figure **3.8** and Table **3.4**. The $E_{1/2}$ value changes from -100 mV to -20 mV, which indicates that the $E_{1/2}$ value depends slightly on the identity of the axial ligand and the counterion in this experiment. The same trend is observed for the OMe complexes (Appendix **3.1 – 3.2**).

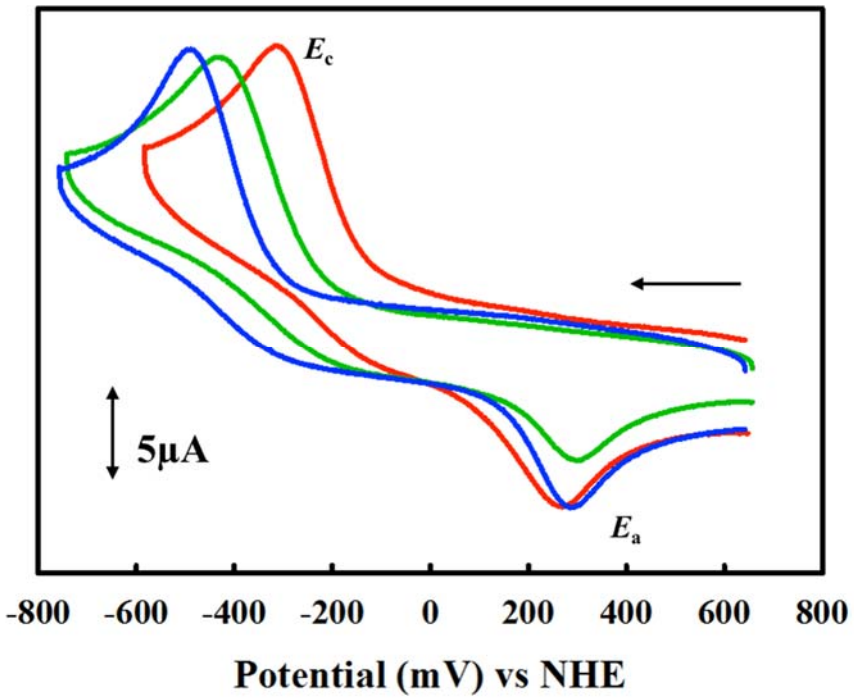

Figure 3.8 **Reduction potentials for $[Co^{III}(salen^{H})(1\text{-MeIm})_2]ClO_4$ (Blue), $[Co^{III}(salen^{H})(coumarin)_2]ClO_4$ (Green), and $[Co^{III}(salen^{H})(coumarin)_2]Cl$ (Red).**

The direction of the arrow signifies the direction of the scans. Conditions: 1 mM complex, 0.1 M $^{n}Bu_4NClO_4$, scan rate 100 mV s^{-1}, DMF, 293 K.

Table 3.4 Reduction potentials (mV) for complexes versus NHE.

Complex	E_c	E_a	$E_{1/2}$	ΔE_p[a]
$[Co^{III}(salen^{H})(1\text{-MeIm})_2]ClO_4$	-490	290	-100	780
$[Co^{III}(salen^{H})(coumarin)_2]ClO_4$	-430	290	-70	720
$[Co^{III}(salen^{H})(coumarin)_2]Cl$	-310	270	-20	580

3.4.4. Preliminary Fluorescence Experiment

Under short wavelength UV light, the free coumarin ligand is fluorescent in comparison to $[Co^{III}(salen^{H})(coumarin)_2]Cl$ (**Figure 3.9**), suggesting that upon coordination, the fluorescence of the coumarin is quenched by the Co(III) ion.

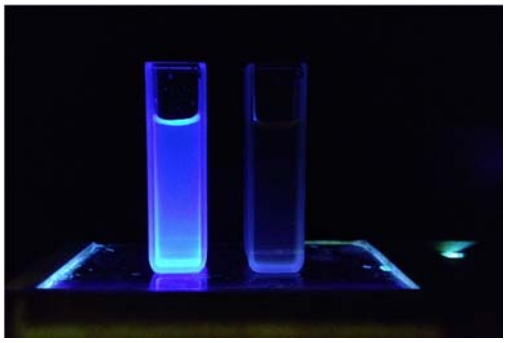

Figure 3.9 Fluorescence experiment using λ_{ex} (254 nm) 6 μM Coumarin (Left) and 3 μM $[Co^{III}(salen^{H})(coumarin)_2]Cl$ (Right).

3.5. Conclusion

In this chapter, the syntheses of $[Co^{III}(salen^{R})(coumarin)_2]ClO_4$ (R = OMe, ^{t}Bu, H, Br) and $[Co^{III}(salen^{R})(coumarin)_2]Cl$ (R = OMe, H, CF_3) complexes are described. Due to the presence of an impurity in the $[Co^{III}(salen^{R})(coumarin)_2]ClO_4$ complexes, we pursued the synthesis of the $[Co^{III}(salen^{R})(coumarin)_2]Cl$ complexes, which were purified, fully characterized, and displayed improved solubility in water and MeOH. X-ray crystallographic analysis of $[Co^{III}(salen^{CF3})(coumarin)_2]Cl$ showed the expected octahedral structure, with two axial coumarin ligands bound. The reduction potentials of complexes were correlated with the electronic properties of the phenolate *para*-substituents and, as expected, the more electron-rich the ligands, gave complexes with more negative Co(III) / Co(II) reduction potentials. Cyclic voltammograms spectra of $[Co^{III}(salen^{R})(coumarin)_2]Cl$ show an irreversible electrochemical process, and the large potential difference between

E_c and E_a is likely due to structural rearrangement and axial ligand release upon reduction. Qualitative emission studies using short wavelength UV light (254 nm) show a much higher fluorescence for the imidazole-coumarin ligand in comparison to the $[Co^{III}(salen^{H})(coumarin)_2]Cl$ complex, suggesting that the coumarin fluorescence is largely quenched upon complexation. Chapter 4 will further detail the photophysical studies with these complexes.

Chapter 4.

Photophysical Properties of $[Co^{III}(salen^{R})(coumarin)_2]Cl$ complexes

4.1. Introduction to Spectrophotometry

An electron in a molecule can be excited from its ground electronic state (S_0) to an excited electronic state (S_n, n ≥ 1), when a photon with a specific energy is absorbed. Photon absorption occurs when the photon energy matches the energy gap between the initial and final states **Equation 4.1**.

$$\Delta E = h\upsilon \qquad \textbf{(4.1)}$$

According to the Pauli exclusion principle, each molecular orbital can hold no more than two electrons.[127] The spin quantum number, m_s, describes the orientation of the electron spin, and the value can be ± ½. The sum of the electron spins in the system is indicated as the total spin angular momentum (S). The spin multiplicity (2S + 1) defines the number of orientations of the spin angular momentum.[128,129] The ground state for most organic molecules is an electronic singlet in which all electrons are spin-paired. When an electron in a singlet ground state is excited to a higher energy level, it can either form an excited singlet state or an excited triplet state **Figure 4.1**.[128,129]

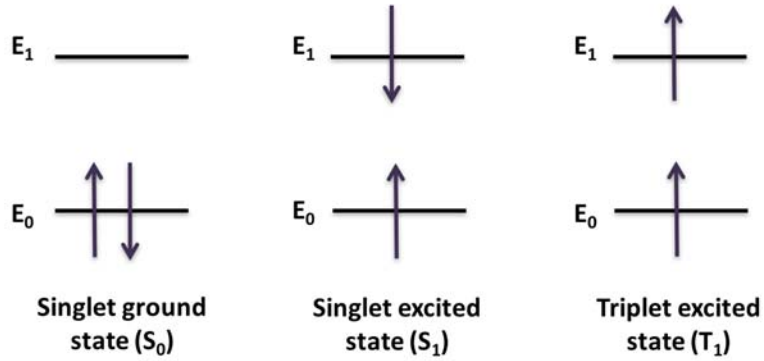

Figure 4.1 Example singlet ground electronic state and excited electronic states.

Photoluminescence begins with the absorption of light to create an excited state. The electron, after being excited to a higher electronic energy level, can decay to the ground state in many different ways. Examples of these pathways are shown in the Jablonski energy diagram (**Figure 4.2)**.

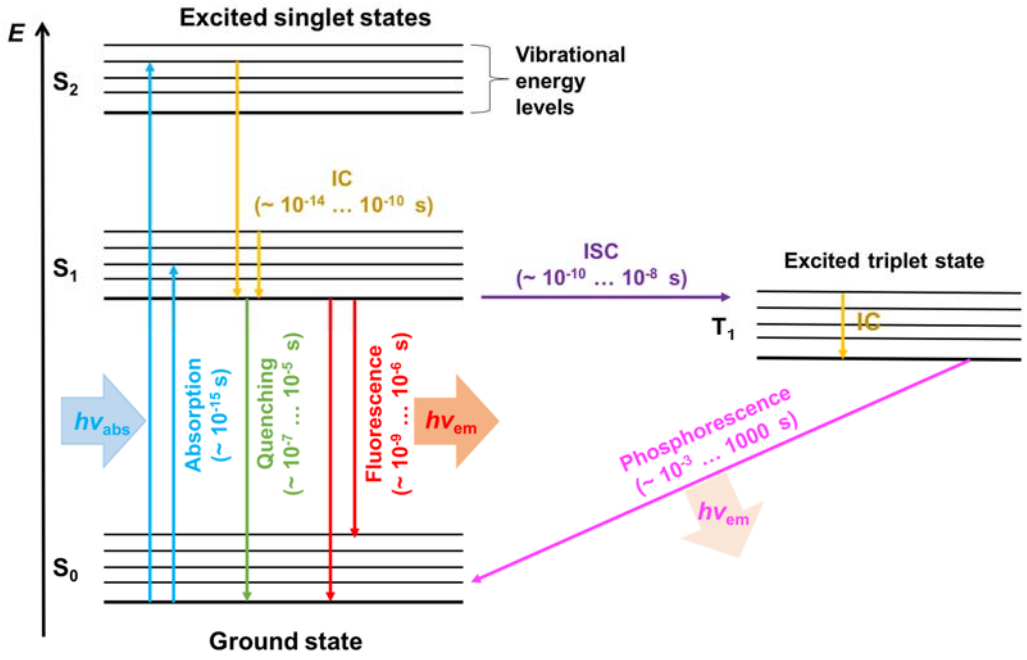

Figure 4.2 Jablonski energy diagram.
($h\nu_{abs}$, absorbance wavelength; $h\nu_{em}$, emission wavelength).[128-130]

During the relaxation process from an excited state following initial photon absorbance, electrons can follow non-radiative or radiative pathways to the ground state. One non-radiative pathway is through vibrational relaxation, where the energy is released within the same molecule, or transferred to other molecules nearby. Another non-radiative pathway is internal conversion (IC), a process by which an electron moves from one electronic state to a lower electronic state, and the excitation energy is transformed to heat. In addition, intersystem crossing (ISC, singlet to triplet) can occur, but the process is forbidden and thus less probable.

Radiative processes result from photon release during decay and occur either via fluorescence or phosphorescence **Figure 4.2**. Fluorescence occurs when the electronic transition is between states with the same spin quantum value (S_1 to S_0, etc.), and usually occurs on the nanosecond timescale (≈ 10^{-9} to 10^{-6} s). Phosphorescence refers to an

electronic transition between different spin quantum values (triplet to singlet), which happens over a longer timescale due to the transition between electronic states with different spin quantum values (≈ 10^{-3} to 10^{3} s).[128-130]

In an absorption spectrum, many bands can exist (S_0 to S_1, S_0 to S_2, S_0 to S_3, etc.), but only the $S_0 \rightarrow S_1$ transition are allowed for absorption and photoluminescence (S_1 to S_0). The absorption spectrum is proportional to the likelihood of a photon being absorbed.[128-130] In order to determine the excitation wavelength that affords the maximum emission wavelength, an absorption spectrum should be obtained first. In absorption spectroscopy, the absorbance (A) is the negative logarithm of transmittance (T) (**Equation 4.2)**.

$$A = -\log_{10} T \qquad \textbf{(4.2)}$$

The Beer-Lambert Law (**Equation 4.3**), shows that, when the light path length (l) and the extinction coefficient (ε) are fixed, the relationship between absorbance (A) and concentration (c) is linear.[131,132]

$$A = \varepsilon l c \qquad \textbf{(4.3)}$$

Absorption spectra are usually shown as a plot of absorbance versus wavelength (nm). The excitation wavelength (λ_{ex}) in fluorescence spectra is usually chosen so as to afford the maximum emission intensity. Therefore, scanning through the absorption spectrum of a molecule while comparing the emission intensity (integrated area under the curve of emission spectra) allows for the determination of the optimal excitation wavelength. After obtaining the excitation and emission spectra, the difference between the excitation and emission wavelengths can be determined, which is known as the Stokes shift.[131,132] During the excitation and emission processes, vibrational relaxation occurs and heat is released, this results in a redshift of the emission wavelength (λ_{em}) in comparison to the excitation wavelength. In this chapter, the luminescence properties of $[Co^{III}(salen^{R})(coumarin)_2]Cl$ complexes (R = OMe **28**, R = H **29** and R = CF_3 **30**) will be discussed. The photophysical properties of coumarin (23) and the $[Co^{III}(salen^{R})(coumarin)_2]Cl$ complexes are compared, including their respective absorption, excitation, and emission profiles. The release of the axial ligands is measured

by monitoring the fluorescence intensity in the presence of a reducing agent and in the presence of a competing ligand.

4.2. Experimental

4.2.1. Instrumentation

Absorption spectra were collected using a Varian CARY 5000 UV-Visible-Near IR spectrophotometer. Measurements were performed in single-beam mode with baseline correction using the same quartz cuvette (1 cm path length) in all experiments. The excitation and emission spectra were collected using a Photon Technology International (PTI) 814 photomultiplier detection system. Signals were collected at 90° to the incident excitation beam. The maximum emission of the coumarin solution was used as a reference. The photophysical data were processed with the Felix32 system. The kinetic studies of coumarin ligand release over 12 hours were performed at 25 °C under constant agitation, and each well in the 96-well plate was excited at 327 nm and emission was collected at 400 nm using a Synergy 4 fluorescence plate reader from BioTek.

4.2.2. Sample Preparation

For the UV-Vis spectroscopy, solutions of 50 μM of $Co^{II}(salen^{R})$, $[Co^{III}(salen^{R})(coumarin)_2]Cl$ and coumarin (**23**) were prepared in 2% DMSO/PBS (0.01 M) pH 7.4. All aqueous solutions used in fluorescence studies were freshly prepared using filtered deionized water. The final concentrations were $[Co^{III}(salen^{R})(coumarin)_2]Cl$ 3 μM, and coumarin ligand 6 μM, in 2% DMSO/PBS (0.01 M) pH 7.4 medium. The ligand release study was completed under aerobic conditions, using $Na_2S_2O_4$ ($E_{1/2}$ = -660 mV vs. NHE)[133] as the reducing agent. A 10-fold excess (30 μM) of $Na_2S_2O_4$ was used to ensure that enough reductant was present. A 10-fold excess (30 μM) of 1-MeIm was used to explore the rate of axial ligand exchange in the absence of reduction.

4.2.3. NMR Sample Preparation

Under N_2, the complex was first solubilized in 250 μL DMSO-d_6 and 250 μL D_2O in a vial to afford a 16 mM, 50% DMSO-d_6 /D_2O solution. The solution was then quickly added into an NMR tube with $Na_2S_2O_4$ powder under N_2. The NMR tube was sealed to ensure the experiment is under anaerobic conditions. Control samples were prepared in the same manner, in the absence of $Na_2S_2O_4$ powder.

4.3. Results and Discussion

4.3.1. Absorption Spectra

The absorption spectra of $Co^{II}(salen^{R})$, $[Co^{III}(salen^{R})(coumarin)_2]Cl$ and coumarin are shown in **Figures 4.3-4.5**. Slight peak shifts and intensity differences are observed upon axial coordination of the coumarin ligand to $Co^{II}(salen^{R})$ to form $[Co^{III}(salen^{R})(coumarin)_2]Cl$.

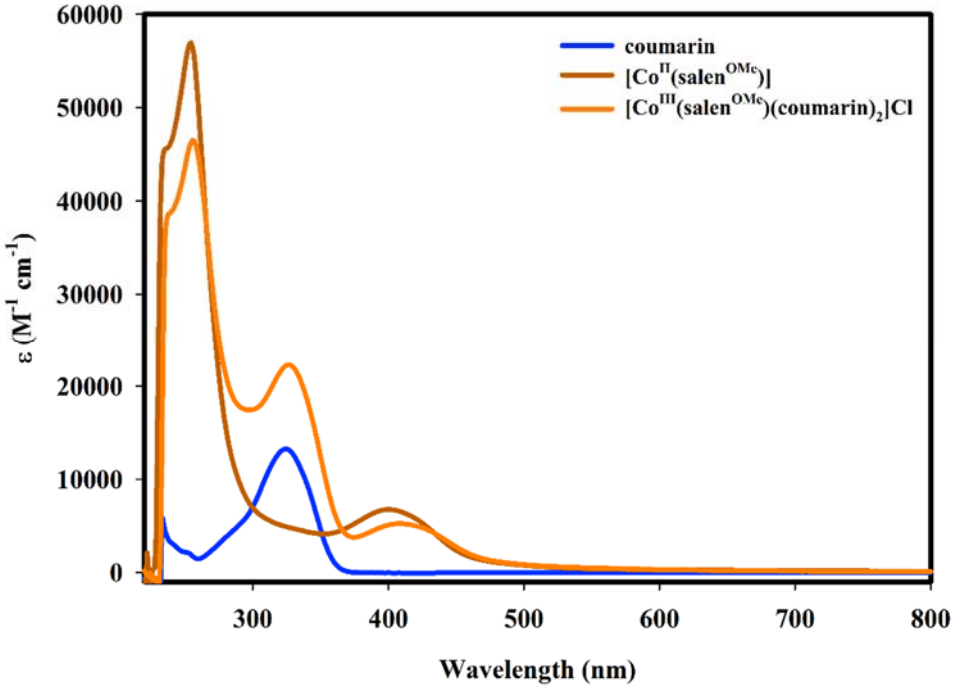

Figure 4.3 Absorbance spectra of $Co^{II}(salen^{OMe})$ (brown), $[Co^{III}(salen^{OMe})(coumarin)_2]Cl$ (orange) and coumarin (blue).
Concentration: 50 μM 2% DMSO/PBS (0.01 M) at 298 K.

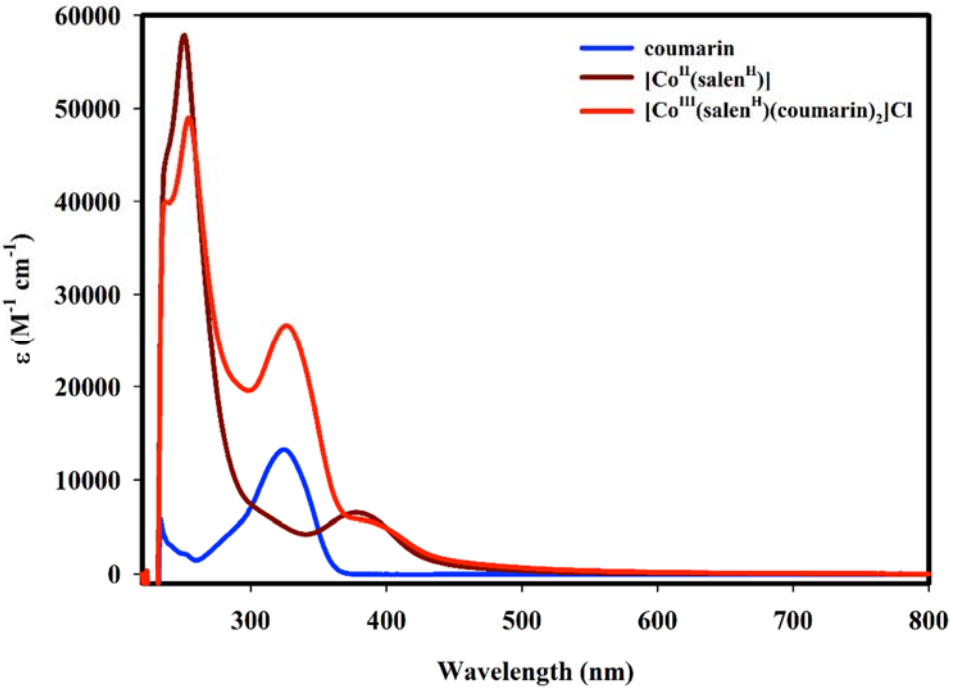

Figure 4.4 Absorbance spectra of $Co^{II}(salen^{H})$ (dark red), $[Co^{III}(salen^{H})(coumarin)_2]Cl$ (red) and coumarin (blue).
Concentration: 50 μM 2% DMSO/PBS (0.01 M) at 298 K.

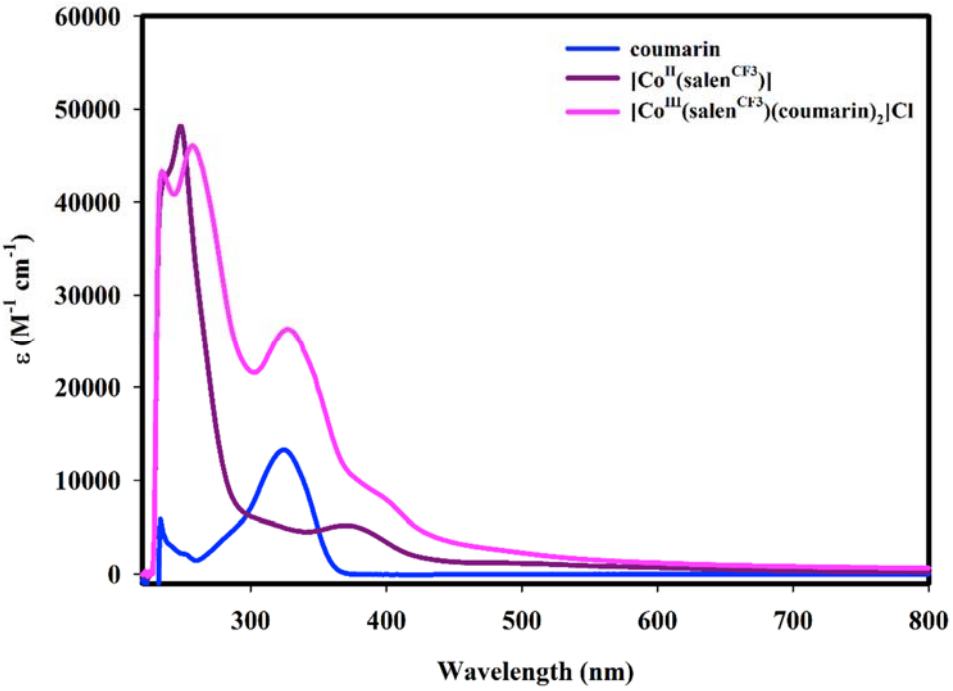

Figure 4.5 Absorbance spectra of $Co^{II}(salen^{CF3})$ (purple), $[Co^{III}(salen^{CF3})(coumarin)_2]Cl$ (pink) and coumarin (blue).
Concentration: 50 μM 2% DMSO/PBS (0.01 M) at 298 K.

4.1.1. Emission Spectra

The optimal excitation wavelength (λ_{ex}) for the coumarin (**23**) was determined to be 327 nm (**Appendix 4.1**), which was used in the emission studies below. Taking into consideration that there are two axial ligands in each Co(III) complex, 6 μM of coumarin and 3 μM of the Co(III) complexes were excited at 327 nm, and the emission spectra of the coumarin ligand and the Co(III) complexes were compared in **Figure 4.6**.

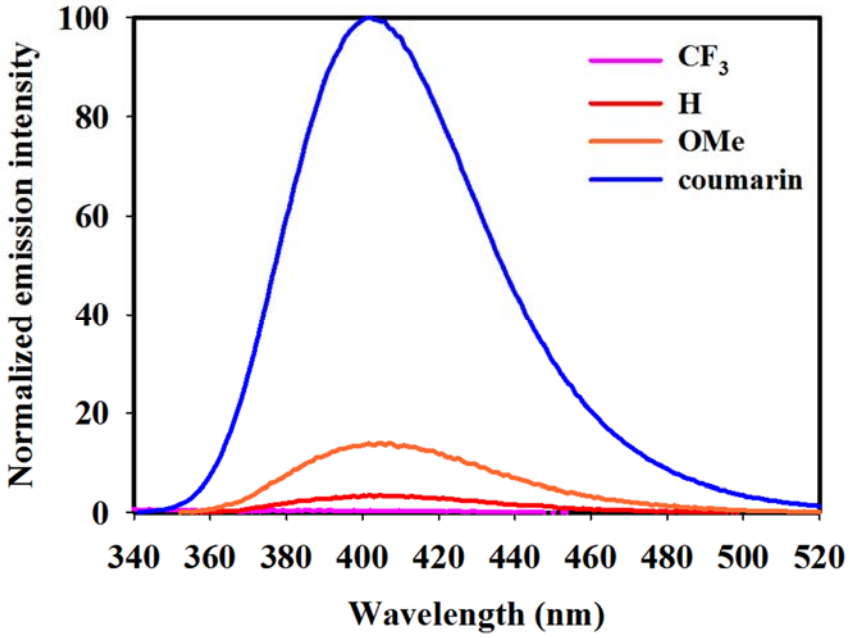

Figure 4.6 Emission spectra of coumarin (blue), [$Co^{III}(salen^{OMe})(coumarin)_2Cl$] (orange), [$Co^{III}(salen^{H})(coumarin)_2Cl$] (red), and [$Co^{III}(salen^{CF3})(coumarin)_2Cl$] (pink).

Conditions: 2% DMSO/PBS (0.01 M) at 298 K, λ_{ex} = 327 nm.

As shown in **Figure 4.6**, the maximum emission intensity is at ca. 400 nm for all compounds, suggesting that in each case the observed emission is due to the coumarin moiety, as both the curve shape and maximum intensity of each spectrum are similar. The spectra were obtained immediately after the solutions were prepared, and were normalized to the spectrum of coumarin (defined as 100). Compared to coumarin, all three complexes exhibited limited emission, indicating that upon complexation the coumarin fluorescence is quenched. However, the three complexes show different emission intensities. The integrated area under curves for the coumarin and the complexes are shown in **Table 4.1**, suggesting a different extent of coumarin ligand release in solution for the three derivatives (OMe > H > CF_3). This difference in fluorescence for the three Co(III) derivatives will be further discussed in **Section 4.4.4**.

Table 4.1 Comparison of the fluorescence intensity of coumarin and the Co(III) complexes upon dissolution.[a]

Compound	Coumarin	OMe	H	CF_3
Area under curve	5.5×10^6	7.6×10^5	1.8×10^5	2.1×10^4
Normalized intensity	100	13.89	3.29	0.38

[a]Conditions: 3 μM complex, 6 μM coumarin, 2% DMSO/PBS (0.01 M) at 298 K, λ_{ex} = 327 nm.

4.3.2. Axial Ligand Release from $[Co^{III}(salen^R)(coumarin)_2]Cl$ Complexes in the Presence of a Reducing Agent

In this experiment, the release of the axial coumarin ligands upon reduction of the Co(III) complexes was investigated using $Na_2S_2O_4$ ($E_{1/2}$ = -660 mV vs. NHE) as a reducing agent.[133] As shown in **Table 3.5**, the reduction potential of the $[Co^{III}(salen^R)(coumarin)_2]Cl$ complexes are more positive in comparison to $Na_2S_2O_4$, thus $Na_2S_2O_4$ should be capable of reducing all three complexes in solution. In this study, technical grade (85% purity) $Na_2S_2O_4$ was used, and since $Na_2S_2O_4$ readily reacts with O_2 in solution, a 10-fold excess of reducing agent was used. A large excess of $Na_2S_2O_4$ is commonly used in the literature to ensure reduction of complexes. [133-135]

In the reduction experiment, a stock solution of $[Co^{III}(salen^R)(coumarin)_2]Cl$ in DMSO and a stock solution $Na_2S_2O_4$ in PBS were mixed and then diluted to afford a 3 μM solution of the complex and 30 μM $Na_2S_2O_4$. The emission spectrum was collected immediately (t = 0). Emission spectra were then collected every 10 min until no further change was observed. For comparison, the emission spectra of the components (3 μM $Co^{II}(salen^R)$, 6 μM coumarin, and 30 μM $Na_2S_2O_4$) were obtained. As mentioned previously, coumarin (6 μM) was always used as a reference.

As shown in **Figure 4.7,** a solution of $[Co^{III}(salen^{OMe})(coumarin)_2]Cl$ in the presence of excess $Na_2S_2O_4$ exhibited a significant increase in coumarin fluorescence over a period of 1.5 hours. The fluorescence intensity did not increase as initially expected to match the value for 6 μM coumarin, but was approximately equal to the solution containing the expected products of the reaction (3 μM $Co^{II}(salen^{OMe})$, 6 μM coumarin, and 30 μM $Na_2S_2O_4$). The maximum emission of the coumarin fluorophore is at 400 nm, and the

$Co^{II}(salen^{R})$ complexes absorb in this energy region, and thus fluorescence quenching by the $Co^{II}(salen^{R})$ complexes is likely (**Figure 4.8**).

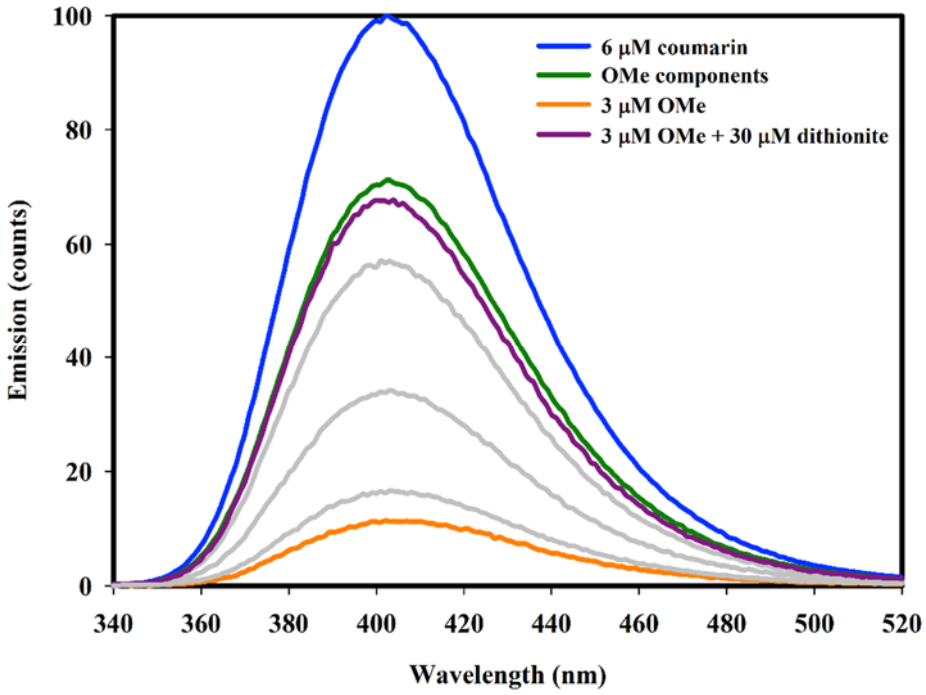

Figure 4.7 **Emission spectra of coumarin (blue), $[Co^{III}(salen^{OMe})(coumarin)_2]Cl$ (orange, at t = 0), components (3 μM $Co^{II}(salen^{OMe})$, 6 μM coumarin, and 30 μM $Na_2S_2O_4$) (green, at t = 0), reaction endpoint under a reducing environment (purple, at t = 1.5 h), and during the reduction process (grey at t = 5 min, 20 min, 40 min, from bottom to top). Reaction duration: 1.5 h.**

Solvent: 2% DMSO/PBS (0.01 M) at 298 K. λ_{ex} = 327 nm, λ_{em} = 400 nm.

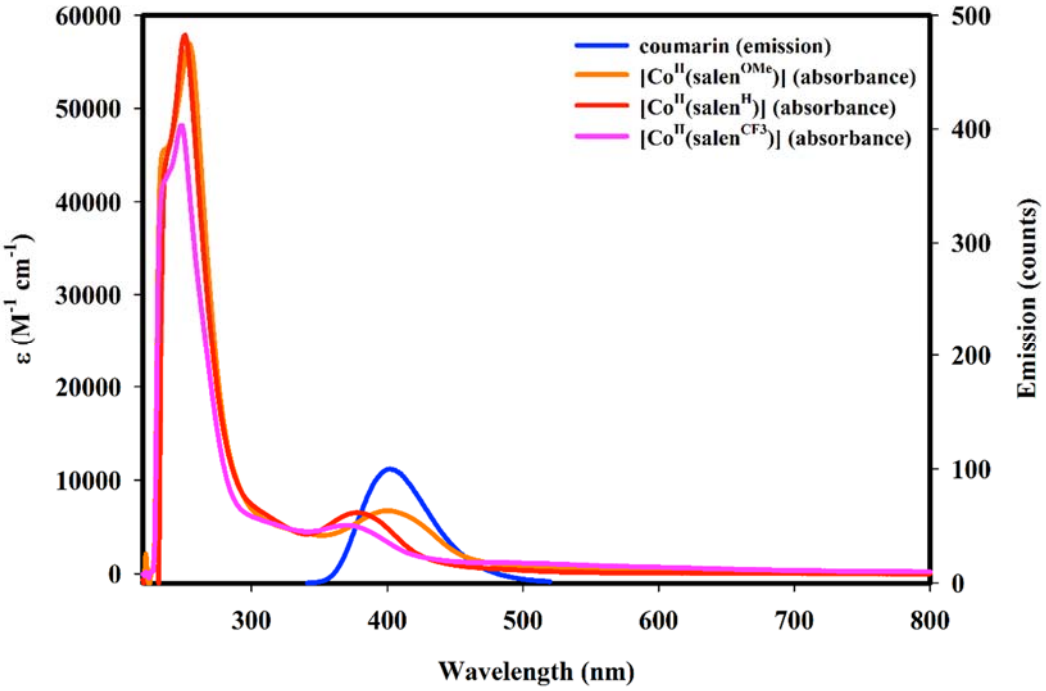

Figure 4.8 Absorbance of 50 μM $Co^{II}(salen^{R})$
(Orange, R = OMe; Red, R = H; Pink, R = CF_3) and emission of 3 μM coumarin (Blue) in 2% DMSO in PBS (0.01 M).

A solution of $[Co^{III}(salen^{H})(coumarin)_2]Cl$ (**Figure 4.9**) in the presence of $Na_2S_2O_4$ also exhibited a significant increase in fluorescence, however the rate of increase was slower in comparison to OMe, and did not reach a maximum until ca. 8 h. Similar to the OMe derivative, the fluorescence intensity did not reach the expected value of 6 μM coumarin, but was approximately equal to the solution containing the expected products of the reaction (3 μM $Co^{II}(salen^{H})$, 6 μM coumarin, and 30 μM $Na_2S_2O_4$). The uncertainty in intensity could be affected by a slight difference in temperature, or component concentrations, etc. This difference can be explained in the same manner as for the OMe derivative, and is likely due to spectral overlap of the reduced Co complex ($Co^{II}(salen^{H})$) and the coumarin fluorophore. Inspection of **Figure 4.8** shows that the absorbance of $Co^{II}(salen^{OMe})$ exhibits the most significant overlap with the emission spectrum of coumarin, which results in increased fluorescence quenching of the coumarin in comparison to $Co^{II}(salen^{H})$ (**Figure 4.7** and **4.9**). For $[Co^{III}(salen^{CF3})(coumarin)_2]Cl$, a minimal amount of fluorescence was observed after 24 h in the presence of $Na_2S_2O_4$ (**Figure 4.10**).

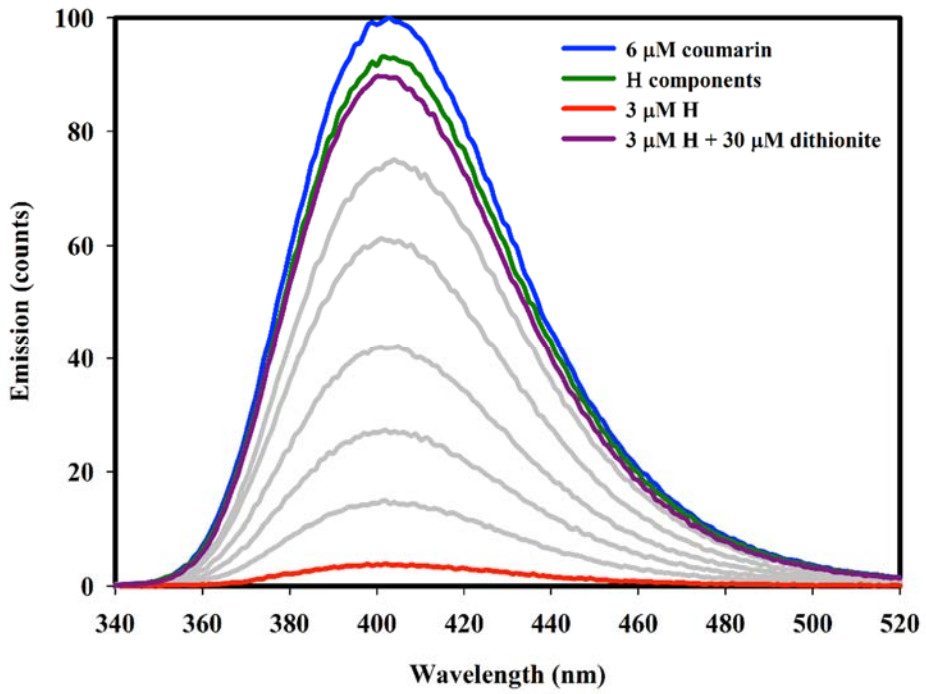

Figure 4.9 **Emission spectra of coumarin (blue), [$Co^{III}(salen^{H})(coumarin)_2$]Cl at t = 0 (red), components (3 μM $Co^{II}(salen^{H})$, 6 μM coumarin, and 30 μM $Na_2S_2O_4$) (green), full release under reducing environment (purple), and fluorescence during the experiment (grey at t = 5 min, 1.5 h, 3.5 h, 5.5 h, 7.5 h from bottom to top). Reaction duration: 8 h.**

Solvent: 2% DMSO/PBS (0.01 M) at 298 K. λ_{ex} = 327 nm, λ_{em} = 400 nm.

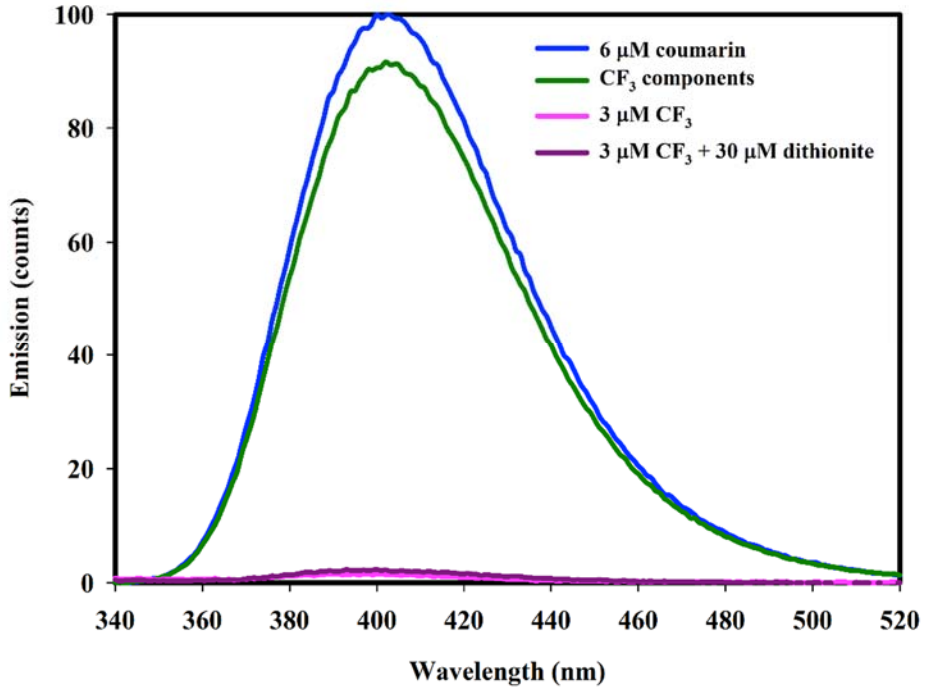

Figure 4.10 Emission spectra of coumarin (blue), [$Co^{III}(salen^{CF3})(coumarin)_2$]Cl at t = 0 (pink), components (3 μM $Co^{II}(salen^{CF3})$, 6 μM coumarin, and 30 μM $Na_2S_2O_4$) (green), and the reaction after 24 h (purple). Monitoring duration: 24 h.

Solvent: 2% DMSO/PBS (0.01 M). λ_{ex} = 327 nm.

It was hypothesized that $Na_2S_2O_4$ would reduce all three complexes due to the low reduction potential of this compound in aqueous solution ($E_{1/2}$ = -660 mV vs. NHE). In addition, we expected the rate of reduction to correlate with the Co(III) / Co(II) reduction potential, and be faster for the CF_3 derivative, followed by H, and then OMe. However, the results are the opposite to that expected based on reduction potentials (**Figure 4.7, 4.9, and 4.10**).

4.3.3. Comparative Fluorescence Release under Reducing Conditions or in the Presence of Excess Ligand

Coumarin release was monitored by fluorescence under reducing conditions as described previously, and compared to coumarin release in the presence of a 10-fold excess of a competing ligand (1-MeIm). For this study a 96-well plate reader was used so that the experiments could be easily measured in triplicate. Solutions were prepared in a black 96-well plate and fluorescence readings (λ_{ex} = 327 nm, λ_{em} = 400 nm) were obtained

every 30 min over a 12 h period. Coumarin fluorescence was used as the control, and it was shown that the fluorescence intensity of coumarin is not affected by the presence of $Na_2S_2O_4$ or 1-MeIm (**Appendix 4.2**). A small decrease in emission is observed over an extended period, which could be due to photobleaching.

Over a period of 2 h, $[Co^{III}(salen^{OMe})(coumarin)_2]Cl$ exhibited a significant increase in coumarin fluorescence in the presence of excess $Na_2S_2O_4$ (ca. 67 % of coumarin control in **Figure 4.11**. From 2 h to 12 h the fluorescence readings remain relatively constant. In the presence of excess 1-MeIm, an increase in fluorescence is also observed (ca. 44% of coumarin control), indicating a significant amount of axial ligand exchange. However, a higher fluorescence intensity is observed under reducing conditions. In the absence of both reducing agent and 1-MeIm, the complex also released coumarin (ca. 26% of coumarin control), suggesting ligand exchange in the buffer solution. 2 eq. of coumarin was used as a reference (100%).

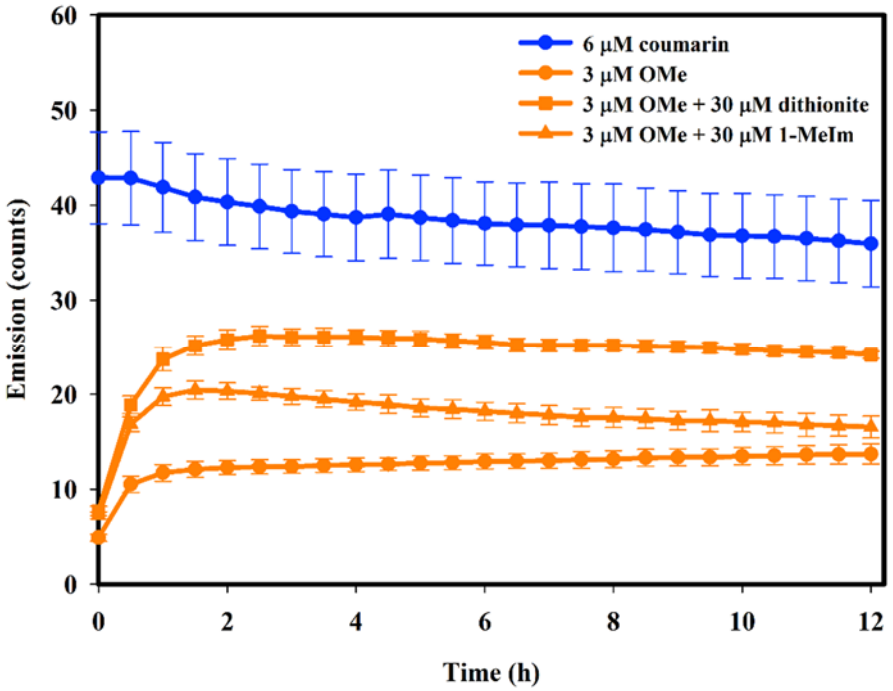

Figure 4.11 **Fluorescence analysis of solutions of $[Co^{III}(salen^{OMe})(coumarin)_2]Cl$ only (circle), under a reducing environment in the presence of $Na_2S_2O_4$ (square), and in the presence of 1-MeIm ligand without reducing agent (triangle). (λ_{ex} = 327 nm, λ_{em} = 400 nm)**

Conditions: 2% DMSO in PBS (0.01 M) at 298 K.

In **Figure 4.12,** over a period of 12 h, [Co^{III}($salen^{H}$)(coumarin)$_2$]Cl exhibited an increase in coumarin fluorescence in the presence of excess $Na_2S_2O_4$ (ca. 60% of coumarin control). In the presence of excess 1-MeIm, an increase in fluorescence is also observed (ca. 44% of coumarin control), indicating a significant amount of axial ligand exchange. However, a higher fluorescence intensity is observed under reducing conditions. In the absence of both reducing agent and 1-MeIm, the complex also released coumarin (ca. 27% of coumarin control), suggesting ligand exchange in the buffer solution. 2 eq. of coumarin was used as a reference (100%).

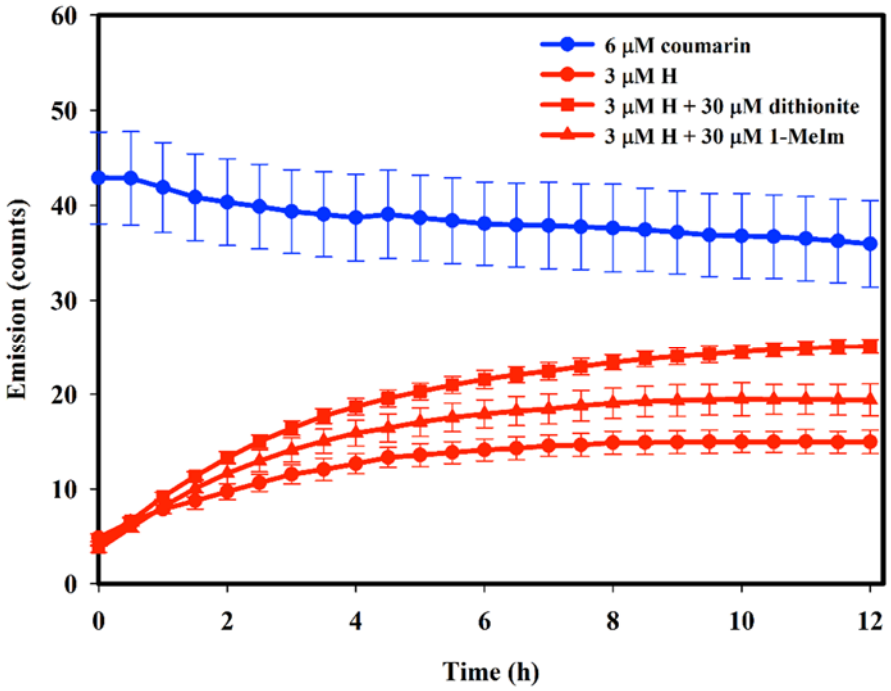

Figure 4.12 Fluorescence analysis of solutions of [Co^{III}($salen^{H}$)(coumarin)$_2$]Cl only (circle), under a reducing environment in the presence of $Na_2S_2O_4$ (square), and in the presence of 1-MeIm ligand without reducing agent (triangle). (λ_{ex} = 327 nm, λ_{em} = 400 nm)

Conditions: 2% DMSO in PBS (0.01 M) at 298 K.

In **Figure 4.13,** over a period of 12 h, [Co^{III}($salen^{CF3}$)(coumarin)$_2$]Cl exhibited a minimal increase in coumarin fluorescence in the presence of excess $Na_2S_2O_4$ or excess 1-MeIm. However, the fluorescence intensity is higher in the presence of $Na_2S_2O_4$ (**Figure 4.13** inset), which indicates increased ligand exchange in the presence of a reductant. In the presence of excess 1-MeIm, the fluorescence intensity is the same as that in the

absence of both reducing agent and 1-MeIm, suggesting minimal ligand exchange in the buffer solution. 2 eq. of coumarin was used as a reference (100%).

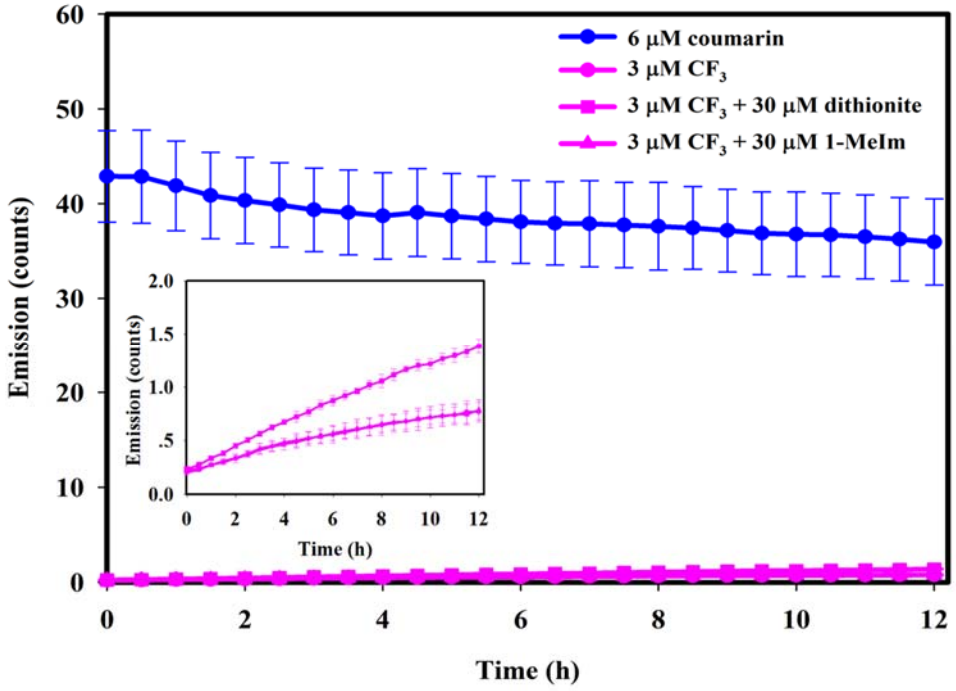

Figure 4.13 Fluorescence analysis of solutions of $[Co^{III}(salen^{CF3})(coumarin)_2]Cl$ only (circle), under a reducing environment in the presence of $Na_2S_2O_4$ (square), and in the presence of 1-MeIm ligand without reducing agent (triangle). (λ_{ex} = 327 nm, λ_{em} = 400 nm)

Conditions: 2% DMSO in PBS (0.01 M) at 298 K.

The rate of axial ligand exchange in the $[Co^{III}(salen^{R})(coumarin)_2]Cl$ complexes can be rationalized by the effect of the *para*-ring substituents on the Lewis acidity at the metal center. The electron-withdrawing CF_3 substituent is expected to increase the Lewis acidity at the metal center to the greatest extent (CF_3 > H > OMe), resulting in increased bond strength between the Co(III) center and the axial ligands, this effect has been investigated previously in the Storr group.[113] This is indeed reflected in the rate of exchange of the Co(III) complexes in the presence of excess 1-MeIm (OMe > H > CF_3). As shown in **Figure 4.11 to 4.13**, the fluorescence intensity, which indicates the amount of ligand release, correlates with the expected Lewis acidity of the Co(III) center (CF_3 > H > OMe). These results are consistent with a literature report that demonstrated increased resistance to ligand exchange (via reduced enzyme inhibition) for Co N,N'-ethylenebis(acetylacetone

iminate) complexes ([Co(acacen)L_2]$^+$) when electron-withdrawing groups are installed on the acacen ligand.[136,137]

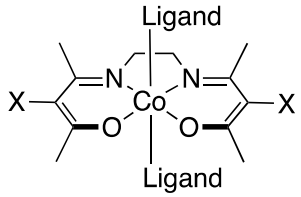

Scheme 4.1 Chemical structure of ([Co(acacen)L_2]$^+$, modification was applied at X on the acacen ligand.

The observed rates (OMe > H > CF_3) of reduction of the [Co^{III}($salen^R$)($coumarin)_2$]Cl complexes are likely influenced by the Lewis acidity at the metal center. The reduction processes studied in this work are relatively slow (timescale of hours), which agrees with reports of similar Co complexes in the literature.[93-95] Due to the slow reduction process and reaction conditions (in air), in which $Na_2S_2O_4$ decomposes, the observed fluorescence increase is likely a combination of both reduction and axial ligand exchange.

4.3.4. Study of the Co(III) Reduction Process with ^{1}H NMR

In order to further investigate the reduction process, ^{1}H NMR spectra were collected over 72 h in the presence of excess $Na_2S_2O_4$. As the Co(III) complexes are reduced by $Na_2S_2O_4$ the paramagnetic Co(II) products (Co($salen^R$)) are expected to form. The Co(II) complexes have been shown in Chapter 2 (**Figure 2.4**) to exhibit broadened signals over a wide chemical shift range consistent with a paramagnetic (S = 1/2) Co(II) complex. Under N_2, the Co(II) complexes are expected to be stable in the reduced form.

For [Co^{III}($salen^{OMe}$)($coumarin)_2$]Cl, at t = 10 min, broad signals over a wide spectral range (50 to -30 ppm) are observed, which increase in intensity up to 1.5 h, and then do not change significantly up to 72 h (**Figure 4.14**). In the diamagnetic spectral region (11 to 0 ppm), the signals became increasingly broadened over time, which could also indicate sample reduction (**Figure 4.15**). A control sample containing only the Co(III) complex did not show any spectral changes over the 72 h period. (**Appendix 4.3-4.4**)

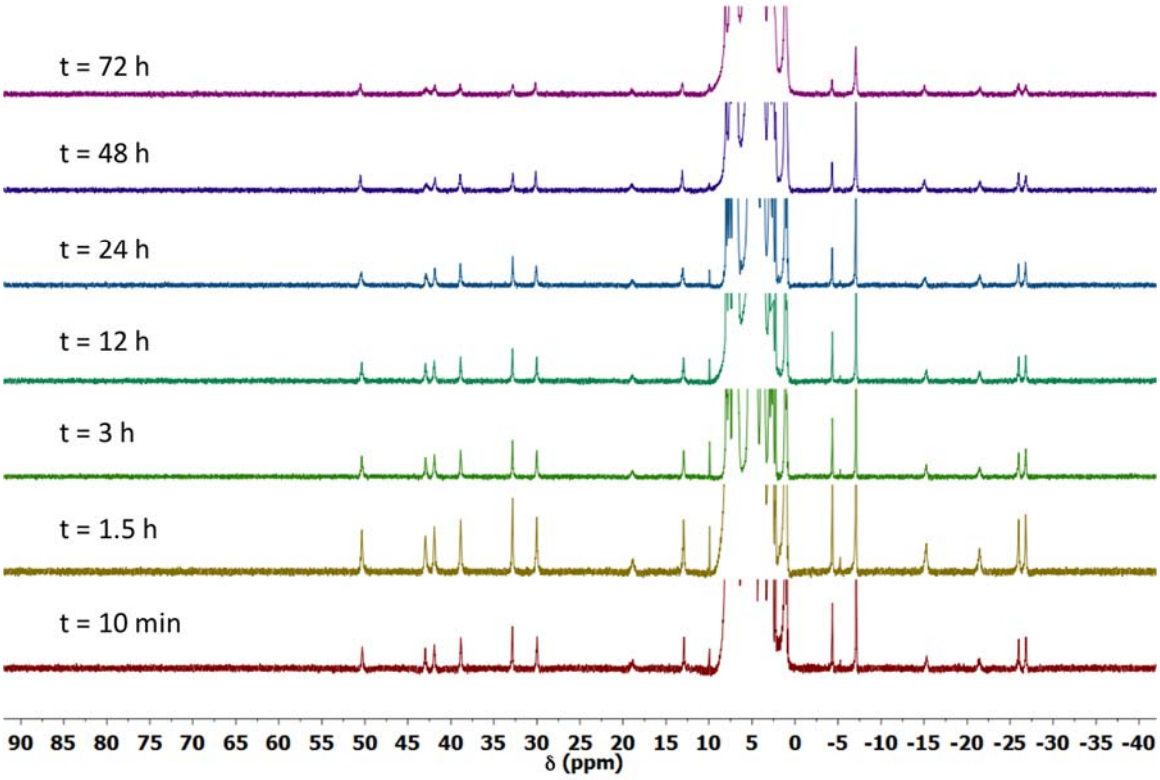

Figure 4.14 ^{1}H NMR spectra of [Co^{III}(salen^{OMe})(coumarin)$_2$]Cl over 72 h in the presence of $Na_2S_2O_4$.

Conditions: 16 mM in 50 % DMSO-*d*$_6$/D$_2$O at 298 K.

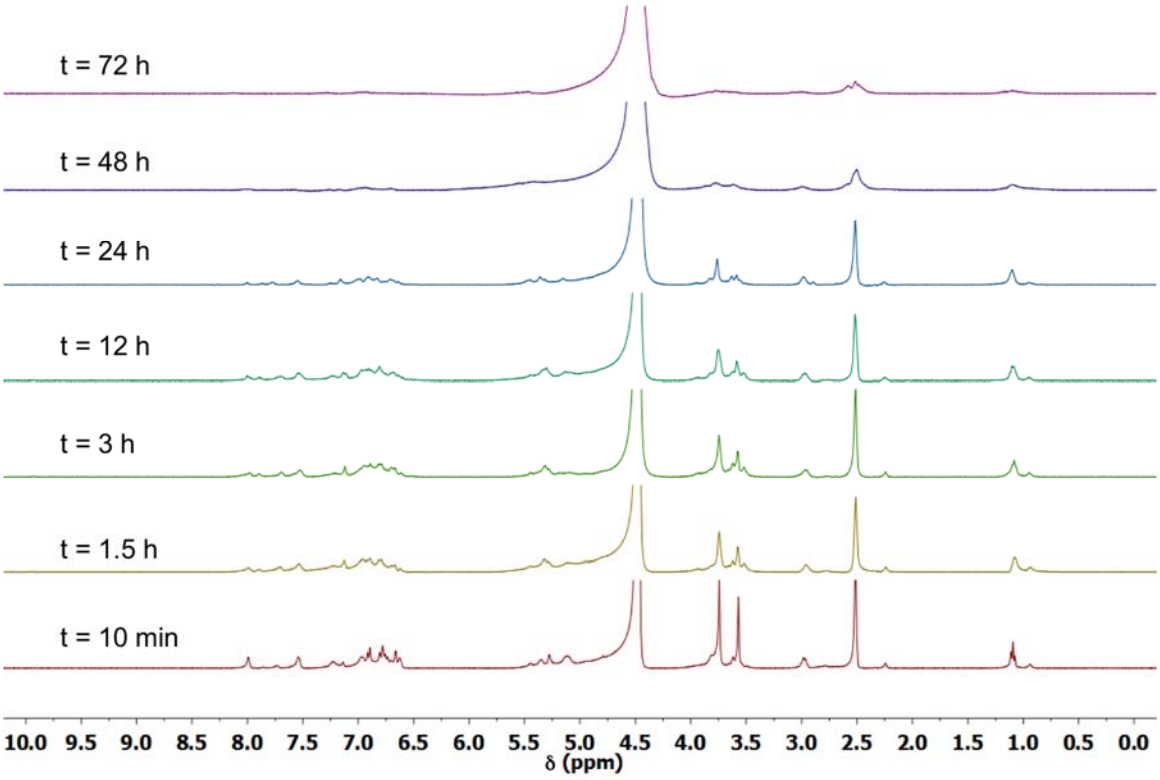

Figure 4.15 ^{1}H NMR spectra of [Co^{III}(salen^{OMe})(coumarin)$_2$]Cl over 72 h in the presence of $Na_2S_2O_4$.
Conditions: 16 mM in 50 % DMSO-d_6/D_2O at 298 K.

For [Co^{III}(salen^{H})(coumarin)$_2$]Cl in the presence of $Na_2S_2O_4$ no observable signals attributed to the Co(II) complex were observed until the 12 h time point, and these signals increased slightly up to 72 h (**Figure 4.16**). The longer time period for this derivative to show paramagnetically-shifted signals in comparison to the R = OMe derivative matches the previously discussed fluorescence experiments. The lower intensity of the signals in the [Co^{III}(salen^{H})(coumarin)$_2$]Cl NMR experiment is likely due to the lower solubility of Co^{II}(salen^{H}) in solution. In the diamagnetic spectral region, the signals become increasingly broadened over time, which might be induced by the unpaired electron, which also indicates sample reduction (**Figure 4.17**). A control sample containing only the Co(III) complex did not show any spectral changes over the 72 h period. (**Appendix 4.5-4.6**)

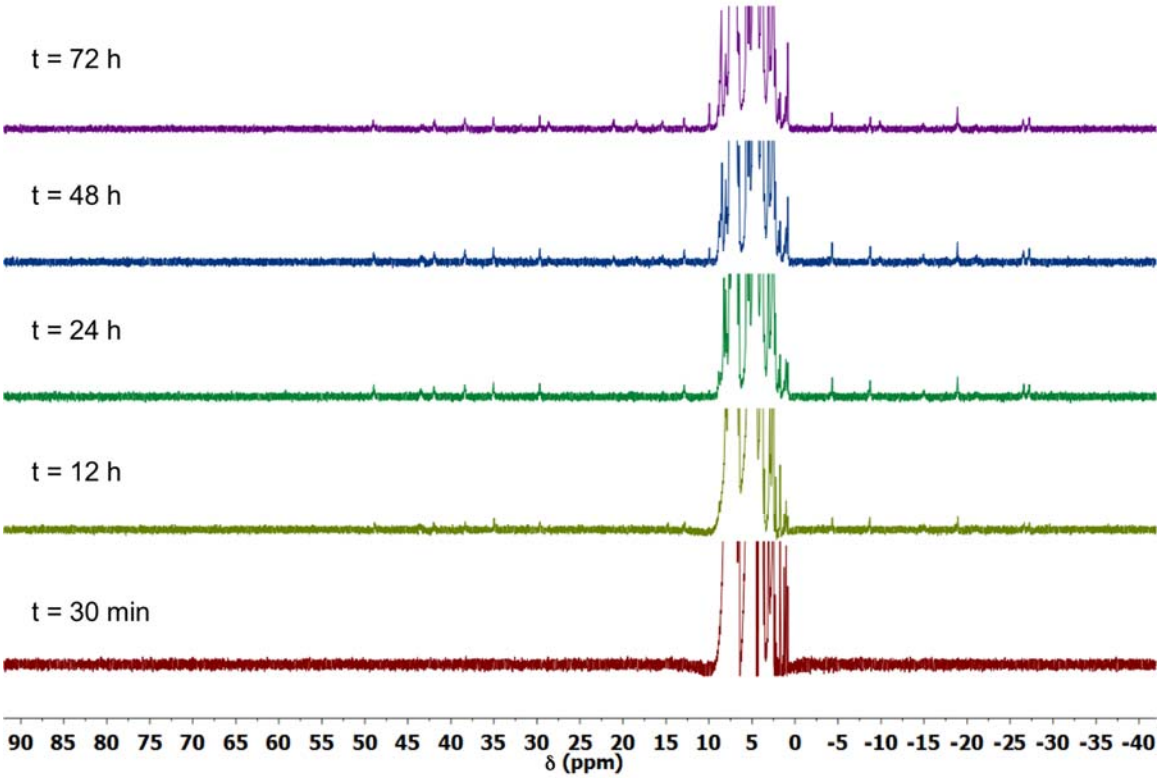

Figure 4.16 **^{1}H NMR spectra of [Co^{III}(salen^{H})(coumarin)$_2$]Cl over 72 h in the presence of $Na_2S_2O_4$.**

Conditions: 16 mM in 50 % DMSO-d_6/D_2O at 298 K.

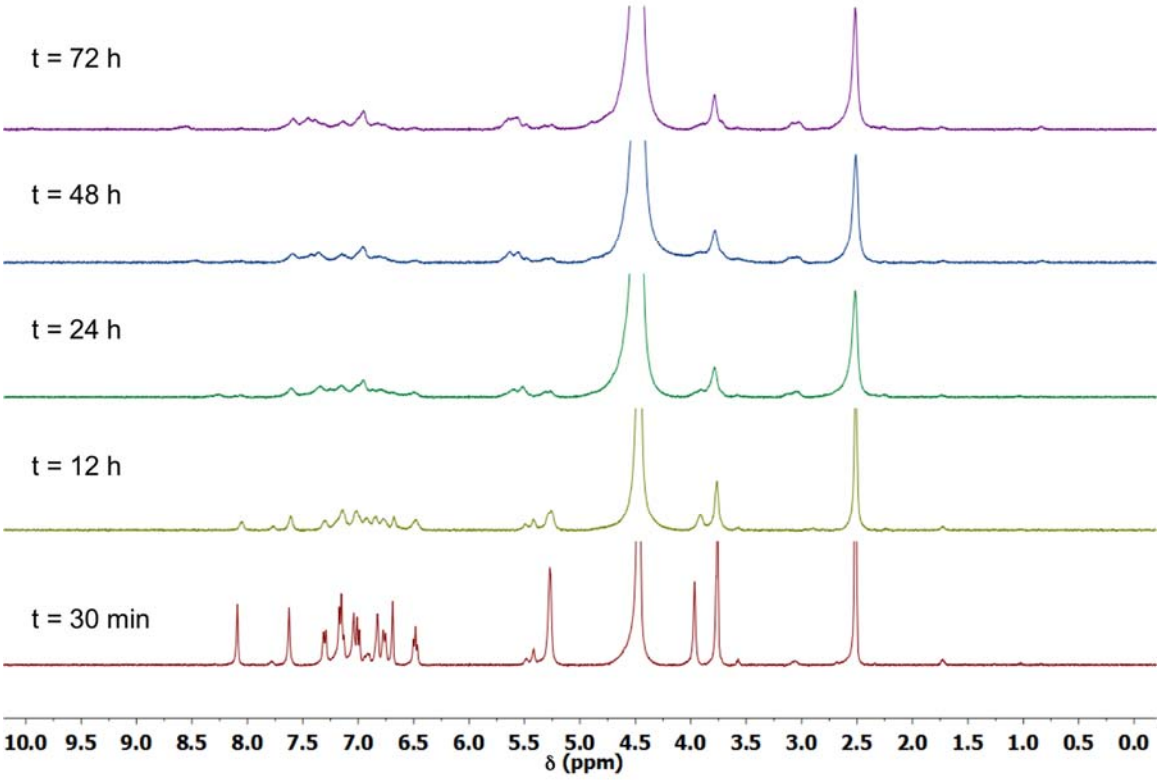

Figure 4.17 ^{1}H NMR spectra of [Co^{III}(salen^{H})(coumarin)$_2$]Cl over 72 h in the presence of $Na_2S_2O_4$.

Conditions: 16 mM in 50 % DMSO-d_6/D_2O at 298 K.

No paramagnetically shifted ^{1}H NMR signals were observed over the course of the 72 h NMR experiment for [Co^{III}(salen^{CF3})(coumarin)$_2$]Cl in the presence of $Na_2S_2O_4$ (**Figure 4.18**). This result correlates with the limited increase in the fluorescence observed for this derivative (**Figure 4.13)**. Over time, the ^{1}H NMR signals in the diamagnetic region broadened, becoming very weak by the 24 h time point (**Figure 4.19**). This broadness could be indicative of a slow reduction process, however no paramagnetically-shifted signals were observed in the ^{1}H NMR spectra (**Figure 4.18**). Another possible explanation for this broadening and disappearance of the signals is precipitation of the complex over the timeframe of the experiment. A control sample containing only the Co(III) complex did not show any spectral changes over the 72 h period. (**Appendix 4.7-4.8**)

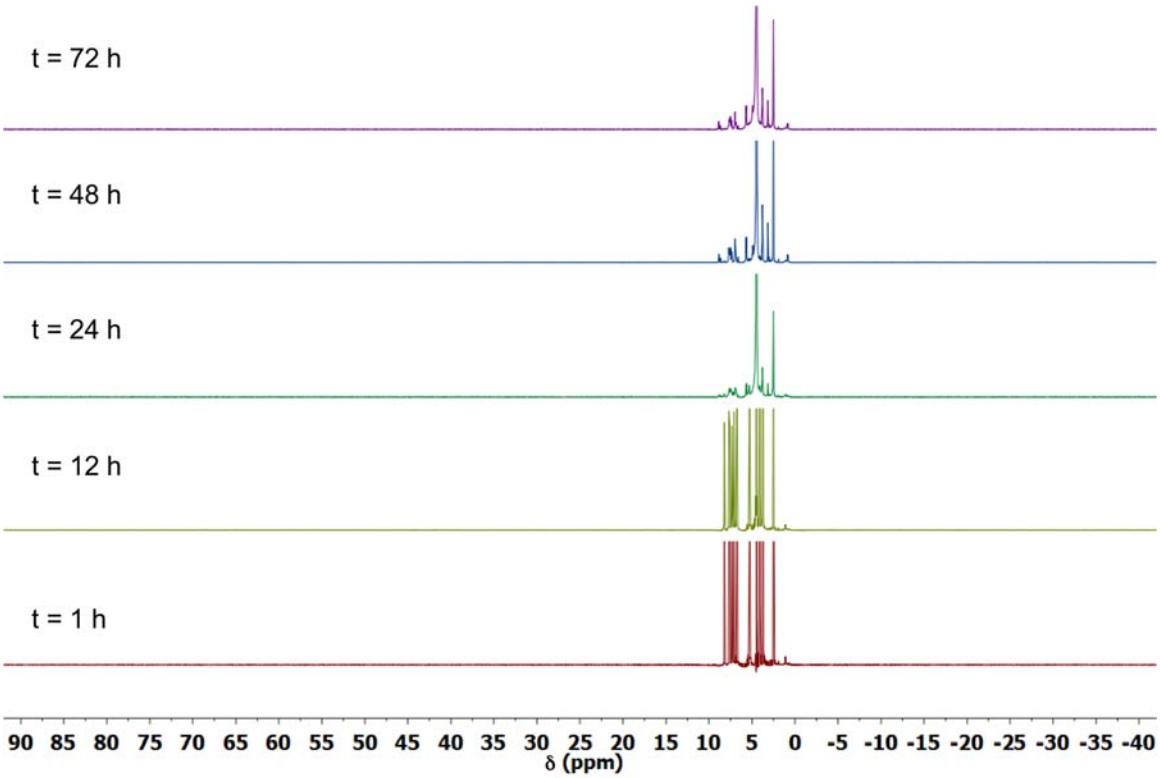

Figure 4.18 **^{1}H NMR spectra of [Co^{III}(salen^{CF3})(coumarin)$_2$]Cl over 72 h in the presence of $Na_2S_2O_4$.**

Conditions: 16 mM in 50 % DMSO-d_6/D_2O at 298 K.

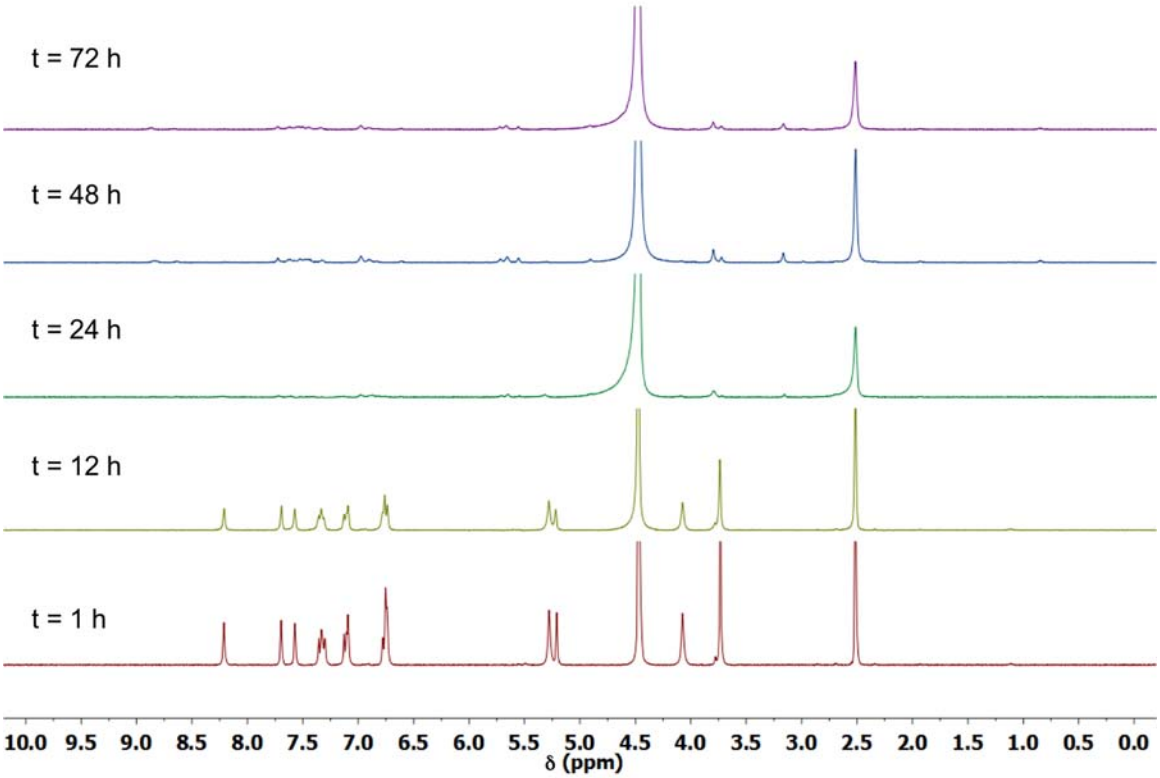

Figure 4.19 ^{1}H NMR spectra of [Co^{III}(salen^{CF3})(coumarin)$_2$]Cl over 72 h in the presence of $Na_2S_2O_4$.
Conditions: 16 mM in 50 % DMSO-d_6/D_2O at 298 K.

Overall, the reduction process observed via the appearance of paramagnetic signals in the NMR study occurs over a similar time period when compared to the results of the coumarin fluorescence release study (**Section 4.4.3**). The reduction rate of the three derivatives is fastest for R = OMe, followed by R = H. The complex where R = CF_3 does not exhibit significant reduction in either study. Interestingly, in the fluorescence study the Co(III) complexes (R = OMe or H) in the absence of reducing agent or competing ligand (1-MeIm) showed increased fluorescence over 12 h with ca. 50% of the intensity in comparison to the reduction experiment (**Figure 4.11** and **4.12**). This indicates that significant ligand exchange occurs in 2% DMSO in PBS solution at 3 μM concentration. This differs from the NMR study, where the diamagnetic NMR spectra of the control showed excellent stability over 72 h, as no spectral changes were observed. The stability difference may result from the concentration difference for the fluorescence and NMR studies (3 μM vs. 16 mM), and the solvent ratio (2% DMSO in PBS vs. 50% DMSO-d_6 in

D_2O). In addition, excitation at regular intervals in the fluorescence experiment (λ_{ex} = 327 nm light (every 30 min over 12 h) may increase the rate of ligand release in comparison to the NMR study.[138]

The paramagnetic ^1H NMR signals observed in the $[Co^{III}(salen^{OMe})(coumarin)_2]Cl$ reduction experiment exhibit slightly different shifts in comparison to the $[Co^{III}(salen^{H})(coumarin)_2]Cl$ reduction experiment (**Appendix 4.9**). The increased number of signals in comparison to the $(Co^{II}(salen^{R})$ species (in 90% DMSO-d_6 in D_2O) shown in **Appendix 4.10-4.11**, suggest that the signals observed in the paramagnetic region are from the coumarin ligand interacting with the paramagnetic Co(II) center, which would also account for the slight shift differences for the OMe and H complexes. Further work is needed to investigate if the coumarin ligands are still bound to the Co(II) center, or have undergone ligand exchange in solution.

4.4. Conclusion

In this chapter, the photophysical properties of the $[Co^{III}(salen^{R})(coumarin)_2]Cl$ complexes were studied. The intact $[Co^{III}(salen^{R})(coumarin)_2]Cl$ complexes show weak fluorescence in comparison to free coumarin, indicating that the fluorescence of coumarin is quenched upon complexation. The reduction of the $[Co^{III}(salen^{R})(coumarin)_2]Cl$ complexes was then monitored in the presence of excess $Na_2S_2O_4$ in solution. In the presence of excess $Na_2S_2O_4$, the $[Co^{III}(salen^{OMe})(coumarin)_2]Cl$ complex showed full axial ligand release (as measured by fluorescence) within 2 h. For $[Co^{III}(salen^{H})(coumarin)_2]Cl$, axial ligand release occurred over an 8 h period. In both cases, partial fluorescence quenching by the reduced $Co^{II}(salen^{R})$ species results in slightly lower fluorescence intensity in comparison to a concentration-matched sample of coumarin. For the $[Co^{III}(salen^{CF3})(coumarin)_2]Cl$ derivative, limited axial ligand release was observed by fluorescence in the reduction experiment.

Axial ligand release for the $[Co^{III}(salen^{R})(coumarin)_2]Cl$ complexes was further investigated over a 12 h period. Under reducing conditions, the fluorescence increase was considerably faster for $[Co^{III}(salen^{OMe})(coumarin)_2]Cl$ in comparison to $[Co^{III}(salen^{H})(coumarin)_2]Cl$, matching the initial fluorescence experiment. In addition, the

fluorescence intensity in the presence of reducing agent is higher for both complexes when compared to ligand exchange alone (addition of 10-fold excess of 1-MeIm), suggesting that ligand release is enhanced under reducing conditions. Experiments with $[Co^{III}(salen^{CF3})(coumarin)_2]Cl$ showed limited fluorescence intensity under all conditions.

The reduction process for the $[Co^{III}(salen^{R})(coumarin)_2]Cl$ complexes was also studied by NMR over a 72 h period. The appearance of broadened ^1H NMR signals over a wide chemical shift range suggests reduction to a paramagnetic Co(II) species. The timeframe for the appearance of the paramagnetic signals matches with the fluorescence data for the OMe and H derivatives. The absence of paramagnetically-shifted signals for the CF_3 derivative suggests limited reduction of this analogue.

These results contradict what is expected based on the Co(III) / Co(II) reduction potentials. From the measured reduction potentials in Chapter 3 (**Table 3.2**), we expected that $Na_2S_2O_4$ would reduce the $[Co^{III}(salen^{R})(coumarin)_2]Cl$ complexes, resulting in structural rearrangement from an octahedral to square planar geometry, and thus the release of the axial fluorescent ligands. However, even though the Co(III) / Co(II) reduction potentials are tuned by the phenolate *para*-substituents, the potential window is narrow for the three derivatives (-0.06 to 0.45 V).

The stability of the complexes towards axial ligand exchange matches the expected axial bond strength based on the Lewis acidity at the metal center (CF_3 > H > OMe). The results in this chapter suggest that Lewis acidity is the dominant factor that affects the stability of complexes. Future work should focus on decoupling these competing processes for this series of complexes.

Chapter 5.

Ongoing and Future Work

5.1. Compound Design

Previously, metal complexes with water-soluble sulfonated ligands were studied as catalysts,[139-141] fluorescent sensors,[142] and therapeutic drugs.[143] In the pharmaceutical industry, solubility in water is a critical parameter in order to achieve a pharmacological response. Low aqueous solubility is a major problem encountered with the formulation of new drugs.[144] In order to develop Co(III) pro-drugs with improved solubility in water, we investigated the synthesis of water-soluble salen ligands. We designed a series of salen ligands with different *ortho*-ring substituents and a sulfonate group at the *para* position (**Figure 5.1**). In this manner, we set out to alter the reduction potential of the resulting Co salen complexes via the *ortho*-substituents, while improving water solubility via the *para*-sulfonate substituent. The synthetic details are shown in **Appendix 5**. [15,140, 142,145,146,

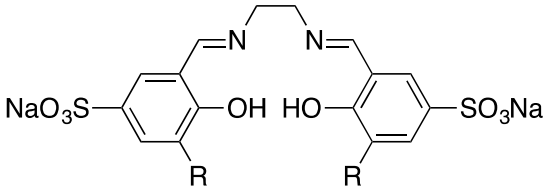

Figure 5.1 Water-soluble salen ligand.

5.2. Results

Salicylaldehydes were purchased from Sigma Aldrich with the exception of 3-chloro-2-hydroxybenzaldehyde, which was prepared from commercially available 2-hydroxybenzaldehyde (**Scheme 5.1**).[15] Two salen ligands (**35** and **39**) have been synthesized, following a 4-step method reported in the literature (**Scheme 5.2**).[145] The nickel complex of sodium 3,3'-((1*E*,1'*E*)- (ethane-1,2-diylbis(azanylylidene)) Bis(methanylylidene)) bis(4-hydroxybenzenesulfonate) was successfully synthesized following the literature method, and it shows good water solubility.[140] However, due to the low solubility of other sodium 5-formyl-4-hydroxybenzenesulfonate precursors (Cl and

OMe) in MeOH, salen ligands could not be synthesized using the same synthetic procedure. In the future, other solvents and/or methods can be attempted for synthesizing the sulfonated salen ligands. We also attempted to synthesize the cobalt complexes of **35** and **39** under a nitrogen atmosphere, however we were unsuccessful. Other synthetic methods can be attempted for cobalt complexes.[147]

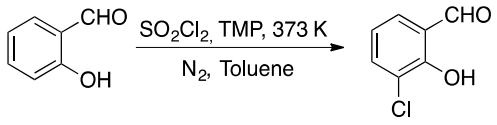

Scheme 5.1 Synthetic methods for 3-chloro-2-hydroxybenzaldehyde

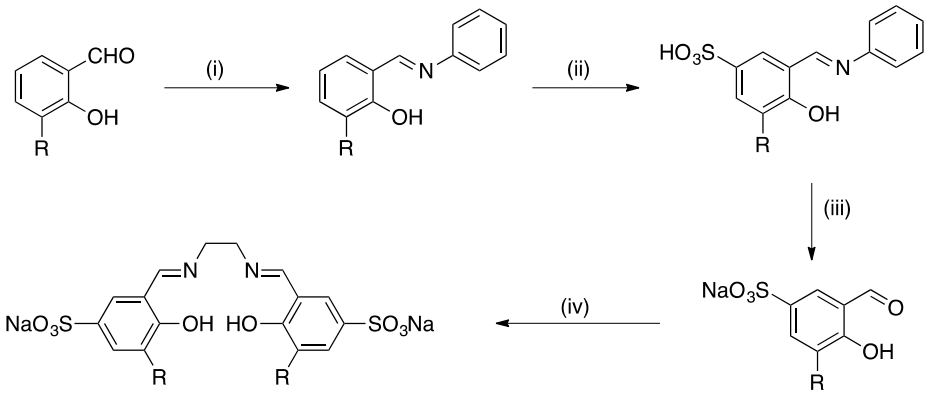

Scheme 5.2 Synthetic methods towards the water soluble salen ligands (R = OMe, ^{t}Bu, H, Cl).

Reaction Conditions: (i) Aniline, EtOH, reflux 2 h; (ii) Concentrated H_2SO_4, 363 K, 2 h. (iii) Na_2CO_3, H_2O, reflux 12 h; (iv) 0.5 eq. ethane-1,2-diamine, MeOH, 2 h, 298 K.

5.3. Future work

We have synthesized and characterized a series of $[Co^{III}(salen^R)(coumarin)_2]Cl$ complexes as detailed in Chapters 3 and 4. Electrochemical measurements showed that the reduction potentials could be altered by installing different phenolate *para*-substituents. The resulting E_c values of the Co(III) / Co(II) redox couple was determined to fall within the range accessible under physiological conditions (-420 mV to -150 mV) and $E_{1/2}$ values

of these complexes (-60 mV to 45 mV) are at the higher edge of this range.[46] Fluorescence studies indicate that the fluorescence of axial coumarin ligands was quenched upon complexation, and that the coumarin fluorescence is restored due to both ligand exchange and reduction of the Co(III) center. The next step of the studies of $[Co^{III}(salen^{R})(coumarin)_2]Cl$ could include using electron paramagnetic resonance (EPR) to study the reduction process by detecting Co(II) signals, to give an improved understanding of the stability of the complexes in biological media.

The $[Co^{III}(salen^{R})(coumarin)_2]Cl$ series of complexes were studied as a proof of concept. Future work should focus on synthesizing Co(III) salen complexes with cancer therapeutics bound in the axial positions. Similar to the coumarin-imidazole conjugate studied in Chapter 3, nucleosides and nucleotides also contain N-donor groups, which could be used to bind to cobalt. Importantly, certain analogues have been introduced as cancer chemotherapies.[148,149] Purine and pyrimidine derivatives such as 5-Fluorouracil and 6-Mercaptopurine (**Figure 5.2**) compete with physiological nucleosides and interact with a large number of intracellular targets such as nucleoside transporters and nucleoside metabolism enzymes, resulting in cytotoxicity.[149]

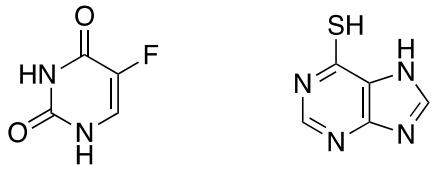

Fluorouracil (5-FU) 6-mercaptopurine (6-MP)

Figure 5.2 Chemical structures of nucleoside analogues.

Many examples of metal-nucleotide and nucleoside complexes have been reported in the literature.[150-152] One proposed route using adenosine analogue, 2-chloro-2'-deoxyadenosine as an example ligand is shown in **Scheme 5.3**.

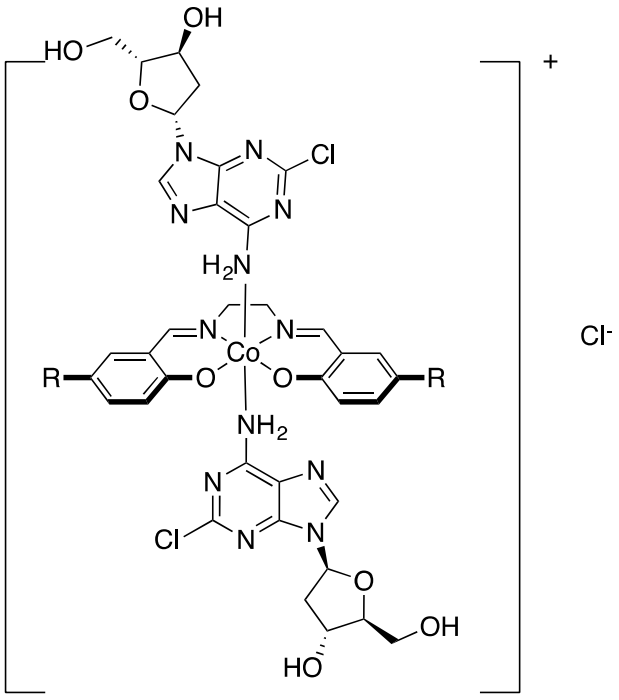

Figure 5.3 Chemical structure of [$Co^{III}(salen^{R})$(2-chloro-2'-deoxyadenosine)$_2$]Cl.

The goal is to develop Co(III) pro-drug compounds with good aqueous solubility, low pro-drug cytotoxicity, and high drug cytotoxicity upon axial ligand release in hypoxic environments. Finally, hypoxia cell and/or tumor models can be used to determine the full potential of these new compounds.

References

(1) Nussbaumer, S.; Bonnabry, P.; Veuthey, J. L.; Fleury-Souverain, S. *Talanta* **2011**, *85*, 2265.

(2) Anand, P.; Kunnumakara, A. B.; Sundaram, C.; Harikumar, K. B.; Tharakan, S. T.; Lai, O. S.; Sung, B.; Aggarwal, B. B. *Pharm. Res.* **2008**, *25*, 2097.

(3) World Health Organization. Cancer. http://www.who.int/mediacentre/factsheets/fs297/en/ (accessed May 30, 2015).

(4) Bergers, G.; Benjamin, L. E. *Nat. Rev. Cancer* **2003**, *3*, 401.

(5) Hanahan, D.; Weinberg, R. A. *Cell* **2011**, *144*, 646.

(6) Lodish, H. F., et al. In *Molecular Cell Biology*; 4 ed.; Freeman, W. H., Ed.; W. H. Freeman and Company: New York, 2000.

(7) Ryan, C. J.; Wilding, G. *Drugs & Aging* **2000**, *17*, 249.

(8) Sahai, E. *Nat. Rev. Cancer* **2007**, *7*, 737.

(9) Whittaker, M.; Floyd, C. D.; Brown, P.; Gearing, A. J. H. *Chem. Rev.* **1999**; *99*, 2735.

(10) Cancer Research UK. *How cancer starts*. http://www.cancerresearchuk.org/about-cancer/what-is-cancer/how-cancer-starts (accessed Mar 23, 2015).

(11) Clarke, R. M.; Storr, T. *Dalton Trans.* **2014**, *43*, 9380.

(12) Kochem, A.; Gellon, G.; Jarjayes, O.; Philouze, C.; Leconte, N.; van Gastel, M.; Bill, E.; Thomas, F. *Chem. Commun.* **2014**, *50*, 4924.

(13) Lee, S.; Zheng, X.; Krishnamoorthy, J.; Savelieff, M. G.; Park, H. M.; Brender, J. R.; Kim, J. H.; Derrick, J. S.; Kochi, A.; Lee, H. J.; Kim, C.; Ramamoorthy, A.; Bowers, M. T.; Lim, M. H. *J. Am. Chem. Soc.* **2014**, *136*, 299.

(14) Leong, S. L.; Young, T. R.; Barnham, K. J.; Wedd, A. G.; Hinds, M. G.; Xiao, Z.; Cappai, R. *Metallomics* **2014**, *6*, 105.

(15) Saper, N. I.; Snider, B. B. *J. Org. Chem.* **2014**, *79*, 809.

(16) Canadian Cancer Society. Canadian Cancer Statistics publication. http://www.cancer.ca/en/cancer-information/cancer-101/canadian-cancer-statistics-publication/?region=sk (accessed Dec 31, 2015).

(17) Shewach, D. S.; Kuchta, R. D. *Chem. Rev.* **2009**, *109*, 2859.

(18) Hanahan, D.; Weinberg, R. A. *Cell* **2000**, *100*, 57.

(19) Kohn, K. W.; Spears, C. L.; Doty, P. *J. Mol. Biol.* **1966**, *19*, 266.

(20) Wang, D.; Lippard, S. J. *Nat. Rev. Drug Discov.* **2005**, *4*, 307.

(21) Jamieson, E. R.; Lippard, S. J. *Chem. Rev.* **1999**, *99*, 2467.

(22) Siddik, Z. H. *Oncogene* **2003**, *22*, 7265.

(23) Rowinsky , E. K.; Donehower , R. C. *New Engl. J. Med.* **1995**, *332*, 1004.

(24) Medina, M. A. *J. Nutr.* **2001**, *131*, 2539S.

(25) Medina, R. A.; Owen, G. I. *Biol. Res.* **2002**, *35*, 9.

(26) Warburg, O. *Science* **1956**, *123*, 309.

(27) DeBerardinis, R. J.; Cheng, T. *Oncogene* **2010**, *29*, 313.

(28) Failes, T. W.; Cullinane, C.; Diakos, C. I.; Yamamoto, N.; Lyons, J. G.; Hambley, T. W. *Chem. Eur. J.* **2007**, *13*, 2974.

(29) Neri, D.; Supuran, C. T. *Nat. Rev. Drug Discov.* **2011**, *10*, 767.

(30) O'Donnell, J. L.; Shannon, A. M.; Bouchier-Hayes, D. In *Anticancer Therapeutics*; John Wiley & Sons, Ltd: 2008, p 245.

(31) Hockel, M.; Vaupel, P. *J. Natl. Cancer Inst.* **2001**, *93*, 266.

(32) Teicher, B. A. *Cancer Metastasis Rev.* **1994**, *13*, 139.

(33) Marie, S. K. N.; Shinjo, S. M. O. *Clinics* **2011**, *66*, 33.

(34) de Arruda Leme, I.; Portari, G. V.; Padovan, G.; Rosa Fá, T.; de Mello-Filho, F.; Marchini, J. *Clinics* **2012**, *67*, 1225.

(35) Vaupel, P.; Kallinowski, F.; Okunieff, P. *Cancer Res.* **1989**, *49*, 6449.

(36) Go, Y. M.; Jones, D. P. *Biochim. Biophys. Acta* **2008**, *1780*, 1273.

(37) Jones, D. P. *J. Intern. Med.* **2010**, *268*, 432.

(38) Kaludercic, N.; Deshwal, S.; Di Lisa, F. *Front. Physiol.* **2014**, *5,* 285.

(39) Mallikarjun, V.; Clarke, D. J.; Campbell, C. J. *Free Radic. Biol. Med.* **2012**, *53*, 280.

(40) Keese, M. A.; Saffrich, R.; Dandekar, T.; Becker, K.; Schirmer, R. H. *FEBS Lett.* **1999**, *447*, 135.

(41) Gutscher, M.; Pauleau, A. L.; Marty, L.; Brach, T.; Wabnitz, G. H.; Samstag, Y.; Meyer, A. J.; Dick, T. P. *Nat. Methods* **2008**, *5*, 553.

(42) Reipa, V. *Bioelectrochemistry* **2004**, *65*, 47.

(43) Lohman, J. R.; Remington, S. J. *Biochemistry* **2008**, *47*, 8678.

(44) Rosenwasser, S.; Rot, I.; Sollner, E.; Meyer, A. J.; Smith, Y.; Leviatan, N.; Fluhr, R.; Friedman, H. *Plant Physiol.* **2011**, *156*, 185.

(45) Waypa, G. B.; Marks, J. D.; Guzy, R.; Mungai, P. T.; Schriewer, J.; Dokic, D.; Schumacker, P. T. *Circ. Res.* **2010**, *106*, 526.

(46) Go, Y. M.; Jones, D. P. *Free Radic. Biol. Med.* **2011**, *50*, 495.

(47) Dijkwel, P. A.; Wenink, P. W. *J. Cell Sci.* **1986**, *84*, 53.

(48) Kizaka-Kondoh, S.; Inoue, M.; Harada, H.; Hiraoka, M. *Cancer Sci.* **2003**, *94*, 1021.

(49) Frezza, M.; Hindo, S.; Chen, D.; Davenport, A.; Schmitt, S.; Tomco, D.; Dou, Q. P. *Curr. Pharm. Des.* **2010**, *16*, 1813.

(50) Orvig, C.; Abrams, M. J. *Chem. Rev.* **1999**, *99*, 2201.

(51) Meggers, E. *Chem. Commun.* **2009**, *9*, 1001.

(52) Weiss, R. B.; Christian, M. C. *Drugs* **1993**, *46*, 360.

(53) Alama, A.; Tasso, B.; Novelli, F.; Sparatore, F. *Drug Discov. Today* **2009**, *14*, 500.

(54) Fujibayashi, Y.; Taniuchi, H.; Yonekura, Y.; Ohtani, H.; Konishi, J.; Yokoyama, A. *J. Nucl. Med.* **1997**, *38*, 1155.

(55) Buss, J. L.; Greene, B. T.; Turner, J.; Torti, F. M.; Torti, S. V. *Curr. Top. Med. Chem.* **2004**, *4*, 1623.

(56) Antony, S.; Aitken, J. B.; Vogt, S.; Lai, B.; Brown, T.; Spiccia, L.; Harris, H. H. *J. Biol. Inorg. Chem.* **2013**, *18*, 845.

(57) Messori, L.; Abbate, F.; Marcon, G.; Orioli, P.; Fontani, M.; Mini, E.; Mazzei, T.; Carotti, S.; O'Connell, T.; Zanello, P. *J. Med. Chem.* **2000**, *43*, 3541.

(58) Shakya, R.; Peng, F.; Liu, J.; Heeg, M. J.; Verani, C. N. *Inorg. Chem.* **2006**, *45*, 6263.

(59) Bergamo, A.; Gagliardi, R.; Scarcia, V.; Furlani, A.; Alessio, E.; Mestroni, G.; Sava, G. *J. Pharmacol. Exp. Ther.* **1999**, *289*, 559.

(60) Hartinger, C. G.; Zorbas-Seifried, S.; Jakupec, M. A.; Kynast, B.; Zorbas, H.; Keppler, B. K. *J. Inorg. Biochem.* **2006**, *100*, 891.

(61) Brabec, V.; Novakova, O. *Drug Resist. Updat.* **2006**, *9*, 111.

(62) Sava, G.; Pacor, S.; Mestroni, G.; Alessio, E. *Clin. Exp. Metastasis* **1992**, *10*, 273.

(63) Harris, T. V.; Szilagyi, R. K.; McFarlane-Holman, K. L. *J. Biol. Inorg. Chem.* **2009**, *14*, 891.

(64) Graf, N.; Lippard, S. J. *Adv. Drug Deliv. Rev.* **2012**, *64*, 993.

(65) Dearling, J. L.; Lewis, J. S.; Mullen, G. E.; Welch, M. J.; Blower, P. J. *J. Biol. Inorg. Chem.* **2002**, *7*, 249.

(66) Ware, D. C.; Palmer, H. R.; Brothers, P. J.; Rickard, C. E. F.; Wilson, W. R.; Denny, W. A. *J. Inorg. Biochem.* **1997**, *68*, 215.

(67) Parker, L. L.; Lacy, S. M.; Farrugia, L. J.; Evans, C.; Robins, D. J.; O'Hare, C. C.; Hartley, J. A.; Jaffar, M.; Stratford, I. J. *J. Med. Chem.* **2004**, *47*, 5683.

(68) Oh, R.; Brown, D. L. *Am. Fam. Physician* **2003**, *67*, 979.

(69) Barceloux, D. G. *J. Toxicol. Clin. Toxicol.* **1999**, *37*, 201.

(70) *IARC Monographs on the Evaluation of Carcinogenic Risks to Humans Chlorinated Drinking water; Chlorination By-Products; Some Other Halogenated Compounds; Cobalt and Cobalt Compounds.*; Lyon, L. A., Ed., 1991; Vol. 52.

(71) *Handbook on the Toxicology of Metals*; Co., A. E. S. P., Ed., 1986; Vol. 2.

(72) Stillman, M. *Angew. Chem. Int. Ed.* **2007**, *46*, 8741.

(73) Kumar, S.; Dhar, D. N.; Saxena, P. N. *J. Sci. Ind. Res.* **2009**, *68*, 181.

(74) Alam, M. S.; Choi, J.-H.; Lee, D.-U. *Biorg. Med. Chem.* **2012**, *20*, 4103.

(75) Sriram, D.; Yogeeswari, P.; Myneedu, N. S.; Saraswat, V. *Biorg. Med. Chem. Lett.* **2006**, *16*, 2127.

(76) Xu, D.; Ma, S.; Du, G.; He, Q.; Sun, D. *J. Rare Earth* **2008**, *26*, 643.

(77) Storr, T.; Scott, L. E.; Bowen, M. L.; Green, D. E.; Thompson, K. H.; Schugar, H. J.; Orvig, C. *Dalton Trans.* **2009**, *16*, 3034.

(78) Zhang, W.; Loebach, J. L.; Wilson, S. R.; Jacobsen, E. N. *J. Am. Chem. Soc.* **1990**, *112*, 2801.

(79) Hughes, D. L.; Smith, G. B.; Liu, J.; Dezeny, G. C.; Senanayake, C. H.; Larsen, R. D.; Verhoeven, T. R.; Reider, P. J. *J. Org. Chem.* **1997**, *62*, 2222.

(80) Cavallo, L.; Jacobsen, H. *Eur. J. Inorg. Chem.* **2003**, *2003*, 892.

(81) Li, Z.; Conser, K. R.; Jacobsen, E. N. *J. Am. Chem. Soc.* **1993**, *115*, 5326.

(82) Kassab, D. J.; Ganem, B. *J. Org. Chem.* **1999**, *64*, 1782.

(83) Martinez, L. E.; Leighton, J. L.; Carsten, D. H.; Jacobsen, E. N. *J. Am. Chem. Soc.* **1995**, *117*, 5897.

(84) Martinez, L. E.; Nugent, W. A.; Jacobsen, E. N. *J. Org. Chem.* **1996**, *61*, 7963.

(85) Larrow, J. F.; Schaus, S. E.; Jacobsen, E. N. *J. Am. Chem. Soc.* **1996**, *118*, 7420.

(86) Chiang, L.; Kochem, A.; Jarjayes, O.; Dunn, T. J.; Vezin, H.; Sakaguchi, M.; Ogura, T.; Orio, M.; Shimazaki, Y.; Thomas, F.; Storr, T. *Chem. Eur. J.* **2012**, *18*, 14117.

(87) Kurahashi, T.; Fujii, H. *Inorg. Chem.* **2013**, *52*, 3908.

(88) Kurahashi, T.; Fujii, H. *J. Am. Chem. Soc.* **2011**, *133*, 8307.

(89) Kauffman, G. B. *J. Chem. Educ.* **2000**, *77*, 165.

(90) Kugel, K. I. i.; Khomskiĭ, D. I. *Phys.Usp.* **1982**, *25*, 231.

(91) Song, Y.; Suntharalingam, K.; Yeung, J. S.; Royzen, M.; Lippard, S. J. *Bioconjug. Chem.* **2013**, *24*, 1733.

(92) Failes, T. W.; Hambley, T. W. *J. Inorg. Biochem.* **2007**, *101*, 396.

(93) Kim, B. J.; Hambley, T. W.; Bryce, N. S. *Chem. Sci.* **2011**, *2*, 2135.

(94) Yamamoto, N.; Renfrew, A. K.; Kim, B. J.; Bryce, N. S.; Hambley, T. W. *J. Med. Chem.* **2012**, *55*, 11013.

(95) Renfrew, A. K.; Bryce, N. S.; Hambley, T. W. *Chem. Sci.* **2013**, *4*, 3731.

(96) Cozzi, P. G. *Chem. Soc. Rev.* **2004**, *33*, 410.

(97) Chiang, L.; Allan, L. E.; Alcantara, J.; Wang, M. C.; Storr, T.; Shaver, M. P. *Dalton Trans.* **2014**, *43*, 4295.

(98) Kochem, A. l.; Kanso, H.; Baptiste, B.; Arora, H.; Philouze, C.; Jarjayes, O.; Vezin, H.; Luneau, D.; Orio, M.; Thomas, F. *Inorg. Chem.* **2012**, *51*, 10557.

(99) Altomare, A.; Cascarano, G.; Giacovazzo, C.; Guagliardi, A. *J. Appl. Crystallogr.* **1993**, *26*, 343.

(100) Sheldrick, G. M. *Acta Cryst. C* **2015**, *71*, 3.

(101) Coletti, A.; Galloni, P.; Sartorel, A.; Conte, V.; Floris, B. *Catal. Today* **2012**, *192*, 44.

(102) Mathavan, A.; Ramdass, A.; Rajagopal, S. *Transition Met. Chem.* **2015**, *40*, 355.

(103) Geneste, H.; Schäfer, B. *Synthesis* **2001**, *2001*, 2259.

(104) Achard, T.; Belokon, Y. N.; Fuentes, J. A.; North, M.; Parsons, T. *Tetrahedron* **2004**, *60*, 5919.

(105) Nielsen, L. P. C.; Stevenson, C. P.; Blackmond, D. G.; Jacobsen, E. N. *J. Am. Chem. Soc.* **2004**, *126*, 1360.

(106) Reznichenko, L. A.; Aleksandrova, E. V.; Mal'tseva, L. F.; Muratova, G. P.; Shipovskaya, L. A.; Vekshina, A. A.; Kochergin, P. M.; Gireva, R. N. *Pharm. Chem. J.* **2001**, *35*, 5.

(107) Fan, G.; Zhao, H.; Duan, Z.; Fang, T.; Wan, M.; He, L. *Catal. Sci. Tech.* **2011**, *1*, 1138.

(108) Hošťálek, Z.; Mundil, R.; Císařová, I.; Trhlíková, O.; Grau, E.; Peruch, F.; Cramail, H.; Merna, J. *Polymer* **2015**, *63*, 52.

(109) Manus, L. M.; Holbrook, R. J.; Atesin, T. A.; Heffern, M. C.; Harney, A. S.; Eckermann, A. L.; Meade, T. J. *Inorg. Chem.* **2013**, *52*, 1069.

(110) Heffern, M. C.; Reichova, V.; Coomes, J. L.; Harney, A. S.; Bajema, E. A.; Meade, T. J. *Inorg. Chem.* **2015**, *54*, 9066.

(111) Kochem, A.; Kanso, H.; Baptiste, B.; Arora, H.; Philouze, C.; Jarjayes, O.; Vezin, H.; Luneau, D.; Orio, M.; Thomas, F. *Inorg. Chem.* **2012**, *51*, 10557.

(112) Orio, M.; Jarjayes, O.; Kanso, H.; Philouze, C.; Neese, F.; Thomas, F. *Angew. Chem. Int. Ed.* **2010**, *49*, 4989.

(113) Chiang, L.; Herasymchuk, K.; Thomas, F.; Storr, T. *Inorg. Chem.* **2015**, *54*, 5970.

(114) Bunce, S.; Cross, R. J.; Farrugia, L. J.; Kunchandy, S.; Meason, L. L.; Muir, K. W.; O'Donnell, M.; Peacock, R. D.; Stirling, D.; Teat, S. J. *Polyhedron* **1998**, *17*, 4179.

(115) Marken, F., Neudeck, A., Bond, A. M. In *Electroanalytical Methods*; Springer Berlin Heidelberg: 2002, p 51.

(116) Hansch, C.; Leo, A.; Taft, R. W. *Chem. Rev.* **1991**, *91*, 165.

(117) Carroll, F. A. *Perspectives on Structure and Mechanism in Organic Chemistry*; 2 ed.; John Wiley & Sons, Inc., 2010.

(118) Hartwig, J. F.; Lippard, S. J. *J. Am. Chem. Soc.* **1992**, *114*, 5646.

(119) Kelland, L. R. *Expert Opin. Investig. Drugs* **2000**, *9*, 1373.

(120) Lakowicz, J. R. *Principles of Fluorescent Spectroscopy*; 3 ed.; Springer, 2006.

(121) Leonetti, F.; Favia, A.; Rao, A.; Aliano, R.; Paluszcak, A.; Hartmann, R. W.; Carotti, A. *J. Med. Chem.* **2004**, *47*, 6792.

(122) Wang, C.; Wu, C.; Zhu, J.; Miller, R. H.; Wang, Y. *J. Med. Chem.* **2011**, *54*, 2331.

(123) Jung, H. S.; Kwon, P. S.; Lee, J. W.; Kim, J. I.; Hong, C. S.; Kim, J. W.; Yan, S.; Lee, J. Y.; Lee, J. H.; Joo, T.; Kim, J. S. *J. Am. Chem. Soc.* **2009**, *131*, 2008.

(124) Musa, M. A.; Cooperwood, J. S.; Khan, M. O. F. *Curr. Med. Chem.* **2008**, *15*, 2664.

(125) Venugopala, K. N.; Rashmi, V.; Odhav, B. *BioMed Res. Int.* **2013**, *2013*, 14.

(126) Lacy, A.; O'Kennedy, R. *Curr. Pharm. Des.* **2004**, *10*, 3797.

(127) Pauli, W. *Science* **1946**, *103*, 213.

(128) Skoog, D. A. H., James, F., Nieman, T., A *Principles of instrumental analysis*; 5 ed.; Thomson Learning/Brooks/cole: Victoria, Australia, 1998.

(129) Bernard Valeur, M. N. B.-S. *Molecular Fluorescence: Principles and Applications*; 2 ed.; John Wiley & Sons, 2013.

(130) Pawlizak, S. University of Leipzig, 2009; Vol. 2015.

(131) Swinehart, D. F. *J. Chem. Educ.* **1962**, *39*, 333.

(132) Lajunen, L. J. H. P., Paavo *Spectrochemical Analysis by Atomic Absorption and Emission*; *RSC*, 2004.

(133) Mayhew, S. G. *Eur. J. Biochem.* **1978**, *85*, 535.

(134) Barman, B. G.; Tollin, G. *Biochemistry* **1972**, *11*, 4755.

(135) Scaife, C. W. J.; Wilkins, R. G. *Inorg. Chem.* **1980**, *19*, 3244.

(136) Matosziuk, L. M.; Holbrook, R. J.; Manus, L. M.; Heffern, M. C.; Ratner, M. A.; Meade, T. J. *Dalton Trans.* **2013**, *42*, 4002.

(137) Takeuchi, T.; Böttcher, A.; Quezada, C. M.; Meade, T. J.; Gray, H. B. *Biorg. Med. Chem.* **1999**, *7*, 815.

(138) Karaoun, N.; Renfrew, A. K. *Chem. Commun.* **2015**, *51*, 14038.

(139) Palopoli, C.; Bruzzo, N.; Hureau, C.; Ladeira, S.; Murgida, D.; Signorella, S. *Inorg. Chem.* **2011**, *50*, 8973.

(140) Correia, I.; Dornyei, A.; Jakusch, T.; Avecilla, F.; Kiss, T.; Costa Pessoa, J. *Eur. J. Inorg. Chem.* **2006**, *2006*, 2819.

(141) Delahaye, É.; Diop, M.; Welter, R.; Boero, M.; Massobrio, C.; Rabu, P.; Rogez, G. *Eur. J. Inorg. Chem.* **2010**, *2010*, 4450.

(142) Zhou, L.; Cai, P.; Feng, Y.; Cheng, J.; Xiang, H.; Liu, J.; Wu, D.; Zhou, X. *Anal. Chim. Acta* **2012**, *735*, 96.

(143) Correia, I.; Pessoa, J. C.; Duarte, M. T.; da Piedade, M. F. M.; Jackush, T.; Kiss, T.; Castro, M. M. C. A.; Geraldes, C. F. G. C.; Avecilla, F. *Eur. J. Inorg. Chem.* **2005**, *2005*, 732.

(144) Savjani, K. T.; Gajjar, A. K.; Savjani, J. K. *ISRN Pharm.* **2012**, *2012*, 195727.

(145) Hager, E. B.; Makhubela, B. C.; Smith, G. S. *Dalton Trans.* **2012**, *41*, 13927.

(146) Palopoli, C.; Bruzzo, N.; Hureau, C.; Ladeira, S.; Murgida, D.; Signorella, S. *Inorg. Chem.* **2011**, *50*, 8973.

(147) Berry, K. J.; Moya, F.; Murray, K. S.; van den Bergen, A. M. B.; West, B. O. *J. Chem. Soc., Dalton Trans.* **1982**, 109.

(148) Jordheim, L. P.; Durantel, D.; Zoulim, F.; Dumontet, C. *Nat. Rev. Drug Discov.* **2013**, *12*, 447.

(149) Galmarini, C. M.; Mackey, J. R.; Dumontet, C. *Lancet. Oncol.* **2002**, *3*, 415.

(150) Melchart, M.; Habtemariam, A.; Parsons, S.; Sadler, P. J. *J. Inorg. Biochem.* **2007**, *101*, 1903.

(151) Anzellotti, A. I.; Liu, Q.; Bloemink, M. J.; Scarsdale, J. N.; Farrell, N. *Chem. Biol.* **2006**, *13*, 539.

(152) Mikulski, C. M.; Minutella, R.; DeFranco, N.; Karayannis, N. M. *Inorg. Chim. Acta* **1985**, *106*, L33.

Appendix

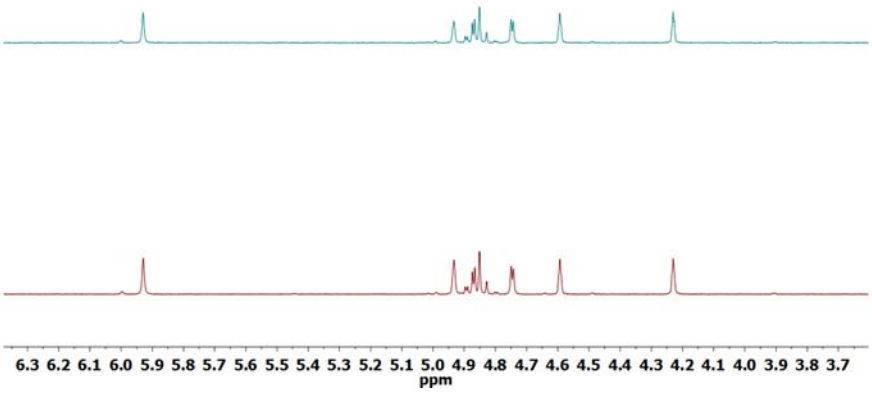

Appendix 2.1: ^{1}H NMR spectra of [Co^{III}(salen^{OMe})(1-MeIm)$_2$]ClO$_4$. Red, spectrum at 10 min; Green, spectrum at 24 h. Conditions: 2% DMSO-d_6 in deuterated PBS, 310 K.

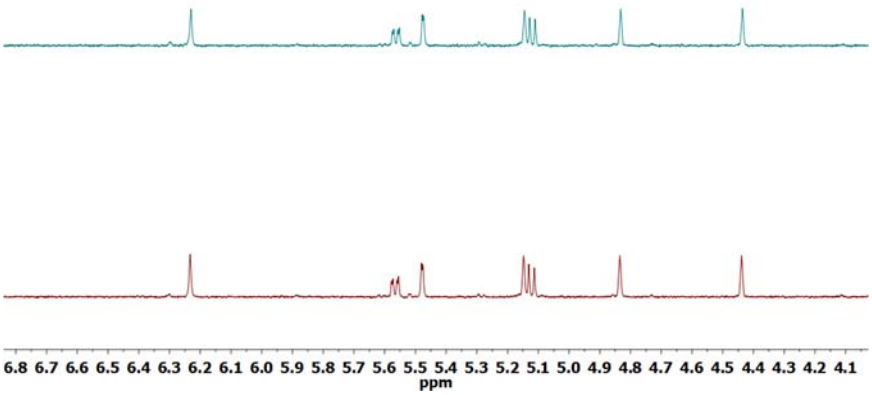

Appendix 2.2: ^{1}H NMR spectra of [Co^{III}(salen^{tBu})(1-MeIm)$_2$]ClO$_4$. Red, spectrum at 10 min; Green, spectrum at 24 h. Conditions: 2% DMSO-d_6 in deuterated PBS, 310 K.

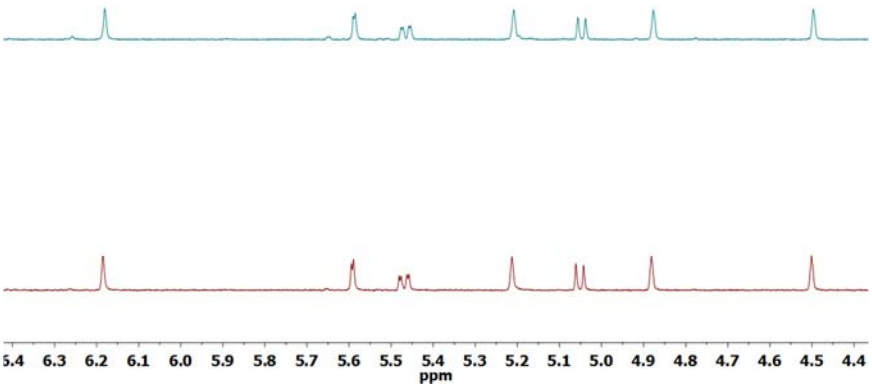

Appendix 2.3: ^{1}H NMR spectra of [Co^{III}(salen^{Br})(1-MeIm)$_2$]ClO$_4$. Red, spectrum at 10 min; Green, spectrum at 24 h. Conditions: 2% DMSO-*d*$_6$ in deuterated PBS, 310 K.

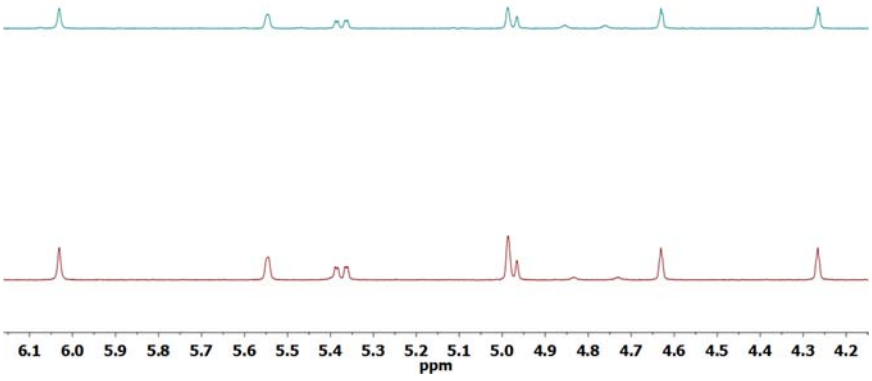

Appendix 2.4: ^{1}H NMR spectra of [Co^{III}(salen^{CF3})(1-MeIm)$_2$]ClO$_4$. Red, spectrum at 10 min; Green, spectrum at 24 h. Conditions: 2% DMSO-*d*$_6$ in deuterated PBS, 310 K.

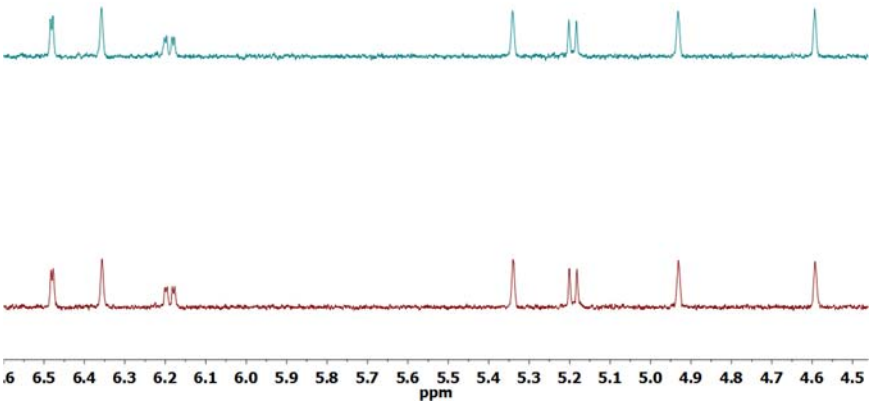

Appendix 2.5: ^{1}H NMR spectra of [Co^{III}(salen^{NO2})(1-MeIm)$_2$]ClO$_4$. Red, spectrum at 10 min; Green, spectrum at 24 h. Conditions: 2% DMSO-d_6 in deuterated PBS, 310 K.

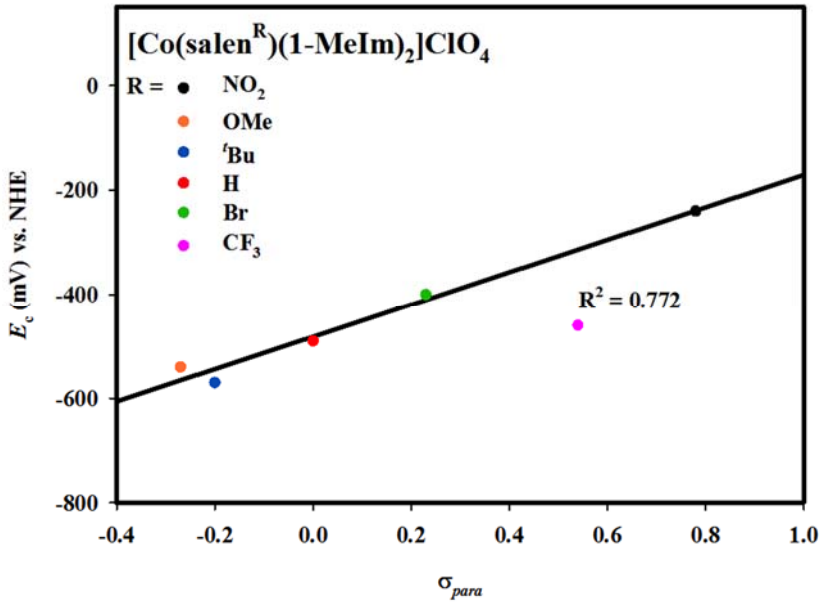

Appendix 2.6: Hammett plot of the E_c value of the [Co^{III}(salen^{R})(1-MeIm)$_2$]ClO$_4$ complexes versus σ_{para} of the *para*-ring substituents.

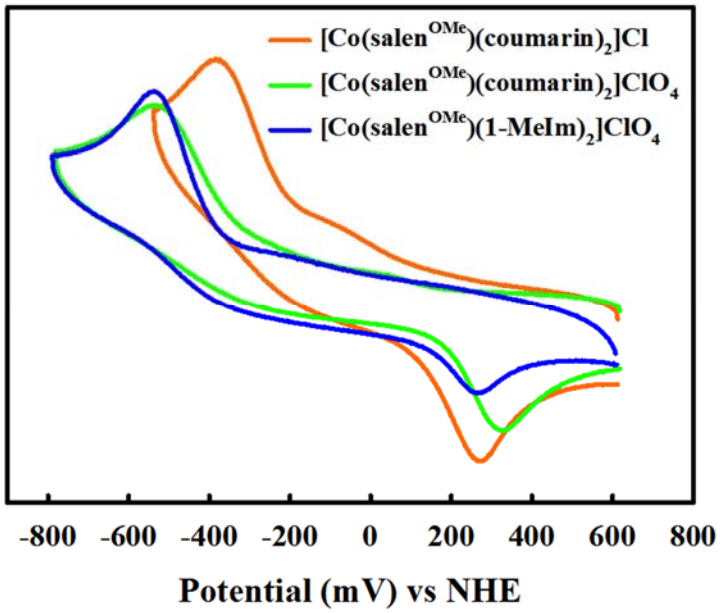

Appendix 3.1 Reduction potentials for $[Co^{III}(salen^{OMe})(1\text{-MeIm})_2]ClO_4$ (Blue), $[Co^{III}(salen^{OMe})(coumarin)_2]ClO_4$ (Green), and $[Co^{III}(salen^{OMe})(coumarin)_2]Cl$ (Orange). The direction of the arrow signifies the direction of the scans. Conditions: 1 mM complex, 0.1 M $^{n}Bu_4NClO_4$, scan rate 100 mV s^{-1}, DMF, 293 K.

Appendix 3.2: Reduction potentials (mV) for complexes versus NHE.

	E_c	E_a	$E_{1/2}$	ΔE_p[a]
$[Co^{III}(salen^{OMe})(1\text{-MeIm})_2]ClO_4$	-540	260	-140	800
$[Co^{III}(salen^{OMe})(coumarin)_2]ClO_4$	-540	320	-110	800
$[Co^{III}(salen^{OMe})(coumarin)_2]Cl$	-390	270	60	660

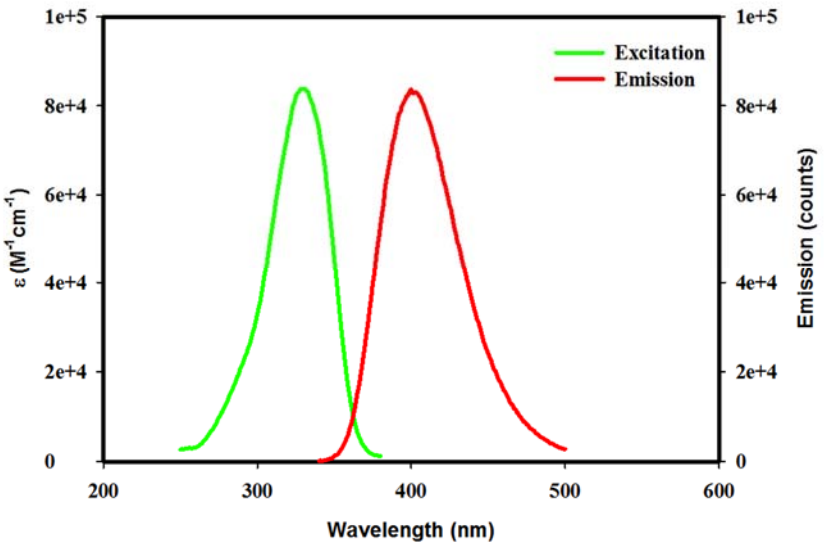

Appendix 4.1: Excitation and emission spectrum of coumarin: emission (green), excitation (red). (λ_{ex} = 327 nm, λ_{em} = 400 nm)

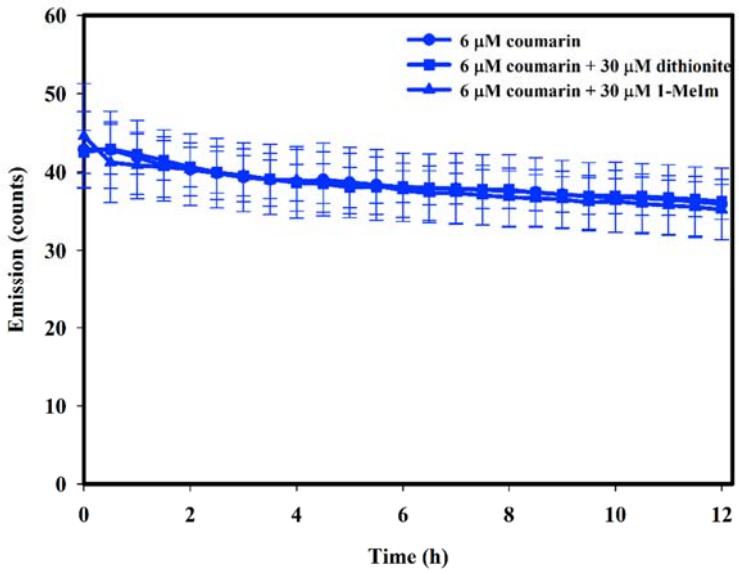

Appendix 4.2: Summary of fluorescence study of coumarin only (circle), under reducing environment (square) and ligand exchange (triangle). (λ_{ex} = 327 nm, λ_{em} = 400 nm)

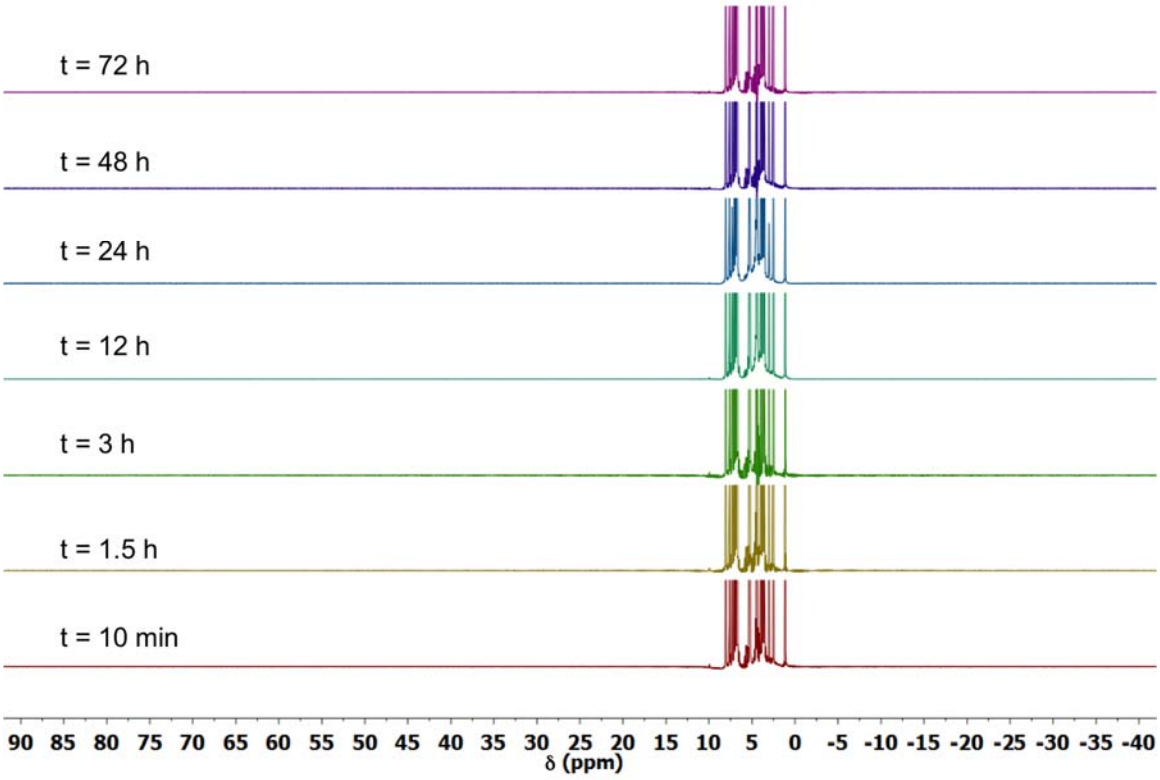

Appendix 4.3: ^{1}H NMR spectra of $[Co^{III}(salen^{OMe})(coumarin)_2]Cl$ (16 mM in 50% DMSO-d_6/D_2O) over 72 hours.

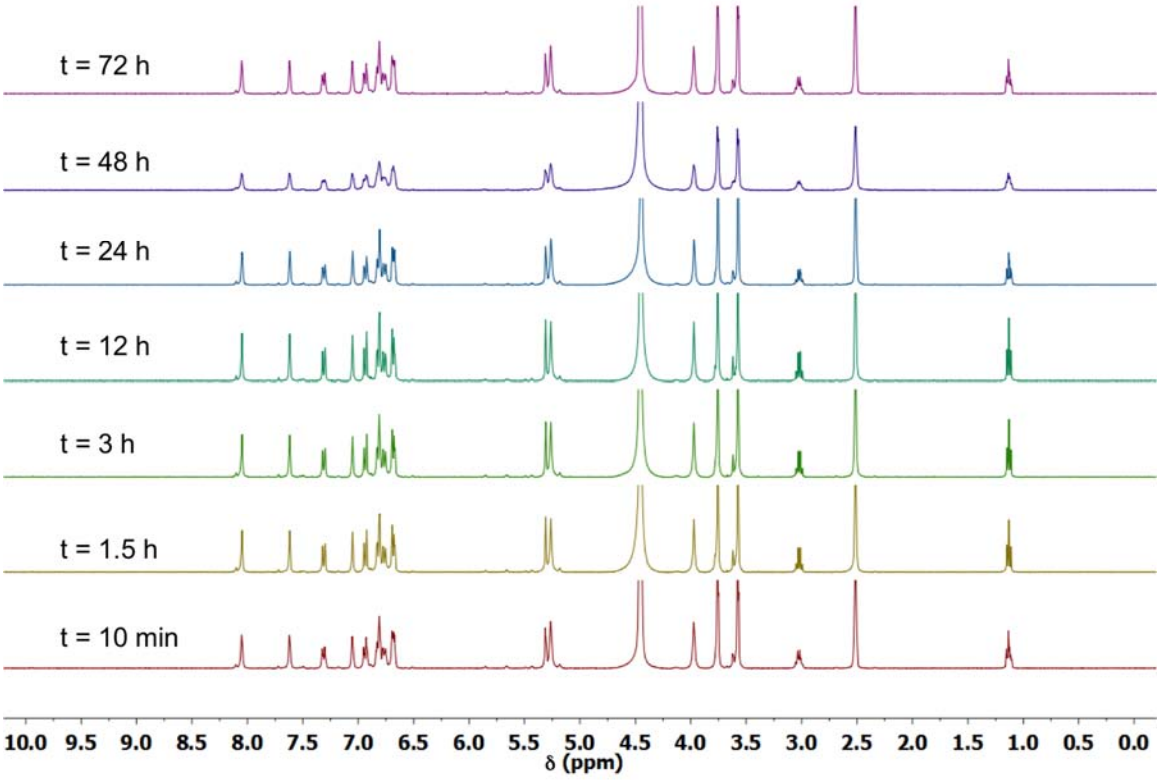

Appendix 4.4: ^{1}H NMR spectra of $[Co^{III}(salen^{OMe})(coumarin)_2]Cl$ (16 mM in 50% DMSO-d_6/D_2O) over 72 hours.

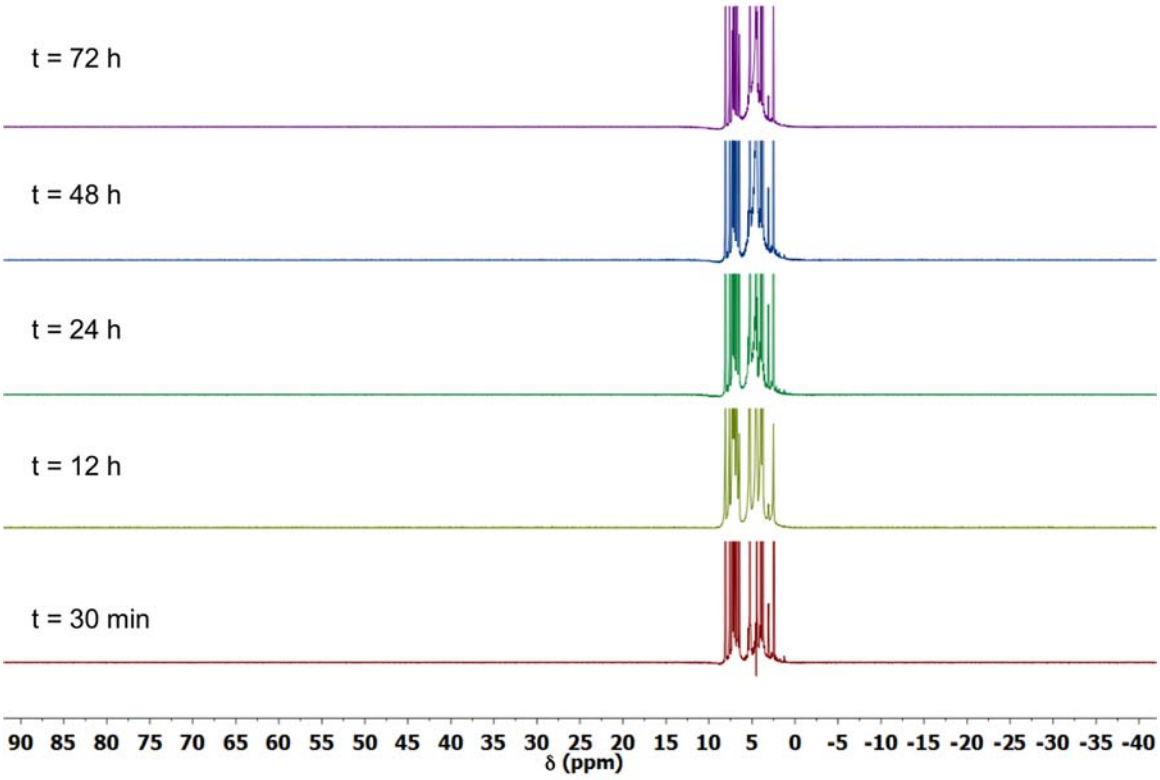

Appendix 4.5: ^{1}H NMR spectra of $[Co^{III}(salen^{H})(coumarin)_2]Cl$ (16 mM in 50% DMSO-d_6 /D_2O) over 72 hours.

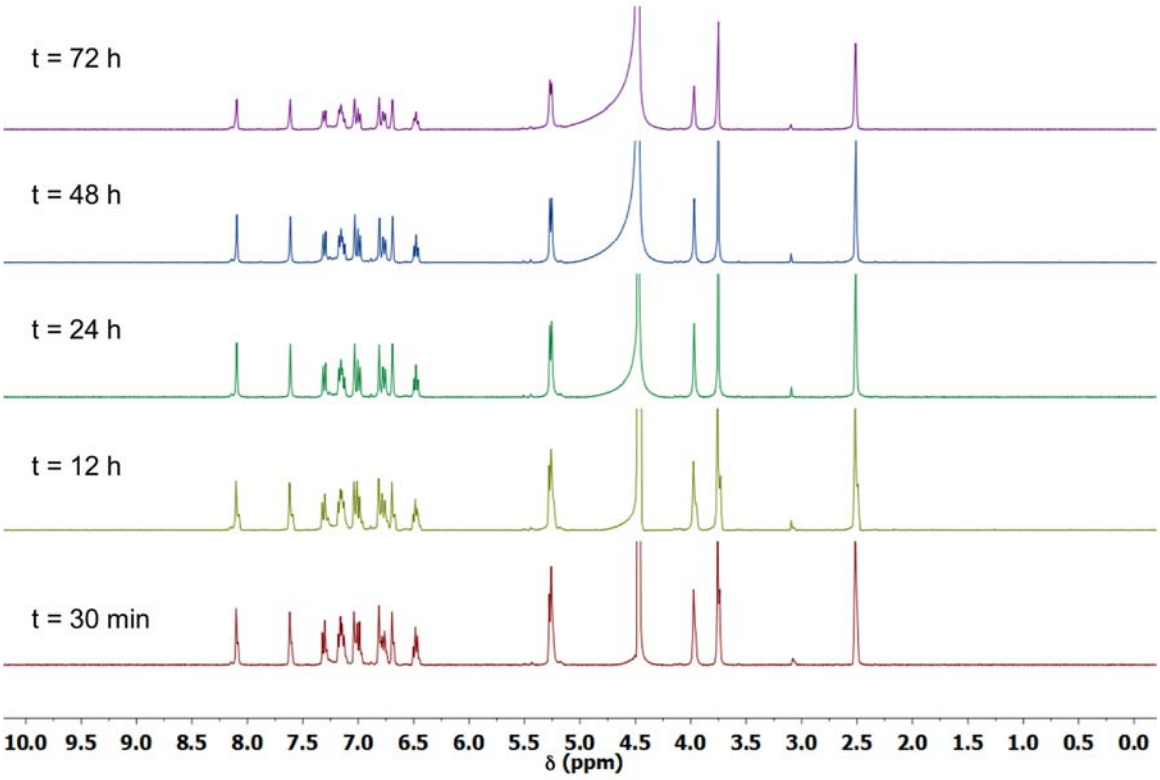

Appendix 4.6: ^{1}H NMR spectra of $[Co^{III}(salen^{H})(coumarin)_2]Cl$ (16 mM in 50% DMSO-d_6 /D_2O) over 72 hours.

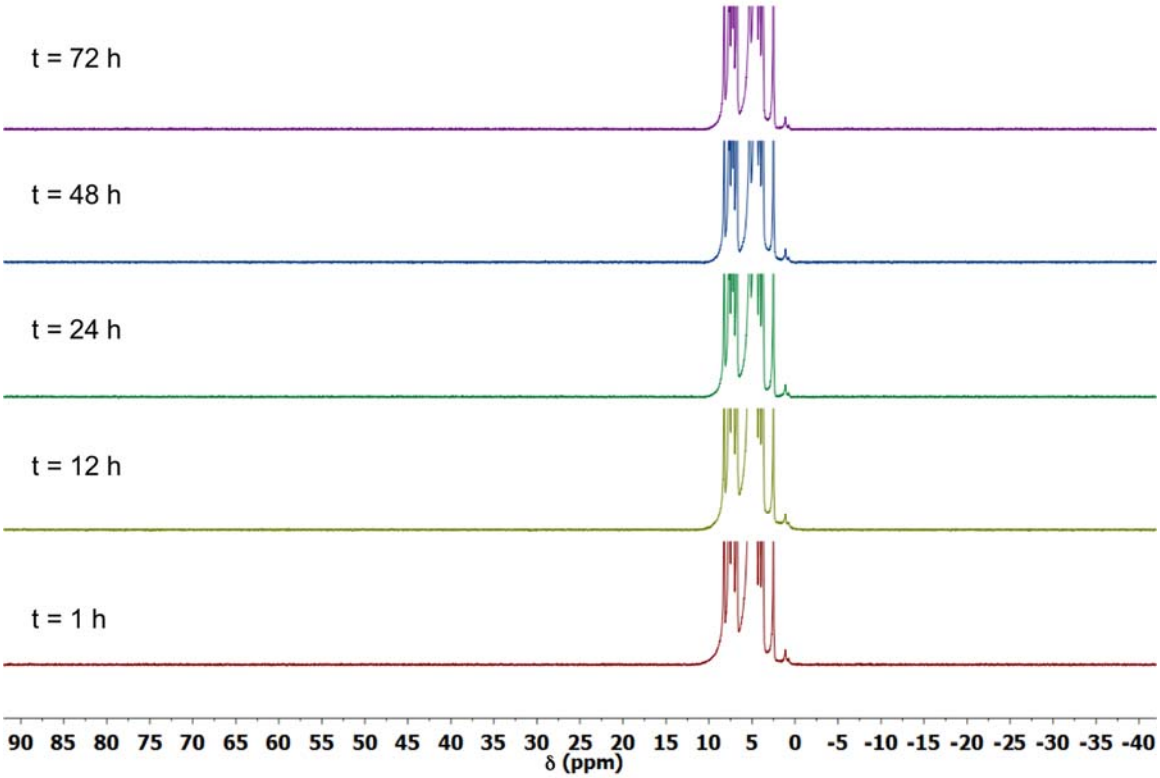

Appendix 4.7: ^{1}H NMR spectra of [Co^{III}(salen^{CF3})(coumarin)$_2$]Cl (16 mM in 50% DMSO-d_6/D_2O) over 72 hours.

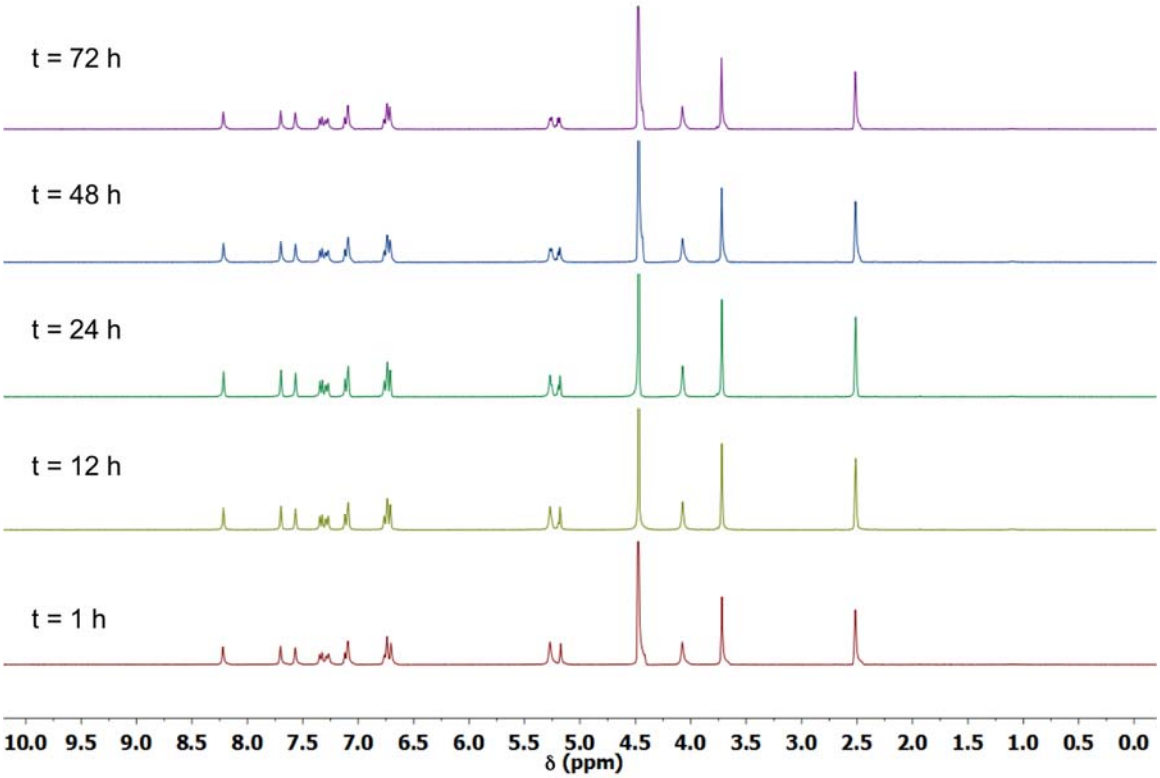

Appendix 4.8: ^{1}H NMR spectra of [Co^{III}(salen^{CF3})(coumarin)$_2$]Cl (16 mM in 50% DMSO-d_6/D$_2$O) over 72 hours.

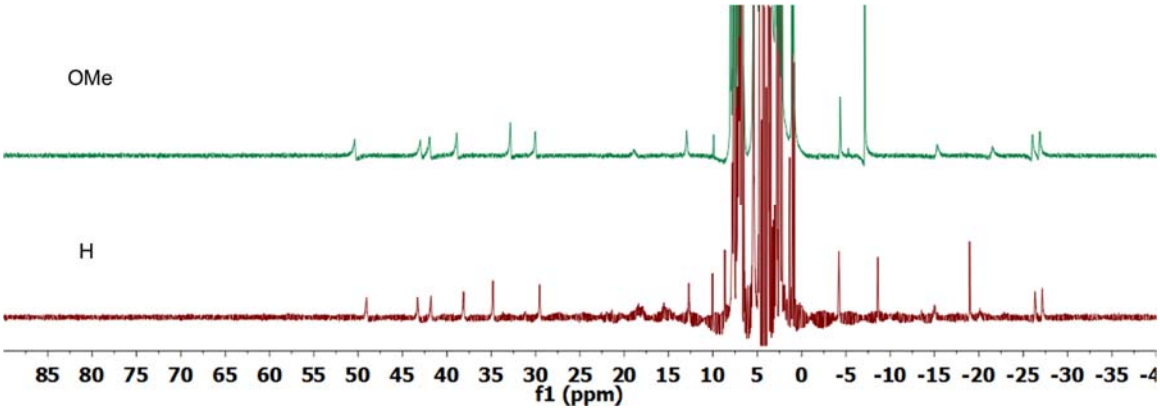

Appendix 4.9: ^{1}H NMR spectra of [Co^{III}(salen^{OMe})(coumarin)$_2$]Cl and [Co^{III}(salen^{H})(coumarin)$_2$]Cl in presence of $Na_2S_2O_4$ at 24 h. Conditions: 16 mM in 50% DMSO-d_6/D$_2$O at 298 K.

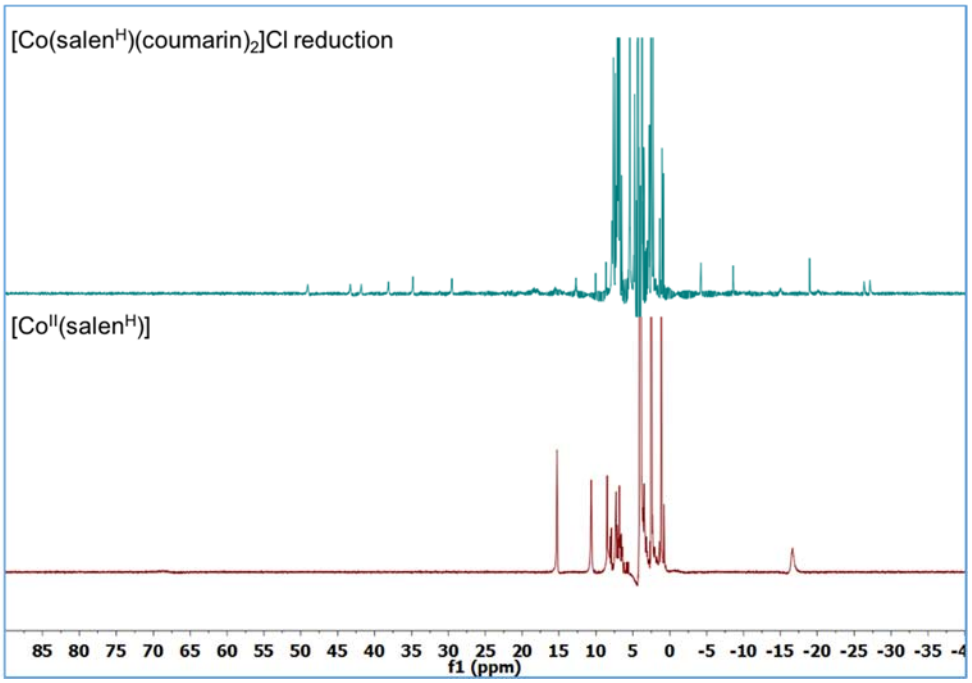

Appendix 4.10: ^{1}H NMR spectra of [Co^{III}(salen^{H})(coumarin)$_2$]Cl (16 mM in 50% DMSO-d_6 /D_2O) in presence of $Na_2S_2O_4$ at 24 h and [Co^{II}(salen^{H})] (90% DMSO-d_6 /D_2O).

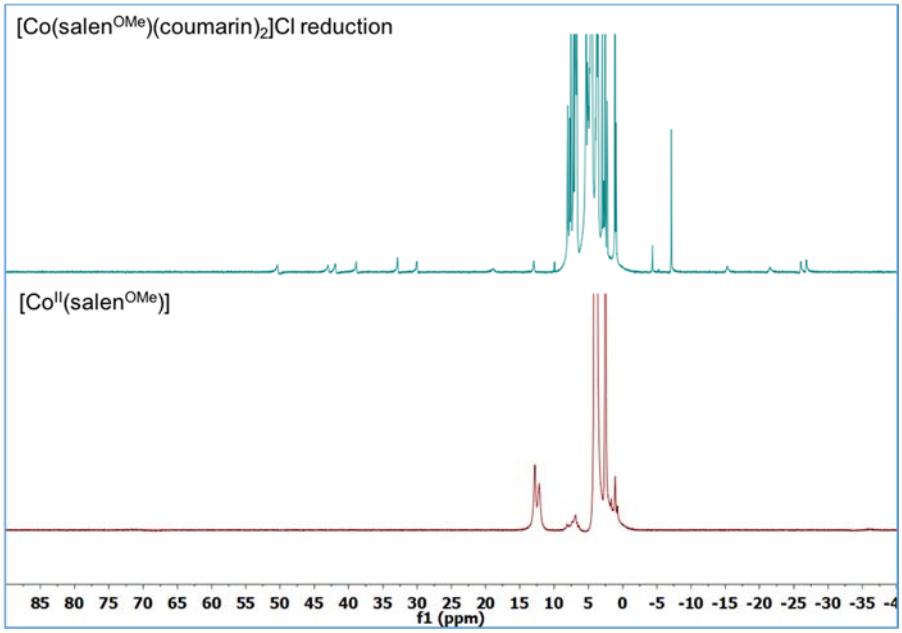

Appendix 4.11: ^{1}H NMR spectra of [Co^{III}(salen^{OMe})(coumarin)$_2$]Cl (16 mM in 50% DMSO-d_6 /D_2O) in presence of $Na_2S_2O_4$ at 24 h and [Co^{II}(salen^{OMe})] (90% DMSO-d_6 /D_2O).

Appendix 5: Syntheses of water soluble salen compounds.

(*E*)-2-((Phenylimino)methyl)phenol (**32**)[145]

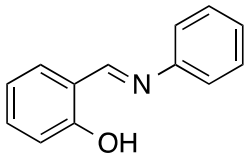

A mixture of aniline (0.37 g, 3.0 mmol) and 2-hydroxybenzaldehyde (0.28 g, 3.0 mmol) and a few drops of acetic acid in dry MeOH (6 mL) was refluxed for 4 h. The reaction mixture was then cooled and poured into ice-cold water. The solid obtained was filtered, washed with ice-cold water, dried and recrystallized from MeOH to afford compound **32**. Yield: 0.54 g, 91%. ^{1}H NMR (400 MHz, $CDCl_3$) δ 8.63 (s, 1H), 7.49-7.35 (m, 4H,), 7.34-7.27 (m, 3H), 7.03 (t, 1H, *J* = 6.6 Hz), 6.98-6.90 (m, 1H). ESI (+)-MS m/z (relative intensity) = 198.0866 ([**32**+H]$^+$). The synthetic procedure for this compound has been reported and characterization matches literature data.[145]

(*E*)-4-Hydroxy-3-((phenylimino)methyl)benzenesulfonic acid (**33**)[145]

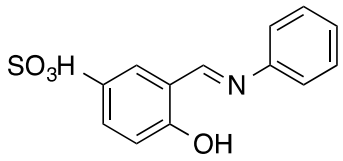

Concentrated sulfuric acid (20 mL of 98% H_2SO_4) was placed in a round-bottom flask fitted with reflux condenser and (*E*)-2-((phenylimino)methyl) phenol (7.42 g, 38.0 mmol) was added slowly with stirring. The mixture was heated at 100–105 °C for 3 h and a colour change from yellow to brown was observed. The hot solution was cooled and poured carefully into a beaker containing 200 mL of ice water. A yellow precipitate formed immediately. The suspension was then reheated until the precipitate had dissolved to form a bright orange solution. Insoluble particles were filtered from the hot solution and the filtrate left to stand at room temperature. The yellow-brown microcrystalline product was filtered and washed with small portions of cold water. The product was used directly for the next step. ESI (-)-MS m/z (relative intensity) = 276.0406 ([**33**-H]$^-$). The synthetic

procedure for this compound has been reported and characterization matches literature data.[145]

Sodium 3-formyl-4-hydroxybenzenesulfonate (**34**)[145]

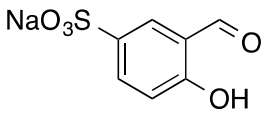

Compound **33** (8.29 g, 30.0 mmol) and Na_2CO_3 (3.17 g, 30.0 mmol) were refluxed vigorously in a round-bottom flask containing 10 mL of distilled water for 2 h. Glacial acetic acid was then added to the cooled solution to adjust to pH 5. An equal volume of EtOH was added and the solution cooled in an ice-bath for several hours. The yellow product was filtered and washed with cold ethanol, and dried in *vacuo*. Yield: 5.05 g, 45%. ^{1}H NMR (400 MHz, D_2O) δ 8.07 (s, 1H, *J* = 2.4), 7.87 (dd, 1H, *J* = 8.8, 2.4 Hz), 7.04 (d, 1H, *J* = 8.8 Hz). ESI (-)-MS m/z (relative intensity) = 200.9904 ([**34**-Na]$^-$). The synthetic procedure for this compound has been reported and characterization matches literature data.[145]

Sodium 3,3'-((1*E*,1'*E*)- (ethane-1,2-diylbis(azanylylidene)) bis(methanylylidene)) bis(4-hydroxybenzenesulfonate) (**35**)[145]

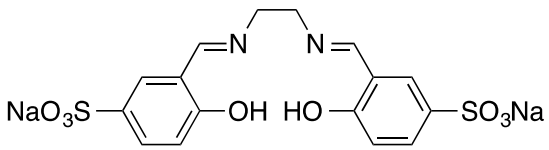

Sodium 3-formyl-4-hydroxybenzenesulfonate (0.20 g, 0.81 mmol) and ethane-1,2-diamine (0.024 g, 0.46 mmol) were dissolved in ethanol (15 mL) and refluxed for 2 h in which time a light yellow precipitate formed. The solid was collected by filtration and was washed with EtOH, then dried under reduced pressure overnight. Yield: 0.16 g, 71%. ^{1}H NMR (400 MHz, DMSO-d_6) δ 8.67 (s, 1H), 7.68 (d, 1H, *J* = 2.2 Hz), 7.52 (dd, 1H, *J* = 8.5, 2.2 Hz), 6.79 (d, 1H, *J* = 8.6 Hz), 3.91 (s, 2H). The synthetic procedure for this compound has been reported and characterization matches literature data.[145]

(*E*)-2-(*tert*-butyl)-6-((phenylimino)methyl)phenol (**36**)[145]

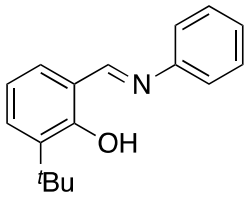

(*E*)-2-(*tert*-butyl)-6-((phenylimino)methyl)phenol was synthesized following the same procedure as compound **32** combining 3-(*tert*-butyl)-2-hydroxybenzaldehyde (0.3 g, 1.7 mmol) and aniline (0.16 g, 1.68 mmol). Yield: 0.34 g. The product was used directly in the next step.

(*E*)-3-(*tert*-butyl)-4-hydroxy-5-((phenylimino)methyl)benzenesulfonic acid (**37**)[145]

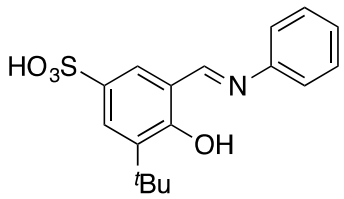

This compound was synthesized following the same procedure as compound **33** combining compound **36** (0.30 g, 1.2 mmol) and sulfuric acid (1 mL, 20 mmol). Yield: 0.09 g). The product was used directly in the next step.

Sodium 3-(*tert*-butyl)-5-formyl-4-hydroxybenzenesulfonate(**38**)[145]

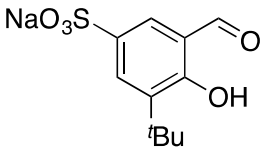

This compound was synthesized following the same procedure as compound **34**, combining compound **37** (0.10 g, 0.30 mmol) and Na_2CO_3 (0.032 g, 0.30 mmol). Yield: 0.04 g, 45%. ^{1}H NMR (400 MHz, D_2O) δ 9.88 (s, 1H), 7.88 (d, 1H, *J* = 2.4 Hz), 7.83 (s, 1H,), 1.33 (s, 9H). The synthetic procedure for this compound has been reported and characterization matches literature data.[145]

Sodium 5,5'-((1*E*,1'*E*)-(ethane-1,2-diylbis(azanylylidene)) bis(methanylylidene)) bis(3-(*tert*-butyl)-4-hydroxybenzenesulfonate) (**39**)[145]

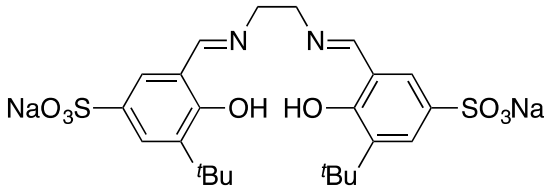

This compound was synthesized using the same method as for compound **34**, combining compound **38** (0.20 g, 0.66 mmol) with ethane-1,2-diamine (0.020 g, 0.33 mmol). Yield: 0.07 g, 34%. ^{1}H NMR (400 MHz, DMSO-d_6) δ 8.68 (s, 1H), 7.56-7.53 (m, 2H), 3.93 (s, 2H), 1.64 (s, 9H). The synthetic procedure for this compound has been reported and characterization matches literature data.[145]

3-chloro-2-hydroxybenzaldehyde (**40**)[15]

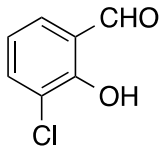

To a solution of 2-hydroxybenzaldehyde (0.25 g, 2.0 mmol) and 2,2,6,6-tetramethylpiperidine (0.028 g, 0.30 mmol) in $PhCF_3$ (10 mL) at 100 °C was added SO_2Cl_2 (325 µL, 4.0 mmol) slowly under N_2. The reaction mixture was heated for 40 min, cooled, and concentrated. The residue was dissolved in DCM, which was washed with saturated NaCl solution and dried over Na_2SO_4. Yield: 1.10 g, 57%. ^{1}H NMR (400 MHz, $CDCl_3$) δ 9.91 (s, 1H), 7.62 (ddd, 1H, *J* = 7.9, 1.6, 0.6 Hz), 7.51 (dd, *J* = 7.7, 1.6 Hz), 7.00 (t, 1H, *J* = 7.8 Hz). The synthetic procedure for this compound has been reported and characterization matches literature data.[15]

(*E*)-2-chloro-6-((phenylimino)methyl)phenol (**41**)[142]

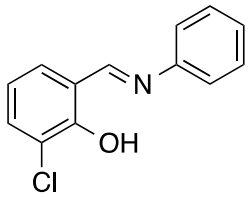

(*E*)-2-chloro-6-((phenylimino)methyl)phenol was synthesized following the same procedure as compound **32**, combining 3-chloro-2-hydroxybenzaldehyde (1.00 g, 6.39 mmol) and aniline (0.600 g, 6.39 mmol). Yield: 1.03 g, 70%. ^{1}H NMR (400 MHz, $CDCl_3$) δ 8.64 (s, 1H), 7.50-7.42 (m, 3H), 7.32 (ddt, 4H, *J* = 8.3, 7.5, 1.3 Hz), 6.90 (t, 1H, *J* = 7.8 Hz). ESI (+)-MS m/z (relative intensity) = 232.0855 ([**41**+H]$^+$). The synthetic procedure for this compound has been reported and characterization matches literature data.[142]

(*E*)-3-Chloro-4-hydroxy-5-((phenylimino)methyl)benzenesulfonic acid (**42**)[142]

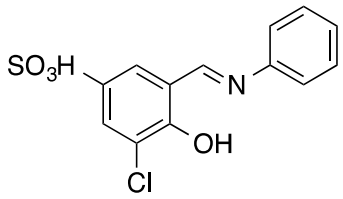

(*E*)-3-Chloro-4-hydroxy-5-((phenylimino)methyl)benzenesulfonic acid was synthesized following the same procedure as compound **32**, combining compound **41** (0.30 g, 1.68 mmol) and sulfuric acid (1.34 mL, 25.0 mmol). Yield: 0.31 g. The compound was used directly in the next step.

Sodium 3-Chloro-5-formyl-4-hydroxybenzenesulfonate(**43**)[142]

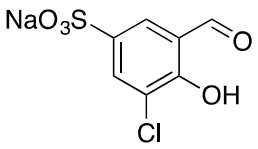

3-Chloro-5-formyl-4-hydroxybenzenesulfonic acid was synthesized following the same procedure as compound **34**, combining compound **42** (0.1 g, 0.3 mmol) and Na_2CO_3

(0.032 g, 0.30 mmol). Yield: 0.04 g, 45%. ^{1}H NMR (400 MHz, D_2O) δ 10.01 (s, 1H), 7.81 (d, 2H, *J* = 9.0 Hz). ESI (-)-MS m/z (relative intensity) = 234.9482 ([**43**-Na]$^-$).

(*E*)-2-Methoxy-6-((phenylimino)methyl)phenol (**44**)[146]

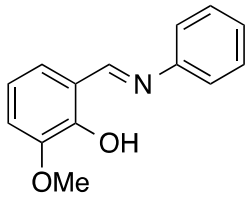

(*E*)-2-Methoxy-6-((phenylimino)methyl)phenol was synthesized following the same procedure as compound **32**, combining 3-methoxy-2-hydroxybenzaldehyde (1.00 g, 6.39 mmol) and aniline (0.600 g, 6.39 mmol). Yield: 1.16 g, 78%. ^{1}H NMR (400 MHz, $CDCl_3$) δ 8.64 (s, 1H), 7.46-7.41 (m, 2H), 7.32-7.27 (m, 3H), 7.04 (dd, 1H, *J* = 7.7, 1.5 Hz), 7.00 (dd, 1H, *J* = 8.1, 1.5 Hz), 6.89 (t, 1H, *J* = 7.9 Hz), 3.95 (s, 3H). ESI (+)-MS m/z (relative intensity) = 228.1025 ([**44**+H]$^+$).

(*E*)-4-Hydroxy-3-methoxy-5-((phenylimino)methyl)benzenesulfonic acid (**45**)[146]

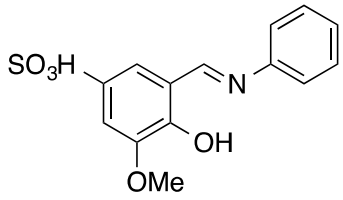

(*E*)-4-Hydroxy-3-methoxy-5-((phenylimino)methyl)benzenesulfonic acid was synthesized following the same procedure as compound **32**, combining compound **44** (0.240 g, 1.06 mmol) and sulfuric acid (0.84 mL, 16 mmol). Yield: 0.21 g, 65%. The compound was used directly in the next step. ESI (+)-MS m/z (relative intensity) = 308.0585 ([**45**+H]$^+$).

Sodium 3-Formyl-4-hydroxy-5-methoxybenzenesulfonate(**46**)[146]

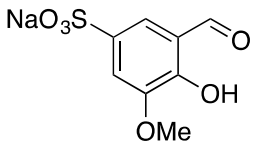

Compound **46** was synthesized following the same procedure as compound **34**, combining compound **45** (0.20 g, 0.65 mmol) and Na_2CO_3 (0.060 g, 0.65 mmol). Yield: 0.16 g, 98%. ^{1}H NMR (400 MHz, D_2O) δ 10.09 (s, 1H), 7.61 (d, 1H, *J* = 2.3 Hz), 7.25 (d, 1H, *J* = 2.4 Hz), 3.86 (s, 3H). ESI (-)-MS m/z (relative intensity) = 230.9896 ([**46**-Na]$^+$).

Ni^{II} complex of sodium 3,3'-((1*E*,1'*E*)- (ethane-1,2-diylbis(azanylylidene)) Bis(methanylylidene)) bis(4-hydroxybenzenesulfonate) (**47**)[140]

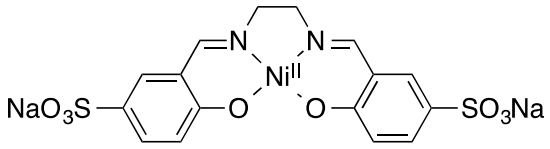

Sodium 3-formyl-4-hydroxybenzenesulfonate (0.10 g, 0.21 mmol) and ethane-1,2-diamine (0.013 g, 0.21 mmol) were dissolved in MeOH (5 mL) containing 4 drops of a tetrabutylammonium hydroxide solution (1M, 0.26 g in 1 mL MeOH). $Ni(CH_3COO)_2$•$4H_2O$ (0.053 g, 0.21 mmol) dissolved in MeOH (5 mL) was slowly added and the mixture became orange. The pH of the mixture was adjusted to 7 by the addition of methanolic HCl. The mixture was stirred for 5 h before collected by filtration. The resulting solid was washed with MeOH and Et_2O and dried in vacuum. Yield: 0.09 g, 85%. ^{1}H NMR (400 MHz, D_2O) δ = 7.95 (s, 1H), 7.77 (s, 1H), 7.35 (t, 1H, *J* = 19.5 Hz), 6.90 (d, 1H, *J* = 8.0 Hz), 3.45(s, 2H).

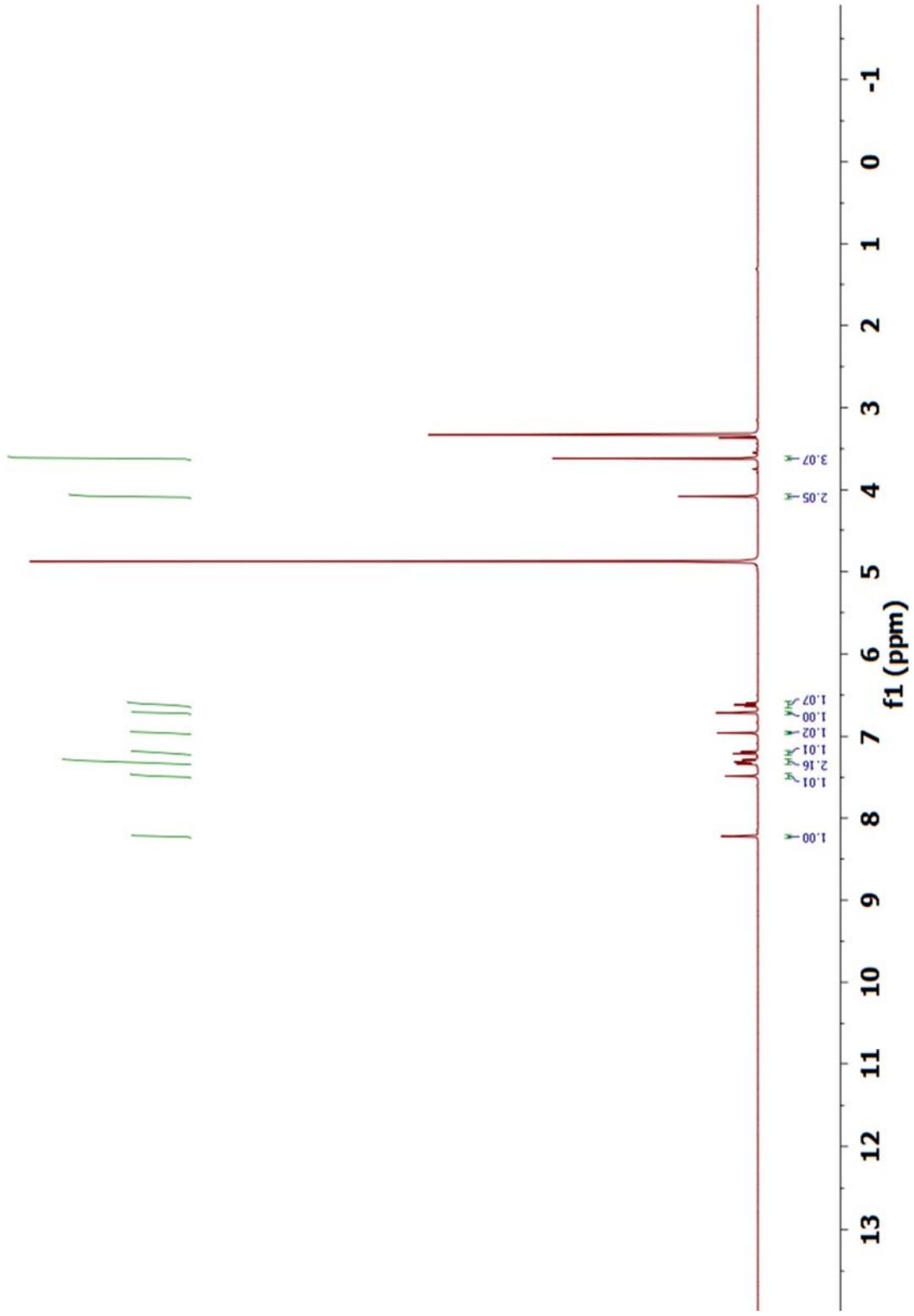

^{1}H NMR spectrum of [Co^{III}(salen^{H})(1-MeIm)$_2$]ClO$_4$ in DMSO-d$_6$.

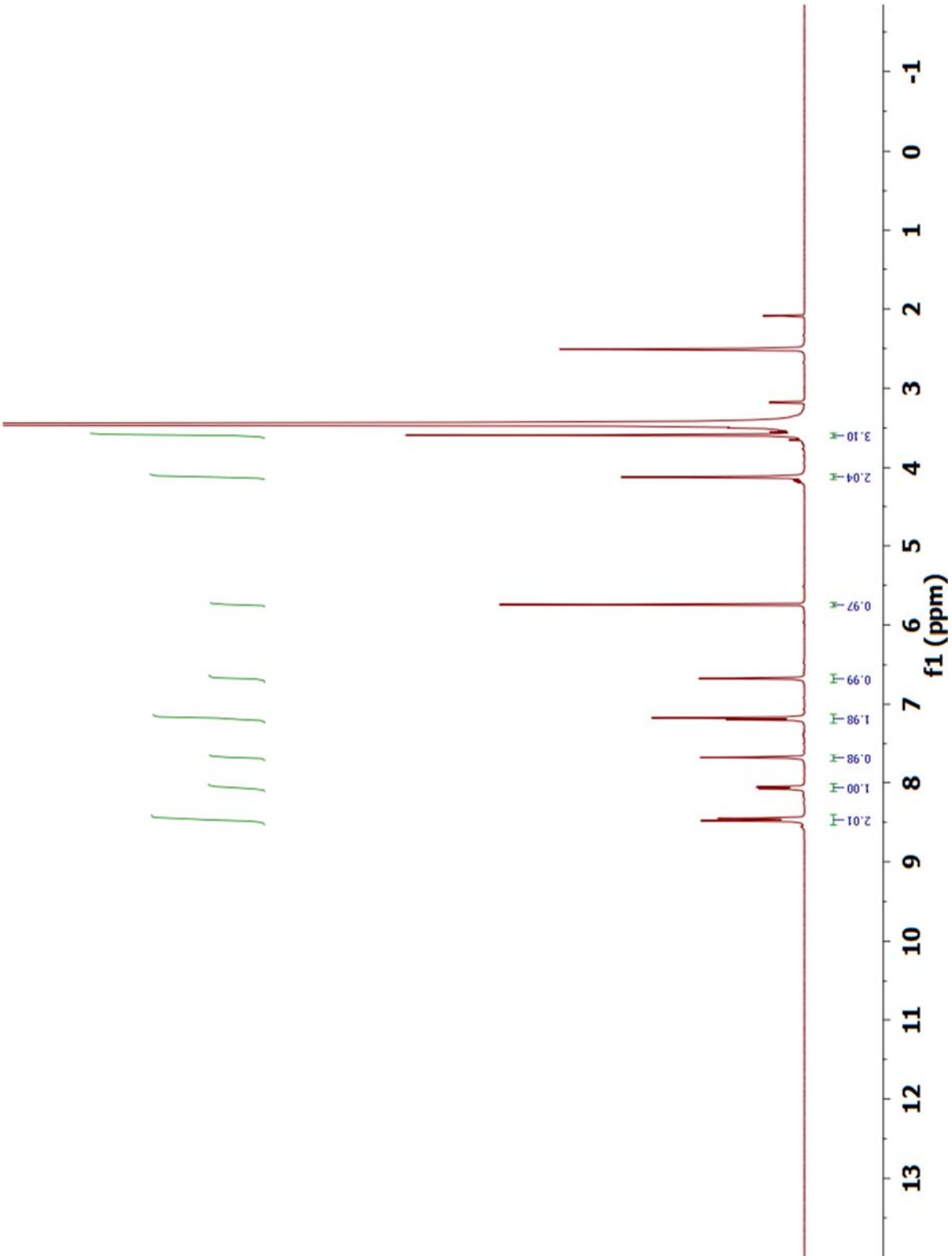

^{1}H NMR spectrum of [Co^{III}(salen^{NO2})(1-MeIm)$_2$]ClO$_4$ in DMSO-d$_6$.

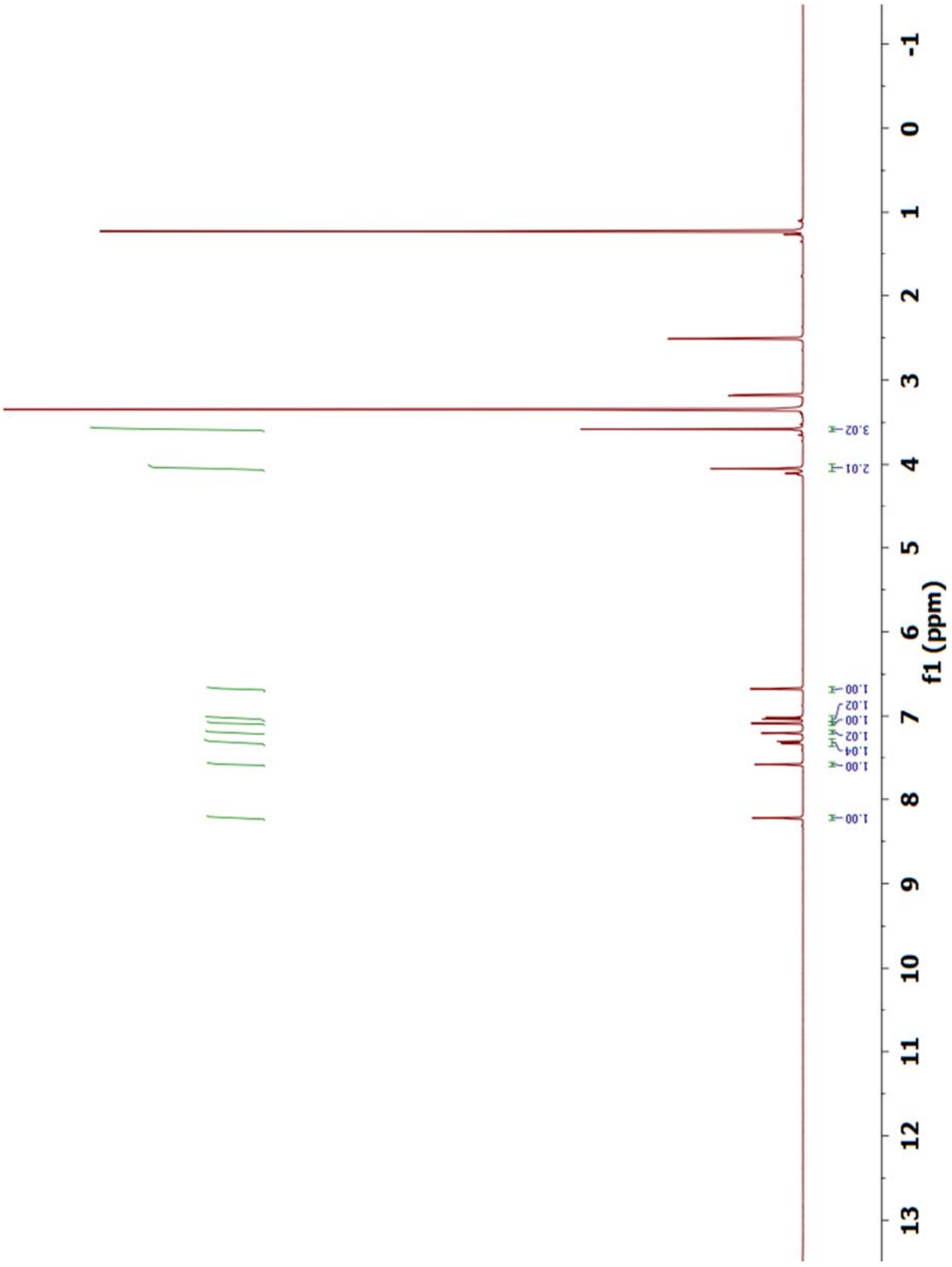

^{1}H NMR spectrum of [Co^{III}(salen^{tBu})(1-MeIm)$_2$]ClO$_4$ in DMSO-d$_6$.

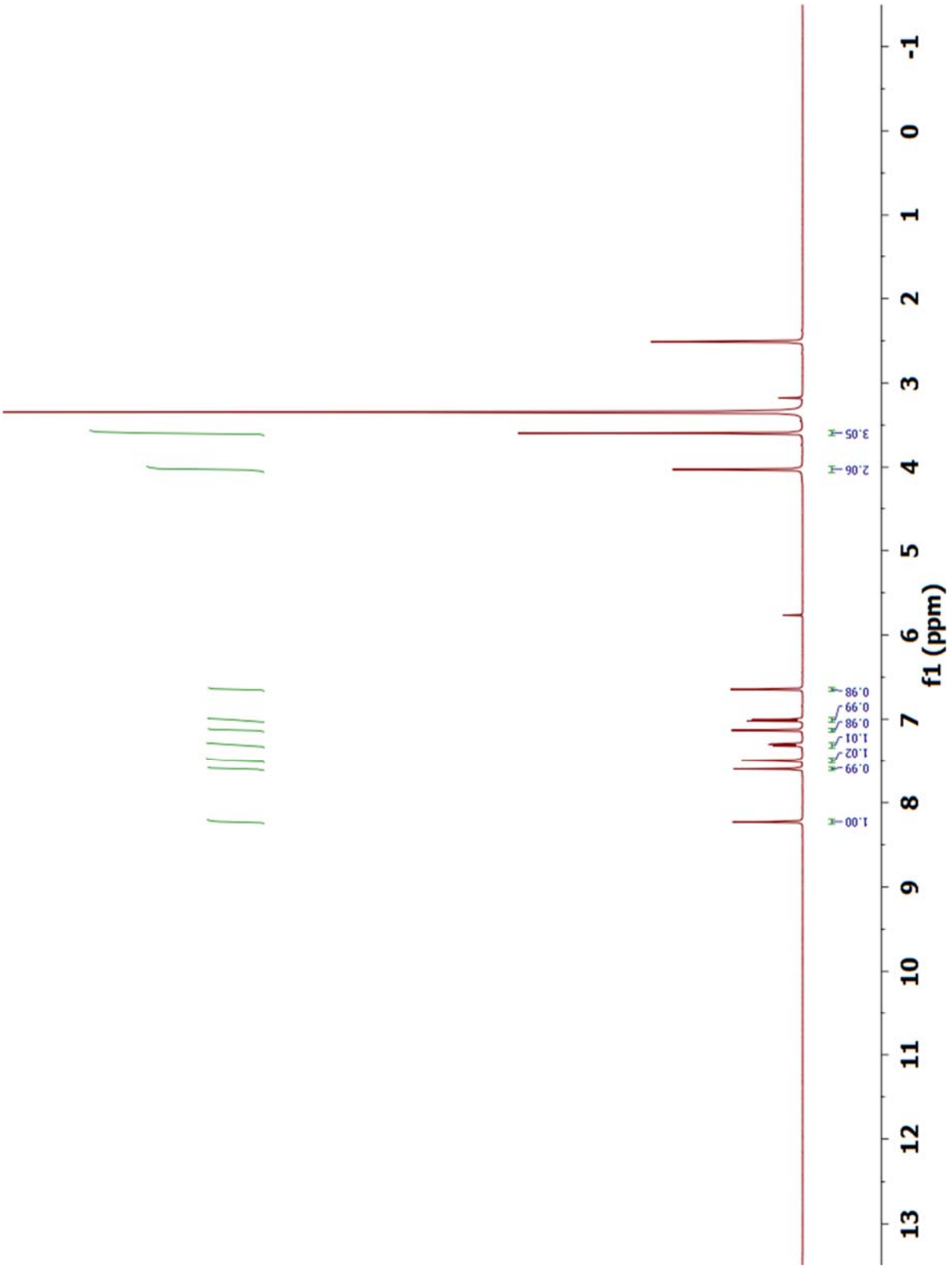

^{1}H NMR spectrum of [Co^{III}(salen^{Br})(1-MeIm)$_2$]ClO$_4$ in DMSO-d$_6$.

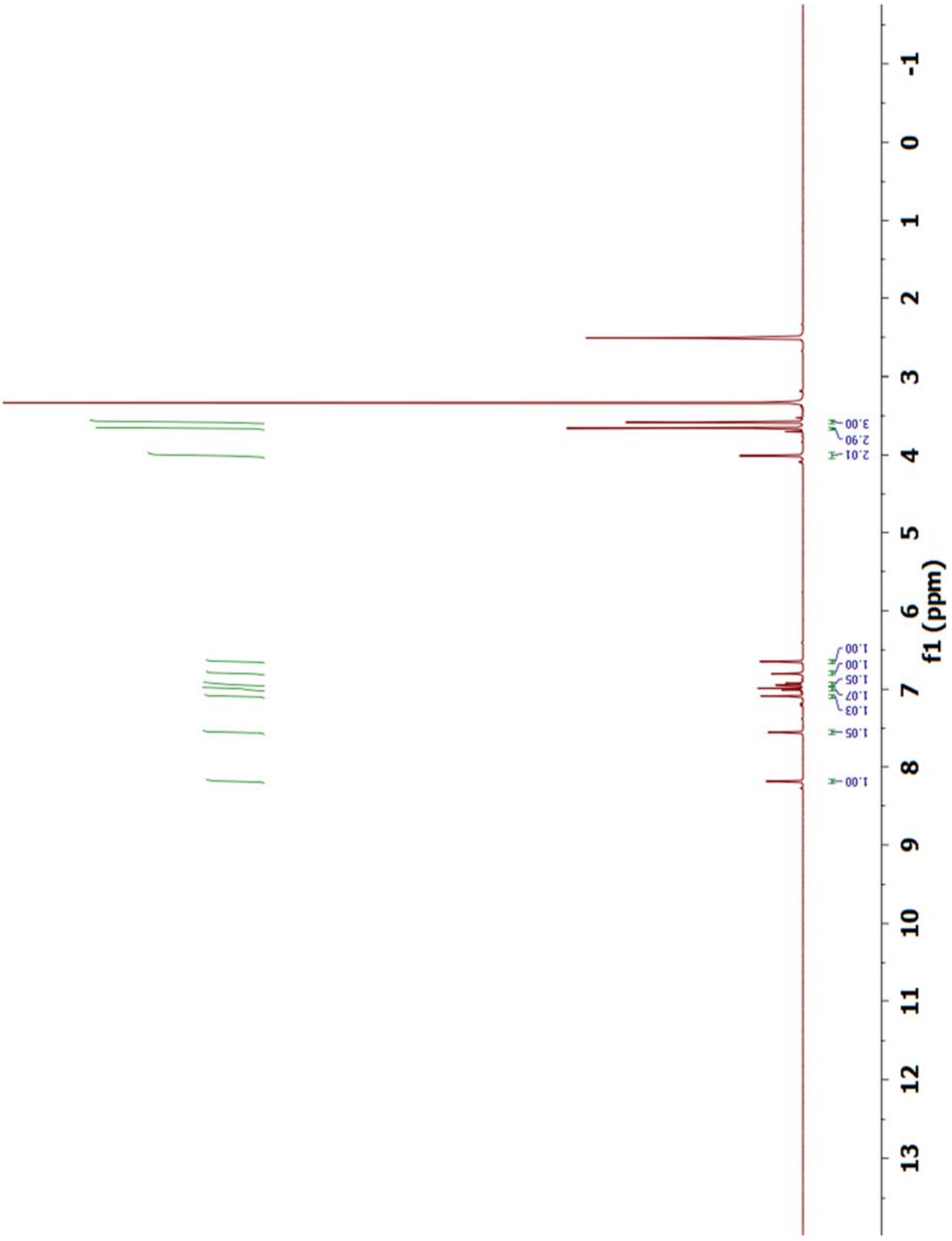

^{1}H NMR spectrum of [Co^{III}(salen^{OMe})(1-MeIm)$_2$]ClO$_4$ in DMSO-d$_6$.

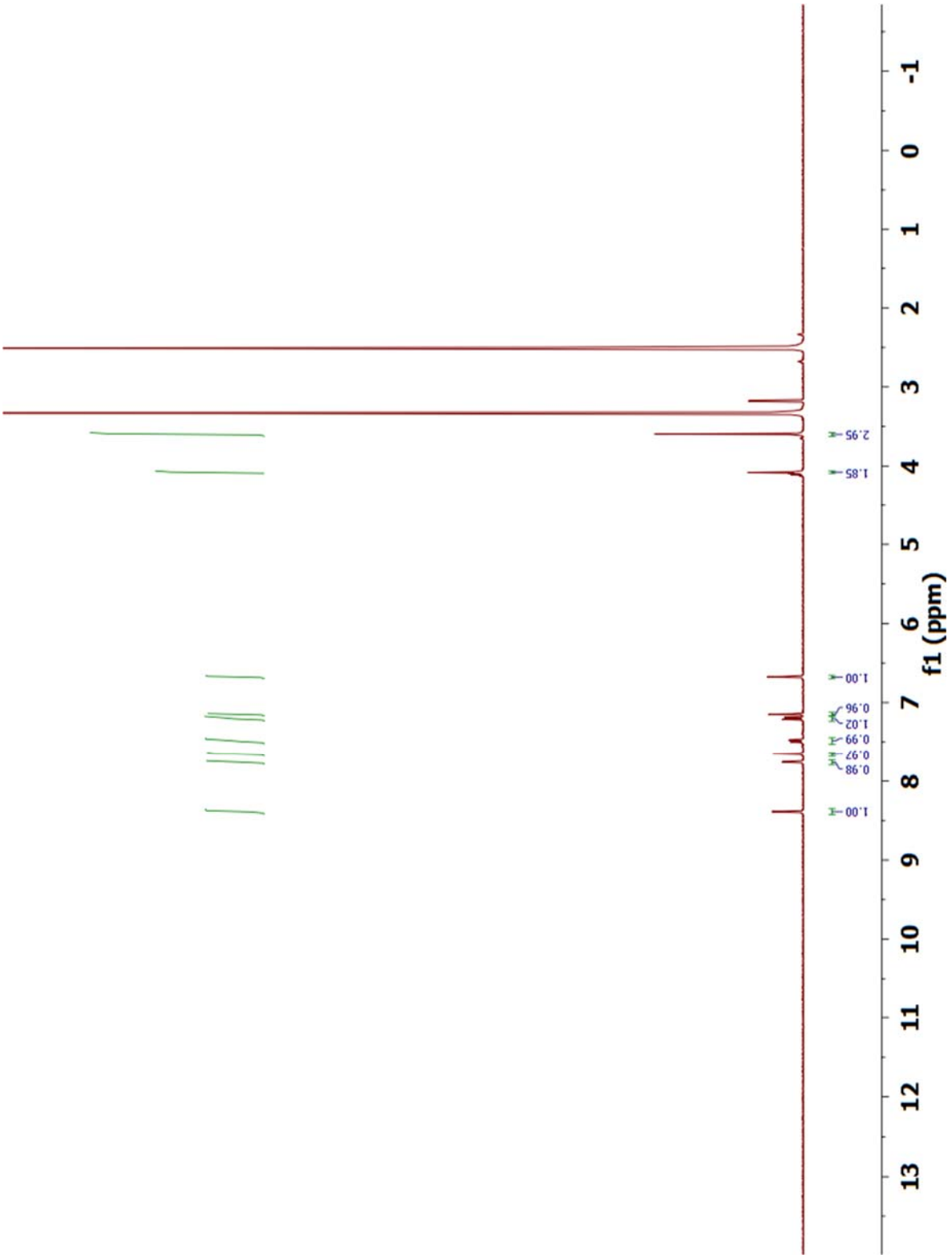

^{1}H NMR spectrum of [Co^{III}(salen^{CF3})(1-MeIm)$_2$]ClO$_4$ in DMSO-d$_6$.

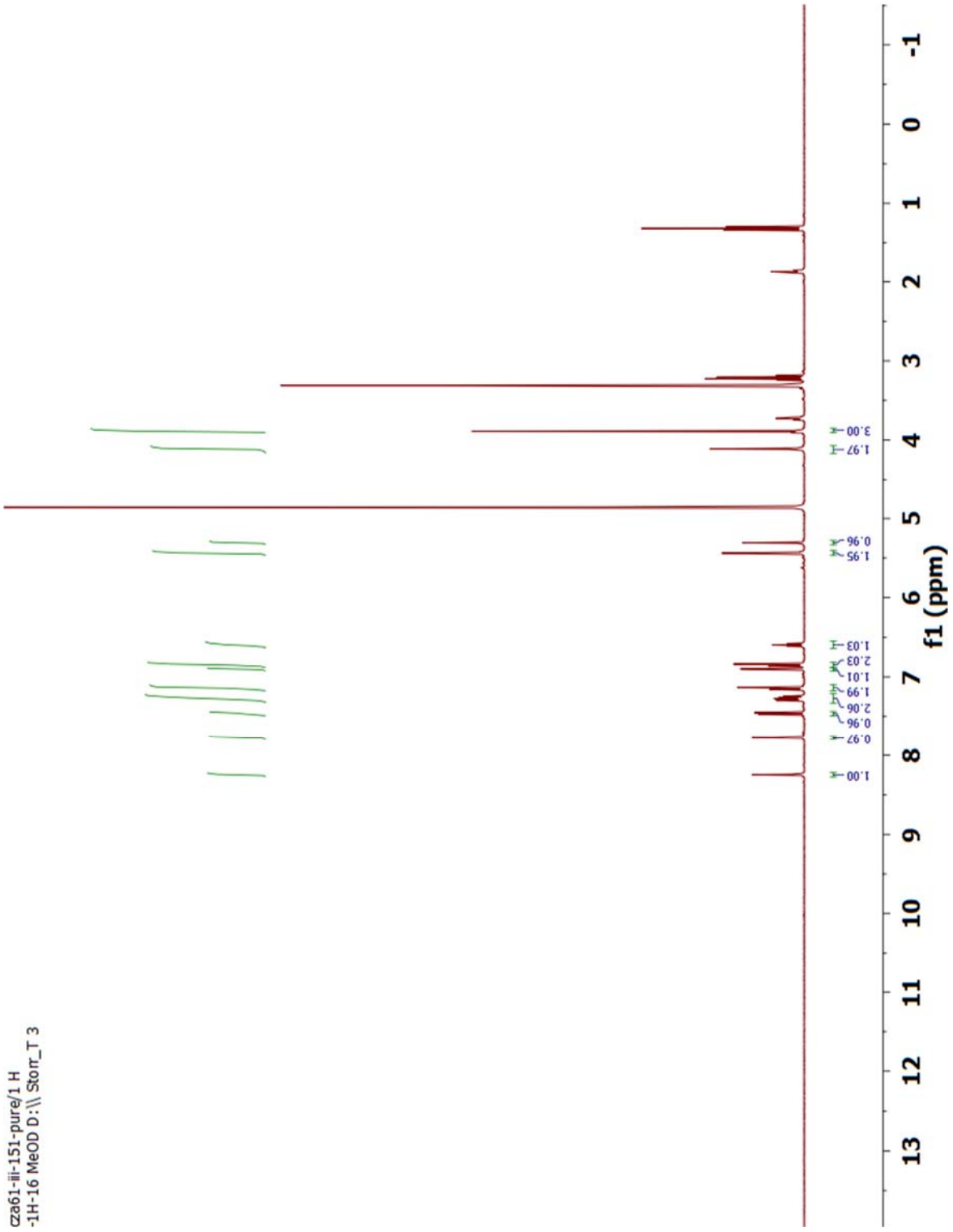

^{1}H NMR spectrum of [Co^{III}(salen^{H})(coumarin)$_2$]Cl in MeOD.

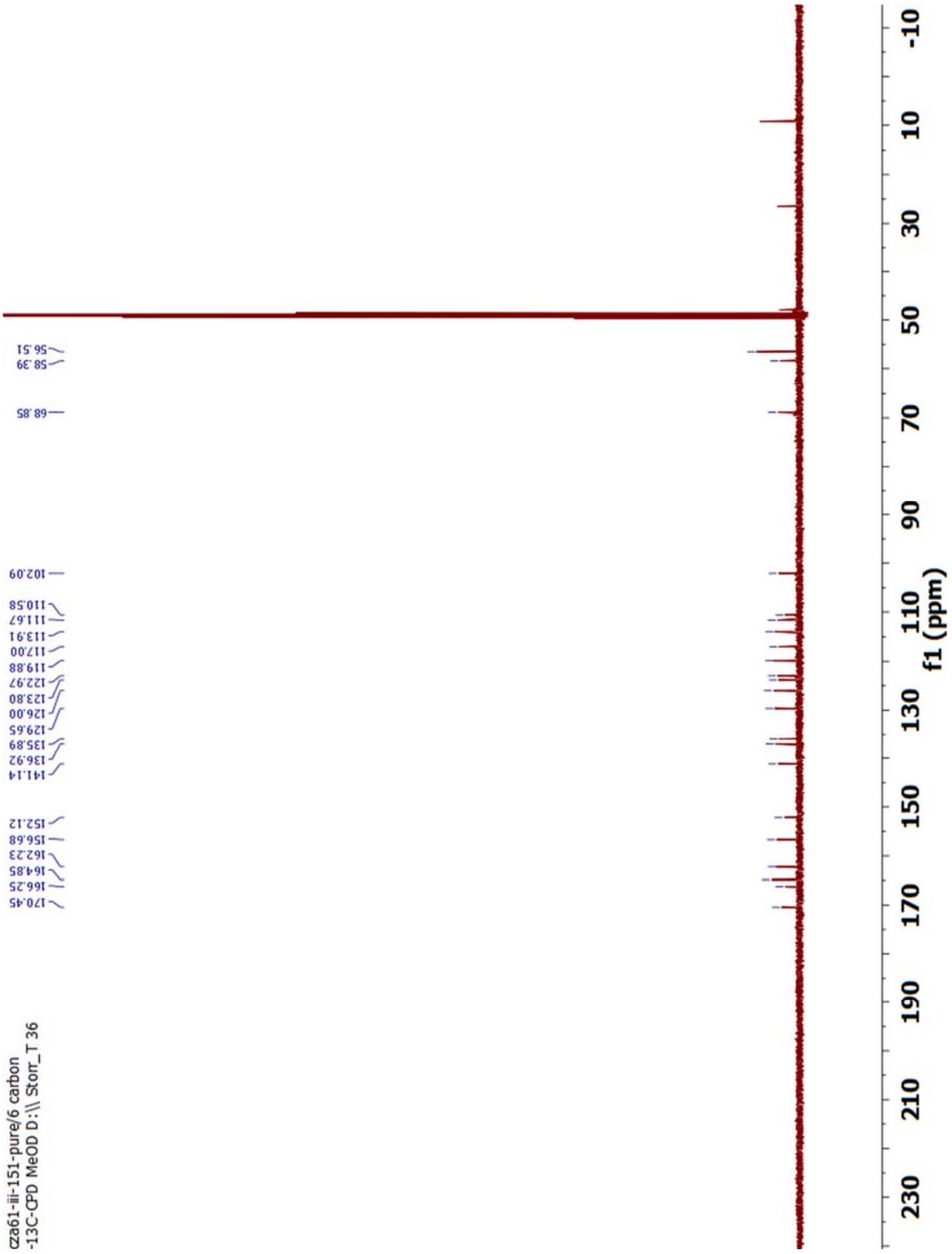

^{13}C NMR spectrum of [Co^{III}(salen^{H})(coumarin)$_2$]Cl in MeOD.

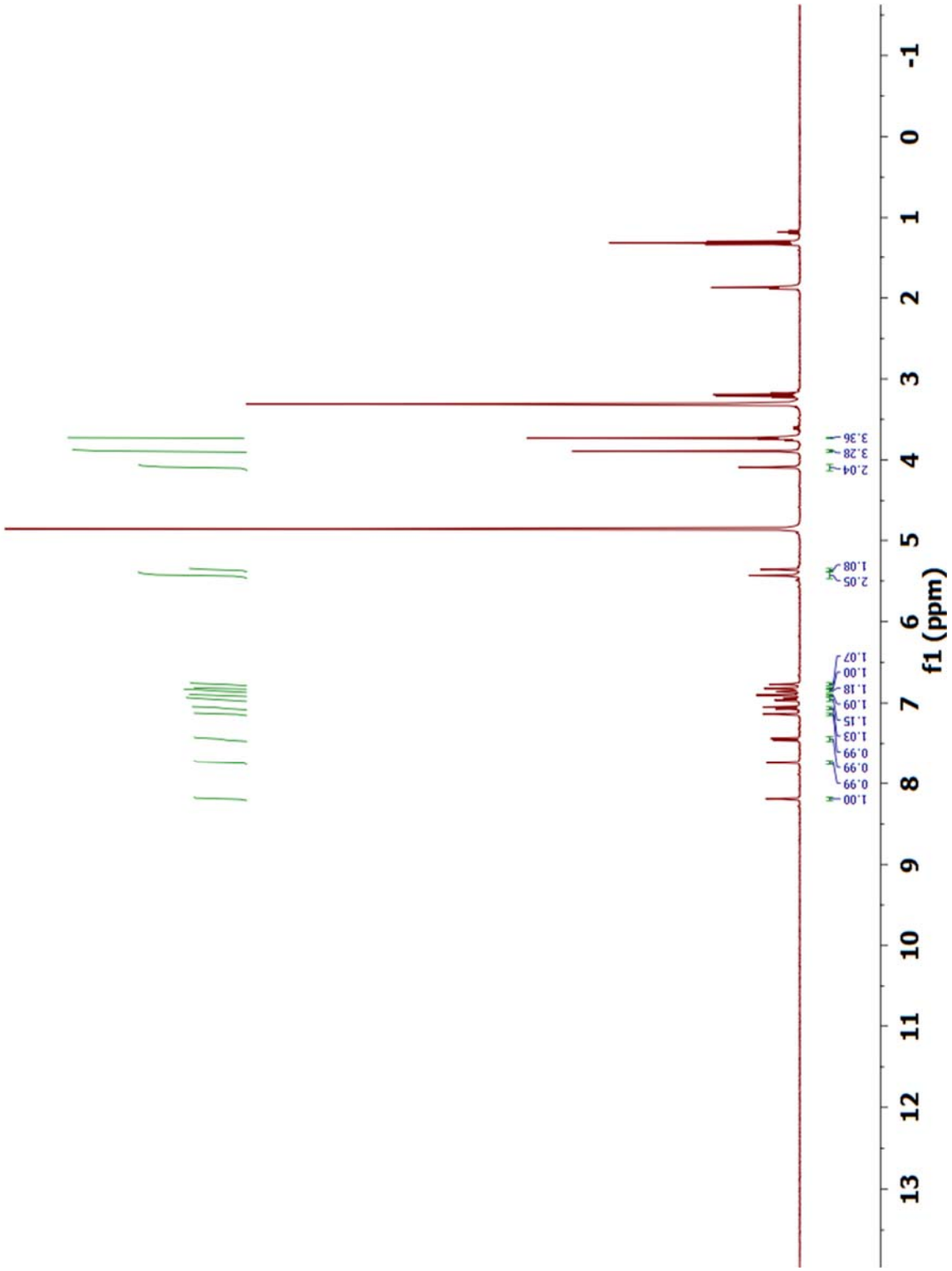

^{1}H NMR spectrum of [Co^{III}(salen^{OMe})(coumarin)$_2$]Cl in MeOD.

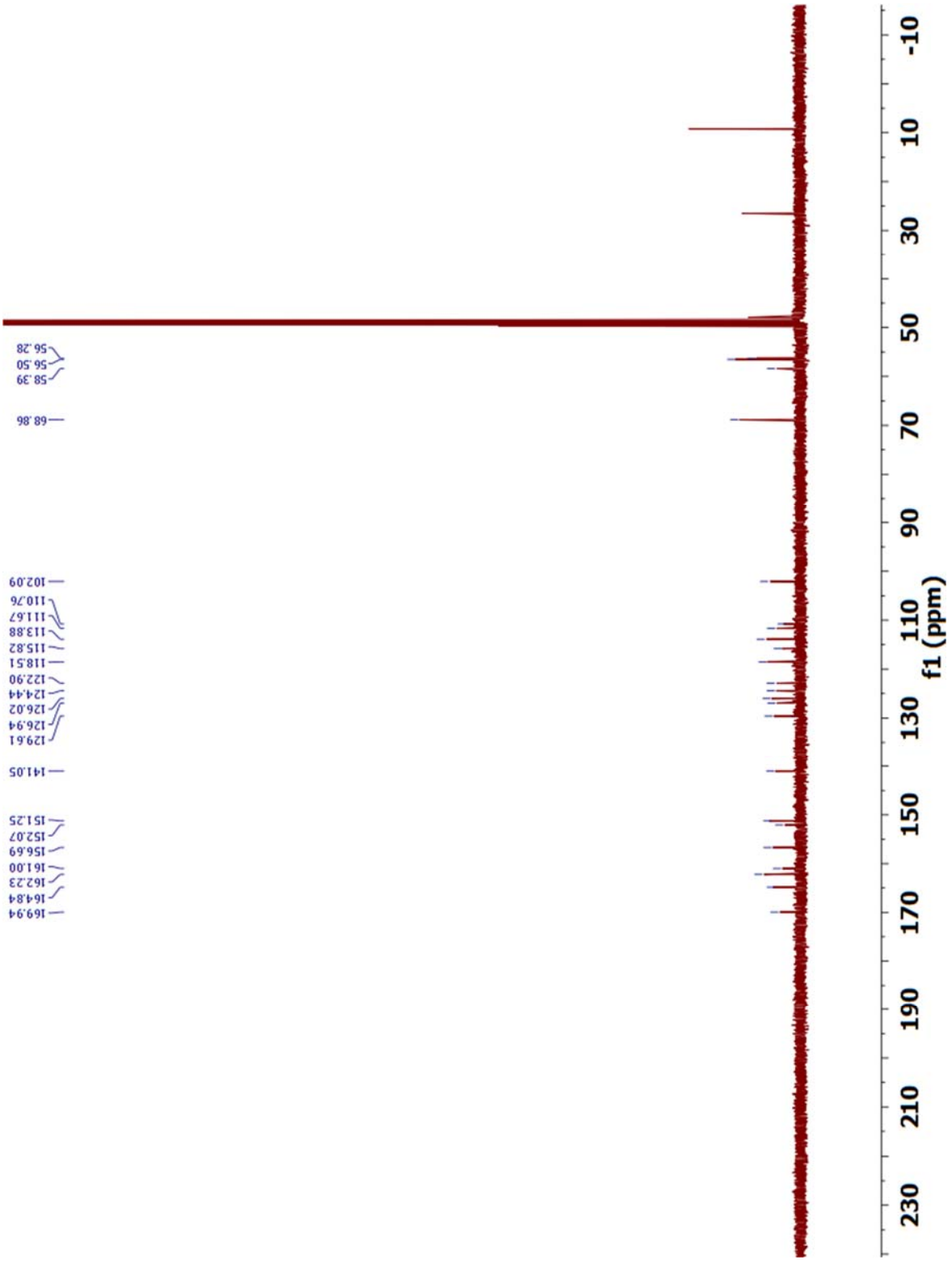

^{13}C NMR spectrum of [Co^{III}(salen^{OMe})(coumarin)$_2$]Cl in MeOD.

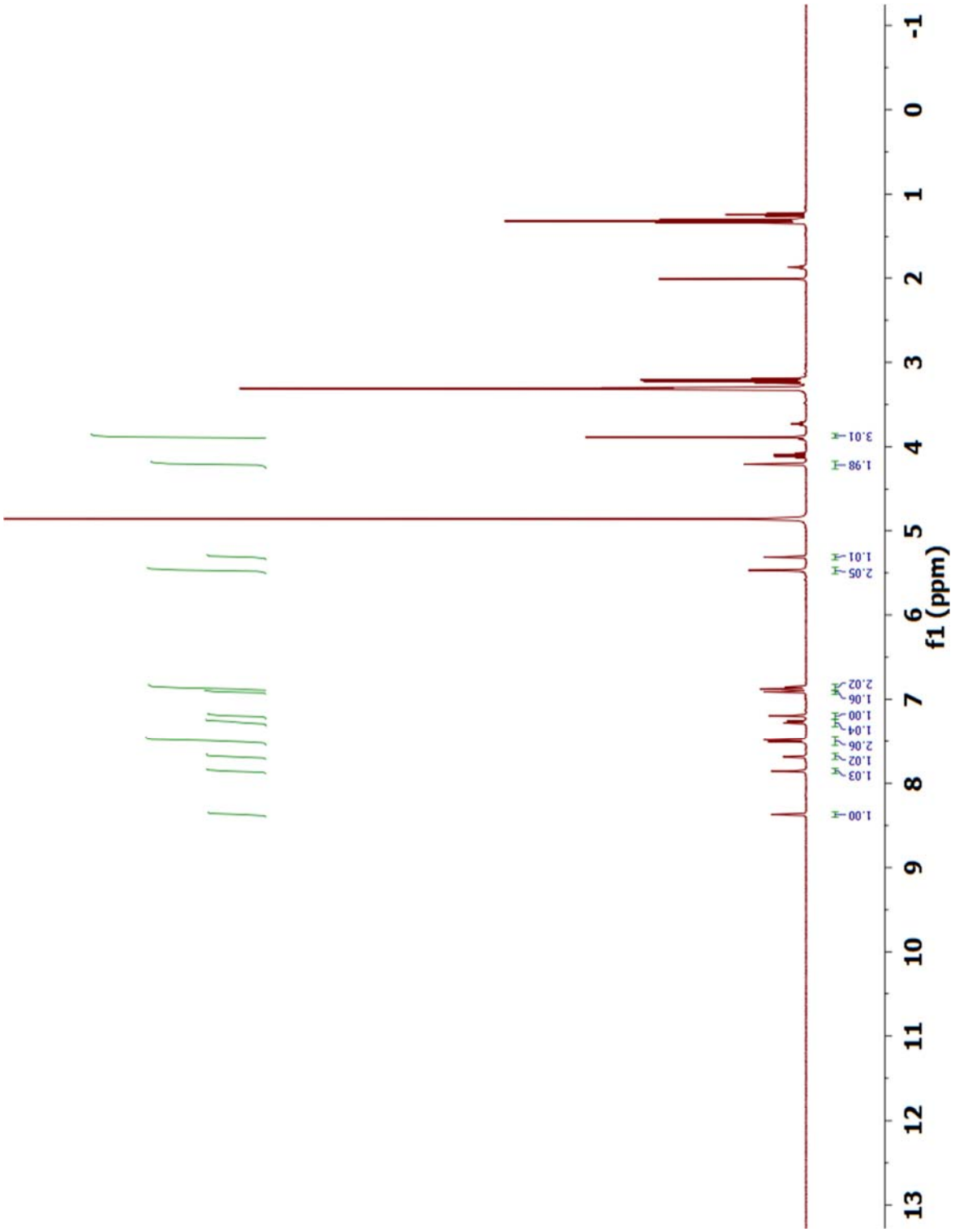

^{1}H NMR spectrum of [Co^{III}(salen^{CF3})(coumarin)$_2$]Cl in MeOD.

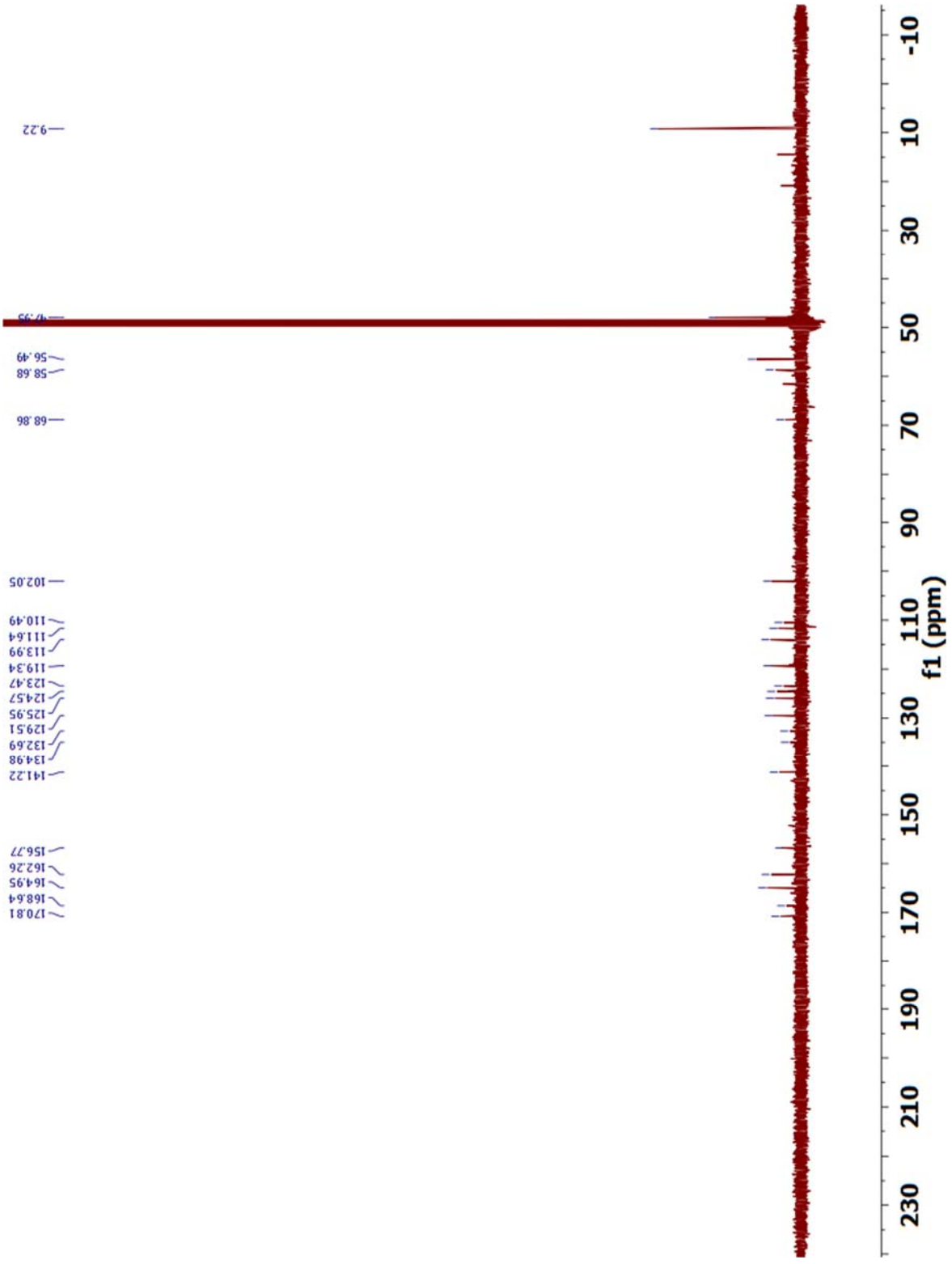

^{13}C NMR spectrum of [Co^{III}(salen^{CF3})(coumarin)$_2$]Cl in MeOD.

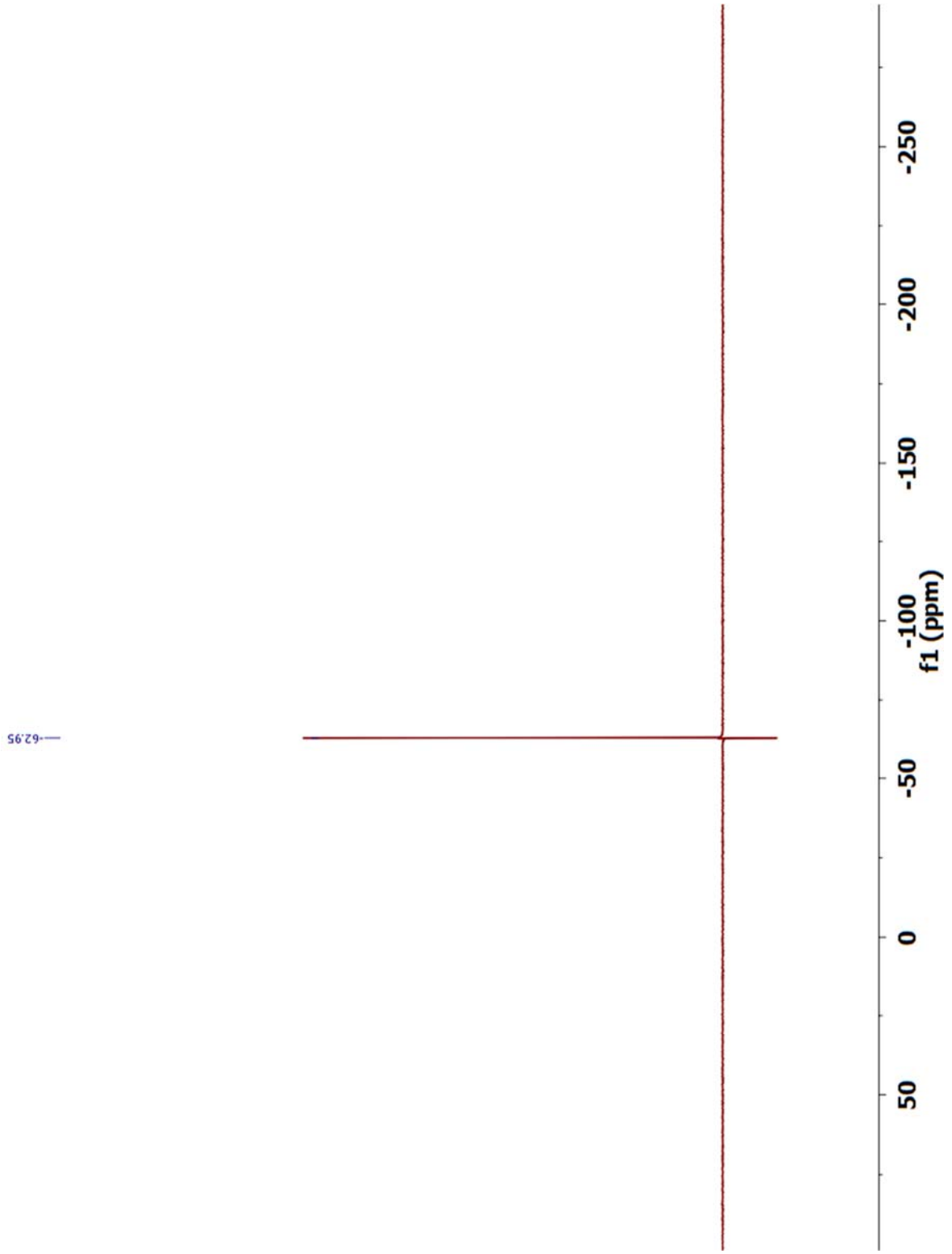

^{19}F NMR spectrum of [Co^{III}(salen^{CF3})(coumarin)$_2$]Cl in MeOD.